Transient Stability Analysis for Power System Networks with Asynchronous Generation

Prem Kethavath

A thesis submitted in fulfilment of the requirements for the degree of Doctor of Philosophy in Electrical and Computer Engineering, The University of Auckland, 2015

"We are at the very beginning of time for the human race. It is not unreasonable that we grapple with problems. But there are tens of thousands of years in the future. Our responsibility is to do what we can, learn what we can, improve the solutions, and pass them on"

Richard P. Feynman

Abstract

Attention is increasing on transient stability and secure mode of operation for power systems with asynchronous generation. This is due to asynchronous mode of generation like windfarms, increasing in capacity and displacing existing high inertia synchronous generation. Participation of wind farms, which are primarily inertia decoupled during transient disturbance, will become necessary to comprehensively analyse framework like energy function and coherency based reduction methods. This thesis investigates the impact of reduced system inertia due to asynchronous generation, on transient stability of power systems.

This thesis proposes an energy function approach to assess power system transient stability impacts following increased penetration of asynchronous generation plants. The asynchronous wind farm generation is considered as an equivalent conventional synchronous generator with negligible inertia. Assessment has been carried out on single machine infinite system and three machine nine bus test system to compute critical energy and critical fault clearing time, from first principles, using potential energy boundary surface method. A new representation of plotting contours of critical clearing times on inertia space has been developed. This enables estimation of additional inertia required for a system due to inertia reduction from asynchronous generators. The results of the simulation and new graphical method confirms that transient stability margin of the system is impacted with increased penetration of asynchronous generation.

This thesis also investigates coherency based analysis technique for network reduction to carry out transient stability analysis for a large power system network that has wind penetration. Identification of coherent groups targets to obtain simplified dynamic equivalent of system by aggregation of coherent generators and replacing it with an equivalent generator. The use of this equivalence can transform a large power system into a reduced model, localized into a small internal area containing the disturbance which impact stability. The New England, 39 bus 10 machine system has been used to demonstrate the methodology. Contingencies are applied with and without wind farm i.e., by replacing few synchronous generators with windfarm of similar capacity.

This thesis also develops transient stability enhancement method for networks with asynchronous generation. When a machine inertia is reduced its first swing stability can be enhanced by line series compensation and also multi-swing stability using bang-bang control on series compensation. Compensation values and the lines that can participate in series compensation during contingencies are found.

Dedicated to
Indian Institute of Technology Kharagpur

Acknowledgements

I like to thank my supervisor, Associate Professor Nirmal Nair, for encouraging me to pursue the fundamental approach of investigating transient stability assessment. He is a valuable source of ideas and knowledge in the realm of power systems. I would also like to thank Dr Akshya Swain, whose contribution has added more perspective to address the controller objectives in this thesis.

The names of Dr Naresh Singhal and Dr Michael Neve deserve special mention for supporting me with process of applying and getting a doctoral scholarship, without which this PhD journey would not have been effectively undertaken.

I like to thank my friend Syed for his constant support and encouragement. I like to thank my friends Girish, Sam, Suman, Arijit, Stuti, Deepthi and Miriam for supporting as a family. Also I like to thank my fellow researchers Dr Waqar Qureshi, Dr Ali Abdolkhani and Dr Kaium Mollah, who have been helping me and encouraging with positive vibes throughout. Finally I like to thank Faculty of Engineering library that provided me with all the additional help needed to complete this PhD.

Contents

List of Figures

List of Tables

Abbreviations

BCU	**B**oundary of stability region-based **C**ontrolling **U**nstable equilibrium point
CCT	**C**ritical **C**learing **T**ime
COA	**C**enter **O**f **A**ngle
DFIG	**D**oubly-Fed **I**nduction **G**enerator
EMF	**E**lectro**m**otive **F**orce
EP	**E**quilibrium **P**oint
FACTS	**F**lexible **A**lternating **C**urrent **T**ransmission **S**ystems
PEBS	**P**otential **E**nergy **B**oundary **S**urface
SEP	**S**table **E**quilibrium **P**oint
SMIB	**S**ingle **M**achine connected to an **I**nfinite **B**us
STATCOM	Static Synchronous Compensator
TCSC	**T**hyristor-**C**ontrolled **S**eries **C**ompensation
UEP	**U**nstable **E**quilibrium **P**oint
WSCC	**W**estern **S**ystem **C**oordinating **C**ouncil

Chapter 1

Introduction

Increasing demand of renewable generation integration to meet the load forecasts, demands for revisiting stability studies for steady state and transient phenomenon [2–4]. Existing practice of considering renewable generation as negative load in stability studies is not valid for high penetration of renewable generation. All the renewable form of power generation are asynchronous type of generation, where inertia is de-coupled compared to synchronous type of generation. The net inertia of a large power system is reduced with higher percentage of asynchronous generation.

There is an increasing need to understand the impact of increased penetration of asynchronous generation towards transient stability studies. Traditional **T**ransient **S**tability **A**nalysis (TSA) involves, implicitly solving of differential and algebraic system equations using time-domain or energy function method. Solving these system equations is at the heart of transient stability analysis. This thesis explores the possibility of using these equations developed for synchronous generators applied to asynchronous generation in large capacity.

1.1 Power system stability and security

Unstable and insecure operation of grid is undesirable in power systems be it at utility, transmission or distribution system level. Electric Power Research Institute reports that there is an estimated loss of $119 to $188 billion annually due to power fluctuations and system outages[5, 6]. These outages are primarily due to operation of elements close to their operation limits pushed by increasing load demand. As generation and transmission facilities are budget constrained the grid undergoes a cycle for demand of new transmission lines. When existing lines are stressed, they lead to failure of their operation and cause outages.

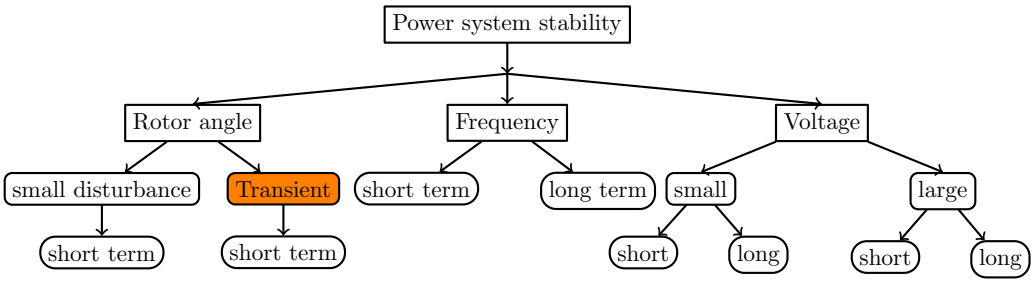

FIGURE 1.1: Types of power system stability

System secure operation is further impacted by increasing renewable generation both at transmission and distribution level due to asynchronous mode of primary generation. This generation is rising because of cheaper source of energy, but the generation technology comes with lower inertia, thus offering reduced synchronising forces over conventional synchronous generation which determines the dynamic security operation limits.

Although power system planning takes into consideration of stressed and ageing condition of network, power outages and fluctuations are common due to severe disturbances. To name a few, disturbance could be trigged by sudden loss of transmission line, sudden loss of load or a generation unit. There could be transient events like lightening, malfunctioning of protective relays, insulation breakdowns etc.. that can lead to change of network configuration.

At the planning stage of power system it is made sure that system can operate and withstand most kinds of disturbance or contingencies. As these disturbances rise stability issues which depend upon severity of the disturbance are categorised and power system stability analysis is performed at planning and operation stage. This analysis makes sure that the system remains in steady or acceptable state of operation following a disturbance. Operation limits for secure mode of operation are determined through stability studies. Stability at planning stages suggest the need for additional assets and necessary controls to maintain or enhance both static and dynamic security limits. During operation, stability analysis is performed to check and determine operation settings of protection devices.

It can be defined "Power system stability is the ability of an electric power system, for a given initial operating condition, to regain a state of operating equilibrium after being subjected to a physical disturbance, with most system variables bounded so that practically the entire system remains intact"[7–9]. System has to remain intact without tripping of loads or generators unless they are intentionally removed to preserve secure operation.

Power system stability problem is high dimensional and complex. It is advised to make simplified assumptions along with degree of detail in representing the system. Power system stability is generally classified into rotor angle, frequency and voltage stability. Fig. 1.1 shows stability classification based on system variable in which instability, severity and duration of disturbance is observed.

Rotor angle stability refers to the ability of synchronous machines in an interconnected power system to remain in synchronism after subjected to a disturbance, i.e. ability of each synchronous machine to restore equilibrium between electromagnetic torque and mechanical torque upon disturbance to remain stable. In an unstable case, angular swings increase in some generators leading to loss of their synchronism relative to other generators. On disturbance the variation of insufficient electromagnetic torque of machine can be categorised into two, the synchronizing torque component which is in phase with rotor angle deviation leading to non-oscillatory instability and also the damping torque component which is in phase with the speed deviation causing oscillatory instability. Transient instability is a sub category of rotor angle stability caused by insufficient synchronising torque.

1.2 Motivation for the thesis

With increasing focus on integrating renewable energy into existing grid, wind energy generation has increasingly attracting large investments and deployments worldwide. Most of the mature research on transient stability is established for synchronous generation. Transient stability studies at planning and operation stages are carried out by analysing all the critical contingencies which can lead to loss of synchronism of generators. Loss of synchronism is the root cause for cascading outages of transformers, transmission lines and loads isolated by protection devices leading to black out. So transient stability studies are very necessary and crucial stability studies for grid operators. In event of a fault causing swing of generators, the generators are kept in synchronous mode of operation by the restoring synchronising forces. These synchronising forces are contributed by individual machine inertia across the grid. With increasing demand of power to meet the power requirement, asynchronous generation are increasing in capacity (e.g. 30% of net grid generation) or displacing existing synchronous generation, reducing the net inertia causing concerns during steady state operation[10, 11]. Reduction in net inertia is unhelpful to maintain stability during transient events.

The transient stability studies offers contingency ranking information based on critical fault clearing time. This information is the underlying principle for all network protection schemes and settings. So transient stability during high penetration are to be

thoroughly understood to avoid catastrophic events triggered by tripping of generators. The impact of increased penetration of wind generators on system dynamic performance is also required[12–14]. In this thesis these impacts will be examined with respect to rotor angle stability using methods like energy function formulation, coherency network reduction, swing equations and robust critical clearing time evaluation.

Doubly-**F**ed **I**nduction **G**enerator (DFIGs), is a variable speed wind turbine generation technology which is gaining more attention amongst all the other wind generation technologies which employ induction generators. These generation technologies are asynchronous in nature and impact of their low inertia is explored in this thesis. Unlike synchronous machine where rotor electrical angle is same as mechanical angle, inertia of the rotor mass is interacting with electrical angle, thus providing synchronous forces. Wind turbine inertia of induction generator is decoupled because the operation and performance of DFIG or any other wind generator is governed by power electronic converter side coupling to the grid [1, 15, 16].

Existing TSA research are based on synchronous machine theory, where transient stability is determined using either time domain and observing rotor angle deviation or using energy function method. As there is no synchronously coupled rotor angle to observe at converter based generation, its effect on other generator rotor angle deviation can only be observed and stability be inferred [12, 17–23]. On the other hand, comprehensive stability study of the entire system using energy function approach will be global and can provide approximate but very robust results well aligned with control theory. This can be achieved by reducing inertia of existing synchronous machines and carrying out either energy function analysis or undertake an explicit time-domain analysis.

1.3 Thesis outline

This thesis is organized into seven chapters and is summarized as follow:

1. **Introduction**
   This chapter provides the statement of the problem, where power system transient stability is defined from the point of view of both conventional and direct methods. It further outlines the motivation for the thesis and lists outputs generated.

2. **Transient stability analysis using energy functions**
   This chapter provides the background needed to undertake transient stability analysis. Swing equation and energy function is provided for **S**ingle **M**achine connected to an **I**nfinite **B**us (SMIB) and multi-machine system. Test cases are provided for 3-machine 9-bus system and 39-bus, 10-machine system.

3. **Stability theory applied to transient energy function method**
   This chapter investigates stability in the sense of Lyapunov. Theory on region of attraction of system to remain stable, application of **P**otential **E**nergy **B**oundary **S**urface (PEBS) method for TSA of 3-machine 9-bus system have been discussed in depth here.

4. **PEBS method with reduced inertia**
   This chapter explores the impact of reduced inertia on critical clearing time of a SMIB and 3-machine 9-bus system and brings out some original contributions.

5. **Asynchronous generation in power system networks**
   This chapter provides the analysis carried out to reflect the absence of inertia of large scale windfarms using traditional synchronous machines system modeling and representation.

6. **Transient stability enhancement of power system with reduced inertia**
   In this chapter, discrete control strategy is used to enhance transient stability of SMIB and 3-machine 9-bus system through series compensation when a machine inertia is reduced. It also proposes method to obtain amount of compensation and the lines which can participate in series compensation that can maintain transient stability when system inertia is reduced.

7. **Conclusions and future work**
   This chapter summarizes the overall thesis and highlights contributions emerging from this research. It also lists some areas of future development that evolves directly from the outputs of this thesis.

1.4 Contributions of thesis

Following are the significant and original contributions of this thesis especially, in understanding impact of reduced inertia caused by asynchronous generation towards transient stability of system using energy function method.

Identification of coherent generator groups in large network with windfarm

39-bus 10-machine system is analysed in DIgSILENT Powerfactory wherein coherent generator groups are identified to reduce the system into fewer machines which swing together. This system is analysed with a DFIG windfarm at a generation bus. It is observed that coherent generator groups remain same, with and without windfarm for the studied network.

PEBS method analysis with reduced inertia

Critical **C**learing **T**ime (CCT) is calculated for SMIB for various reduced inertia values. It is observed that with decrease of inertia, CCT is reduced. 3-machine 9-bus system is analysed by reducing inertia in steps for two machines. PEBS method is used to obtain critical clearing time and critical energy for various combination of inertia. Also results were provided to prove that assuming wind generation as negative load reduce stability limit and also that assumption is invalid for large amount of wind generation.

Equi-CCT contours

A new method for presenting critical clearing times obtained for several combinations of inertia, called as equi-CCT lines are plotted on the inertia space. The graphical representation of CCT for several inertia combinations offers a quantifiable amount of inertia required for maintaining desired stability margin. This is a novel and new contribution.

PEBS based stability enhancement with discrete control

Discrete control strategy using bang-bang control applied on SMIB with reduced inertia has improved transient stability. On a 3-machine 9-bus system, when inertia of a machine is reduced by providing series compensation on transmission lines, stability is improved, this analysis is repeated for a wide range of inertia and limit on compensation value is calculated. For each set of these combinations CCT is obtained using PEBS method. These set of values are presented as equi-CCT contours with the inertia and compensation as axis. It is observed that with a limit on compensation, only a few lines seems to be able to participate in compensation or give desired CCT when machine inertia is reduced.

1.5 Publications & Presentations

1. Naik, P.K., Qureshi, W.A., Nair, N.-K., "Identification of Coherent Generator Groups in Power System Networks with Windfarms", in Australasian Universities Power Engineering Conference 2011 (AUPEC 11), $25^{th} - 28^{th}$ September 2011, Brisbane, Australia

2. Naik, P.K., Bahadornejad, M., Nair, N.C., Vyatkin, V., "IEC 61850 based smart distribution protection: Solutions for sympathetic tripping," Innovative Smart Grid Technologies Asia (ISGT), 13-16 November 2011, Perth, Australia

3. Prem Kumar "Transient stability assessment with large scale wind penetration", Oral presentation at NewZealand Wind Energy Conference and Exhibition 2012, $2 - 4^{th}$ Apr. 2012 Hamilton, NewZealand

4. Nair, N.-K C, Naik, P.K, Chakrabarti, B., Goodwin, D. "Managing transmission system operation in New Zealand with high renewable penetration", in IEEE PES General Meeting 2012, July 2012, San Diego, USA

5. Prem Kumar Naik, "Transient stability assessment with large scale wind penetration", Student Poster Contest at the 2012 IEEE PES General Meeting, San Diego, CA, USA on July 24, 2012

6. Prem K Naik, Akshya Swain and Nirmal-Kumar C Nair, "Stability improvement with series compensation on transmission networks with asynchronous generation", Student Poster Contest Program at IEEE PES GM 2014", Washington, DC, USA, from July 27-31, 2014

7. Naik, P. K., Nair, N.-K. C., and Swain, A. K. (2015), "Impact of reduced inertia on transient stability of networks with asynchronous generation". Journal International Transactions on Electrical Energy Systems, doi: 10.1002/etep.2079.

8. Prem K. Naik, Akshya K. Swain and Nirmal K C. Nair, "Discrete control of series compensated transmission networks with asynchronous generation", (submitted to Journal International Transactions on Electrical Energy Systems)

Chapter 2

Transient stability analysis using energy functions

In this chapter power system stability problem and its practices are reviewed. Introduction to direct methods to determine stability is provided. System of equations are derived to demonstrate dynamics of single machine connected to infinite bus and its corresponding energy function. System of equation to study dynamics of multi-machine system in center of angle formulation and its energy function is derived. Energy function analysis is then performed on 3-machine 9-bus system as a case study. For a large system coherent generator groups are identified for a 39-bus 10-machine system.

2.1 Power system transient stability analysis

Upon fault, if the post-fault trajectory of the system does not converge to an acceptable steady state then the system will encounter instability. Depending on the parameter of interest and its behaviour the type of instability is categorised. If the system or bus voltage is of unacceptable value during the fault and does not attain acceptable value on reaching steady state it is suffering from voltage instability. If the frequency is out of acceptable limit so it suffers from frequency instability. Further, these instabilities can be fault specific.

Similarly the system can suffer oscillatory instability which mostly arises due to rotor angle dynamics of machines where rotor angles can be bounded with an oscillatory behaviour causing sub-synchronous resonance. These oscillations can be stable and periodic causing power oscillations of low frequency.

In transient stability studies, power system is modelled be a set of differential and algebraic equations to capture the dynamic behaviour alongside non-linear power flow equations. They are solved as coupled equations and larger the system more the complexity. The most standard method is to numerically solve these system equations in time domain and obtain the quantities of variables of interest as function of time. These variables can be machine rotor angle, power flow, voltage or can be a combination of all. Depending on the dynamics of these variables nature of stability is decided whether a system is held secure and operating within acceptable limits.

2.2 Step by step transient stability analysis

A step-by-step integration of system differential and algebraic equations in time domain is conventional transient stability analysis method. Initial system state is obtained from solving pre-fault system equations, fault-on dynamic equations use these initial state(end of pre-fault) for integration. The fault/disturbance duration includes occurrence and removal of fault. After the fault is cleared, post-fault dynamic equations also get numerically integrated using solvers. Following simulation of fault-on and post-fault trajectories, fundamentally rotor angles of machines are obtained. The angles are plotted in reference to machine of high inertia and if these machine rotor angles are bounded, the system is stable, else system is unstable. Fig. 2.17 and Fig. 2.18 illustrate corresponding to a 3-machine 9-bus system in **C**enter **O**f **A**ngle (COA) formulation, for a particular fault it is observed that the Critical Clearing Time (CCT) is in between 0.31 and 0.32 seconds. In conventional method it is required to perform simulation runs numerous times with increasing fault duration until bounds on CCT are found. CCT is the maximum duration between the inception of fault and its removal such that the system just loses transient stability. The trial and error approach to obtain CCT is the basic disadvantage of this method, which is over come by direct energy function methods.

2.3 Transient stability analysis from direct methods

The transient energy method is assessing the transient stability of power systems directly. It allows critical clearing times to be calculated directly from a single solution. It also provides a quantitative measure about the degree of stability. Direct methods come with a disadvantage when compared to conventional methods as the models used in direct methods are in less detail or reduced models of generator, exciter, governor, compensator, regulators etc.. or their characteristics response is out of duration of

stability study. Transient stability analysis with direct method aim to acquire knowledge of stable equilibrium point which is surrounded by a stability region called region of attraction and determination of stability its boundary[24].

Method explored here is to obtain stability information directly using a function. The value of energy obtained from the function that describes system transient energy is computed at end of disturbance. This value is compared with a critical-threshold value, difference in values is energy margin and is the parameter of interest also an indicator of stability[25, 26].

A power system provided with transient stability models during for fault-on and post-fault post-fault configurations, following are the basic steps involved in stability assessment using direct methods are as follows:

step 1 System dynamic equations are formulated.

step 2 Stable and unstable equilibrium points of system are computed.

step 3 Energy function pertaining to post-fault system is constructed.

step 4 Critical energy V_{cr} of the system is calculated, this is the energy at UEP $V(\delta_u, 0)$.

step 5 Now the energy $V(\delta, \omega)$ at the instant of fault clearing time is computed, if this energy is less than V_{cr}, then the post-fault system trajectory is stable

step 6 Else repeat repeat above step by incrementing clearing time until critical clearing time that satisfies above step.

For the above the knowledge of stability region of post-fault system is essential. If initial state of post-fault system lies inside the stability region of a desired post-fault SEP, then without conducting further numerical integration one can ensure that post-fault system trajectory will reach to SEP.

2.3.1 Advantages and challenges in using direct methods

Direct methods have made a significant progress since its first appearance in 1940s, it is only in recent years its practical appearance for transient stability analysis is emerging. Transient stability can be determined using direct methods with out performing time consuming solution for post fault system, direct methods are appreciated not only for speed of solution and also for providing quantitative measure for degree of stability[27]. Direct methods are attractive when stability of certain network configurations are to be compared. For example when there is need for quick determination of stability for operation limits while it is constrained by transient stability limit[28]. They also provide information that help to decide on preventive and emergency control actions.

From an analytical point of view, direct methods were originally developed for power systems with autonomous post-fault systems. There are several challenges and limitations involved in practical applications of direct methods for power system transient stability analysis, some of which are inherent with methods while others are related to their applicability to power system models. These challenges come from modelling limitation, function determination, reliability, limitations in scenario and accuracy[26].

2.4 Energy function of single machine infinite bus system

Synchronous machine is major source of power generation, which is driven by a turbine to convert mechanical energy into electrical energy. Interconnection and synchronous operation of large number of machines form the generation of power System. More details of operation and construction can be obtained from[29–31].

2.4.1 Synchronous machine electrical output

A three phase generation circuit in per-phase equivalent is represented in Fig. 2.1. With armature current I_a, generator internal voltage E_a, with $E_a = |E_a|\angle\delta$, and Z_d as synchronous impedance can be presented by equations below as

$$Z_d = R + jX_d \tag{2.1}$$

$$V_t = E_a - I_a Z_d \tag{2.2}$$

The phaser diagram for Eqs. (2.1) and (2.2) are shown in Fig. 2.2 with R neglected.

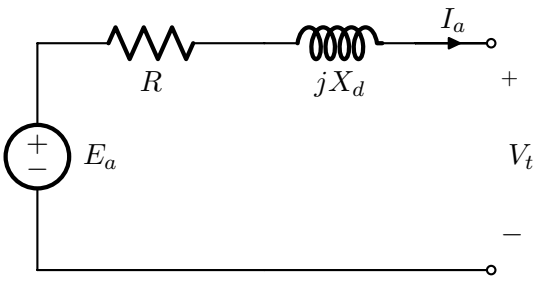

FIGURE 2.1: Per phase equivalent of synchronous machine

Corresponding to Fig. 2.1, a generator is delivering power at an angle δ between terminal voltage V_t and machine generated voltage E_a. Complex power(p.u) delivered by the generator to the system in given by

$$S = P + jQ = V_t I_a{}^* = |V_t||I_a|(\cos\theta + j\sin\theta) \tag{2.3}$$

equating real and imaginary quantities of Eq. (2.3) to obtain active and reactive power as

$$P = |V_t||I_a| \cos\theta \tag{2.4}$$

$$Q = |V_t||I_a| \sin\theta \tag{2.5}$$

Field voltage E_a is kept constant by maintaining field current I_f constant. A generator with larger δ, delivers more power to the network exerting higher counter torque on prime mover. The input from the prime mover is re-established so the speed is in correspondence to frequency of infinite bus. Real power P derived as function of power

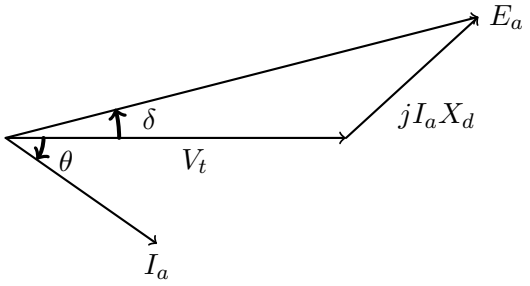

FIGURE 2.2: Per phase vector equivalent of synchronous generator delivering lagging current

angle δ as follows with $V_t = |V_t|\angle 0^o$ and $E_a = |E_a|\angle\delta$ in p.u

$$I_a = \frac{|E_a|\angle\delta - |V_t|}{jX_d} \qquad \text{and} \qquad I_a^* = \frac{|E_a|\angle -\delta - |V_t|}{-jX_d} \tag{2.6}$$

At the generator terminals complex power delivered to the system is

$$\begin{aligned} S = P + jQ = V_t I_a^* &= \frac{|V_t||E_a|\angle -\delta - |V_t|^2}{-jX_d} \\ &= \frac{|V_t||E_a|(\cos\delta - j\sin\delta) - |V_t|^2)}{-jX_d} \end{aligned} \tag{2.7}$$

Splitting real and imaginary parts of Eq. (2.7) for active and reactive power and as function of rotor angle δ gives rise to below equations

$$P = \frac{|V_t||E_a|}{X_d}\sin\delta \tag{2.8}$$

$$Q = \frac{|V_t|}{X_d}(|E_a|\cos\delta - |V_t|) \tag{2.9}$$

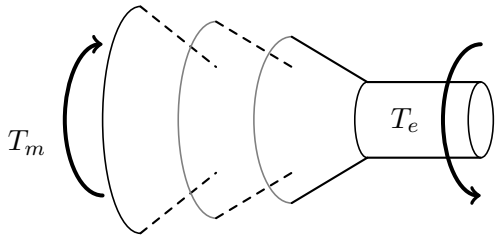

FIGURE 2.3: Rotor shaft direction of rotation with mechanical and electrical torque

2.4.2 Swing equation

Classical power system model is used for stability studies to analyse first swing transients. T_m is the mechanical torque, T_e is the electrical torque to the shaft. Resultant torque will accelerate the shaft in the direction of rotation θ_m, as shown in Fig. 2.3 synchronous machine rotor equation is derived to produce Eq. (2.10) with few assumptions, this model is valid for multi-machine system. Mechanical power input is assumed to be constant. The generator is represented by a constant electromagnetic field behind a transient reactance and loads are represented as passive impedance. T_a is acceleration torque in event of disturbance, Equation (2.10) is the governing equation for obtaining rotor angle responses of the system. These equations can be found in [29–31].

$$
\begin{aligned}
T_a &= T_m - T_e \,\text{N-m} \\
J\frac{d\omega_m}{dt} &= T_a = T_m - T_e \,\text{N-m} \\
J\frac{d^2\theta_m}{dt^2} &= T_a = T_m - T_e \,\text{N-m} \\
\theta_m &= \omega_{sm}t + \delta_m \,\text{rad} \\
J\frac{d^2\delta_m}{dt^2} &= T_a = T_m - T_e \,\text{N-m} \\
\theta_m T_a &= P_a \,\text{W} \\
J\omega_m\frac{d^2\delta_m}{dt^2} &= P_a = P_m - P_e \,\text{W} \\
J &= \frac{2H}{\omega_{sm}^2} \,\text{Kg} - \text{m}^2 \\
\frac{2H}{\omega_s^2}\frac{d^2\delta}{dt^2} &= P_a = P_m - P_e \,\text{per-unit} \\
M\frac{d^2\delta}{dt^2} &= P_m - P_e
\end{aligned}
\tag{2.10}
$$

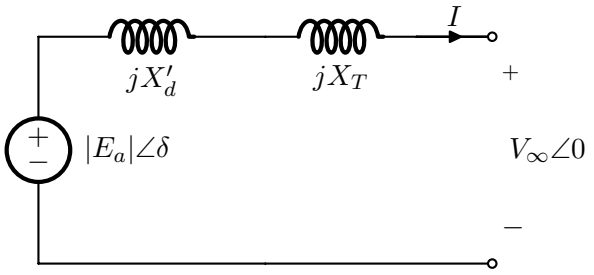

FIGURE 2.4: SMIB phase equivalent for stability study

T_e	Electromagnetic torque, in N-m
T_m	Mechanical torque to the prime mover, in N-m
θ_m	Angular displacement of rotor with respect to a stationary axis, in radians
ω_m, ω_s	Synchronous speed of machine in radians per second
δ_m, δ	Angular displacement of the rotor from the synchronous rotating reference axis, in radians
J	Moment of inertia of the rotor mass, in Kg-m^2
P_e	Electrical power across air gap
P_a	Accelerating power
H	Inertia constant

2.4.3 Power-angle curve

For stability studies a synchronous machine is assumed to be connected to an infinite bus through a loss less transformer and transmission line, as shown in Fig. 2.4. The power transfer from synchronous machine to infinite bus is expressed as

$$P_e = P_e^{max} \sin\delta \tag{2.11}$$
$$P_e^{max} = \frac{|E_a||V_\infty|}{X}$$

with $X = X'_d + X_T$, X'_d is machine transient reactance and X_T is reactance of transmission system. The relation between electrical output P_e and angle δ is the power-angle curve shown in Fig. 2.5. P_m is the mechanical power input, δ_s and δ_u are equilibrium points

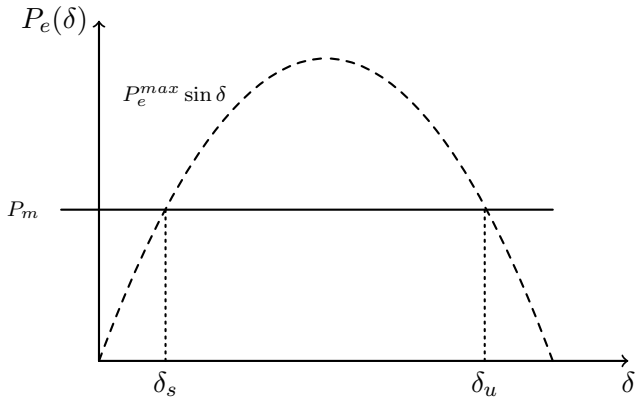

FIGURE 2.5: Power-angle curve of SMIB

2.4.4 Determination of stable and unstable equilibrium points

Equilibrium points are obtained at steady state condition on equating the acceleration Eq. (2.10) to zero

$$\begin{aligned} 0 &= P_m - P_e^{max} \sin\delta_s \\ \delta_s &= \sin^{-1}\left(\frac{P_m}{P_e^{max}}\right) \end{aligned} \tag{2.12}$$

From Fig. 2.5 it can be seen where the equilibrium point δ_s, is a **S**table **E**quilibrium **P**oint (SEP) and $\delta_u = \pi - \delta_s$ an **U**nstable **E**quilibrium **P**oint(UEP) are placed. To determine if a point is stable or not one method is to linearise the system equation around the EP and find the roots of the linearised characteristic equation at EP. If the roots lie on the left half of the complex plane (LHP) then the equilibrium point is stable else unstable.

Another method is to assume an infinitesimal change in angle $\delta = \delta_s + \Delta\delta$ as the speed is zero at equilibrium point $\omega = 0$, system state is $(\delta_s + \Delta\delta, 0)$. Here ω and acceleration $\alpha = [P_m - P_e(\delta)]/M$ are both negative which causes δ to decrease with time, resultant torque pull the system towards δ_s. Similarly at point δ_u system state is same but the acceleration $\alpha = [P_m - P_e(\delta)]/M$ and ω are both positive, forcing the system angle to move away from δ_u, making it an unstable point.

2.4.5 Equal-area stability criterion

The stability condition explained before can also be proved using equal-area criteria under the power-angle curve. Figure 2.6 is a pre-fault configuration of a machine connected to an infinite bus through two parallel loss-less lines, P_{e1}^{max} is pre-fault maximum

electrical output given by

$$P_{e1}^{max} = \frac{|E||V_\infty|}{X_g + X_l}$$

$X_g = X'_d$, $X_g + X_l$ is the net reactance between machine and infinite bus.

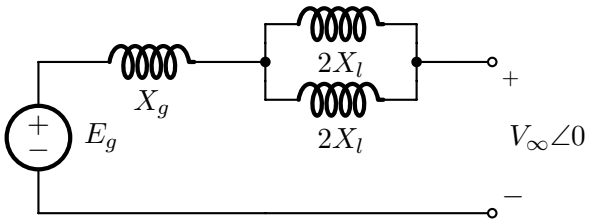

FIGURE 2.6: Per-fault configuration of SMIB

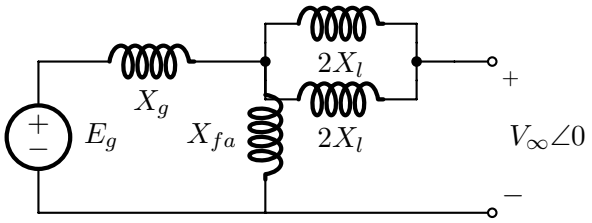

FIGURE 2.7: on-fault configuration of SMIB

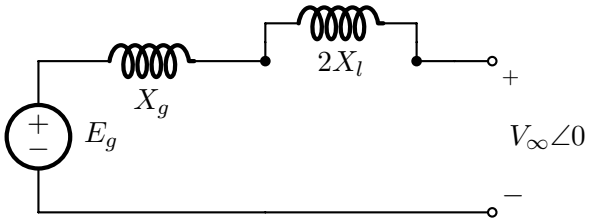

FIGURE 2.8: post-fault configuration of SMIB

Fig. 2.7 is the configuration upon severe fault on transmission line. Maximum electrical output during fault (P_{e2}^{max}) can be obtained using delta-star conversion of admittance

$$P_{e2}^{max} = \frac{X_{fa}|E||V_\infty|}{X_l X_{fa} + X_l X_g + X_g X_{fa}}$$

X_{fa} is fault impedance, let a transmission line be removed in clearing a fault, post-fault configuration is shown in Fig. 2.8 and post-fault maximum electrical output P_{e3}^{max} is given by equation

$$P_{e3}^{max} = \frac{|E||V_\infty|}{X_g + 2X_l}$$

In Fig. 2.9 shown are power-angle curves of pre, on and post-fault configurations and even the direction in which system is moving. Angle, speed and acceleration at several points on power-angle curves are summarised in the table below.

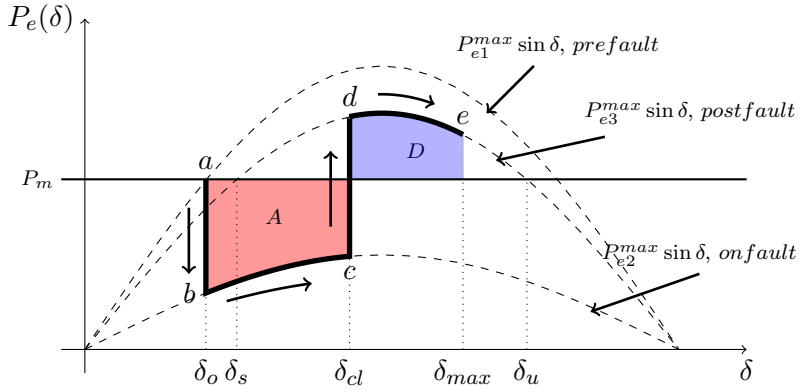

FIGURE 2.9: Equal area criterion under power-angle curve

Curve	Point	$\alpha = P_m - P_e$	ω	δ
pre-fault	a	$= 0$	0	δ_o
on-fault	b	> 0	0	δ_o
	c	> 0	ω_{cl}	δ_{cl}
post-fault	d	< 0	ω_{cl}	δ_{cl}
	e	< 0	0	δ_{max}

Note whenever speed is 0 it is in reference to synchronous speed. Here δ_{max} is such that the decelerating area D is equal to accelerating area A. This can be proven with swing equation Eq. (2.10) multiplied by ω on both sides to give

$$M\omega\frac{d\omega}{dt} = [P_m - P_e(\delta)]\frac{d\delta}{dt}$$

and intergrating within limits δ and δ_{max}

$$\int_{\omega(\delta_o)}^{\omega(\delta_{max})} M\omega\, d\omega = \int_{\delta_o}^{\delta_{max}} [P_m - P_e(\delta)]\, d\delta$$

we know that speed is 0 at δ_o and δ_{max}, so

$$0 = \int_{\delta_o}^{\delta_{max}} [P_m - P_e(\delta)]\, d\delta$$

This integral can be spilt at δ_{cl} fault clearing angle into two area, also electrical output equation changes at δ_{cl}, thus

$$\int_{\delta_o}^{\delta_{cl}} [P_m - P_{e2}^{max} \sin\delta]\, d\delta = \int_{\delta_{cl}}^{\delta_{max}} [P_{e3}^{max} \sin\delta - P_m]\, d\delta$$

This relation is basically establising equal area criterian ($A = D$). After the fault is removed, as its a loss-less system, post-fault configuration still satisfies the equal area criteria.

Although ω is zero at point **e**, system will keep moving due to inertia until it reaches point **g**, that is where the kinetic energy(KE) of the system becomes zero and at the same it gains PE. This can be explained using figure Fig. 2.10 also called extended equal area criterion. When the system reaches point **e** speed is 0 so is KE and also point **e** is

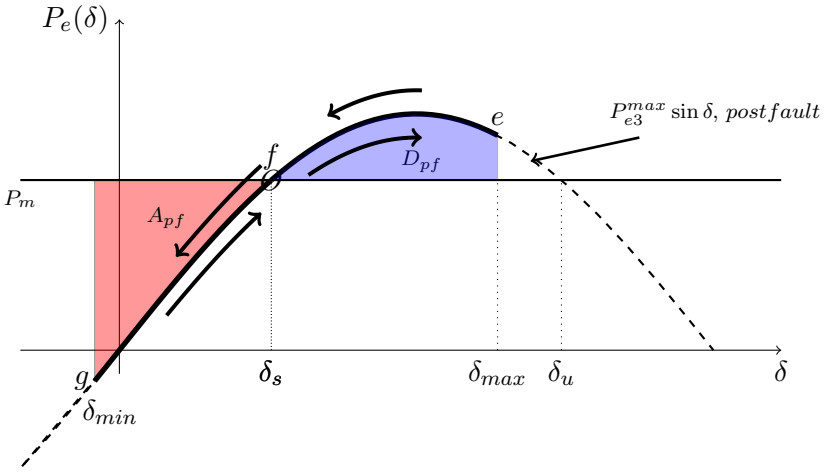

FIGURE 2.10: Acceleration and deceleration areas of post-fault system

an angle away from equilibrium attaining maximum PE, at this point **e** $P_m \neq P_e$, thus $\alpha < 0$, pulling system towards post fault SEP (δ_s).

At δ_s point **f**, although $\alpha = 0$ rotor is still spinning and has attained maximum speed $-\omega_{max}$ hence with maximum KE, which is also transient PE ($\delta = \delta_s$) at this point has completely converted to KE. Machine will now tend to move beyond point **f** losing KE and simultaneously gaining PE ($\delta \neq \delta_s$) until reaches point **g** (δ_{min}) system KE is completely converted to maximum PE, at point **g** $D_{pf} = A_{pf}$ satisfying equal-area criterion. As per present loss-less undamped model, the system will oscillate forever between points **e** and **g**.

2.4.6 Transient energy function from equal-area criterion

The equal-area criterion is established in previous section, now this criterion can be used to show that total energy as sum of kinetic and potential energy terms

$$V(\delta, \omega) = V_{pe}(\delta) + V_{ke}(\omega), \tag{2.13}$$

Potential energy $V_{pe}(\delta)$ is function of displacement and KE of speed, $V_{ke} = \frac{1}{2}M\omega^2$ and for a loss-less system rate of change of total energy (dV/dt) is zero.

$$0 = \dot{V}_{pe} + \dot{V}_{ke}$$

well know that $\dot{V}_{ke} = M\omega\dot{\omega}$, so it makes $\dot{V}_{pe} = -M\omega\dot{\omega}$ on simplification it yields to

$$dV_{pe}(\delta) = -M\dot{\omega}d\delta$$

and on substituting $M\dot{\omega}$ in acceleration Eq. (2.10) we obtain

$$dV_{pe}(\delta) = -[P_m - P_e(\delta)]\, d\delta$$

from power angle curve we learned that transient PE is gained by sytem on moving from point δ_s to δ and it is equal to area between P_m and P_e, and integrate PE differential equation from limits δ_s to δ.

$$\int_{V_{pe(\delta_s)}}^{V_{pe(\delta)}} dV_{pe(\delta)} = -\int_{\delta_s}^{\delta} [P_m - P_e(\delta)]d\delta$$

$V_{pe} = 0$ at δ_s

$$V_{pe}(\delta) = -\int_{\delta_s}^{\delta} [P_m - P_e(\delta)]d\delta \tag{2.14}$$

P_e here is $P_{e3}^{max} \sin\delta$ upon integration and applying limits, we get

$$V_{pe}(\delta) = -[P_m(\delta - \delta_s) - P_{e3}^{max}(-\cos\delta + \cos\delta_s)]$$

We need to obtain maximum value of this PE for post-fault configuration beyond which the system is unstable, it is obvious from what we derived before that if δ goes beyond δ_u the system is unstable thus providing a limiting condition on δ and energy $V_{pe}(\delta_u)$. The injected transient energy (KE+PE) due to fault or in other terms the transient energy gained by the post-fault system should be less than the maximum PE to remain stable. The equal-area criterion establishes that area $A = D$ when the system is stable. δ_{cl} is angle when fault is cleared, referring to Fig. 2.9 the accelerating area is given by Eq. (2.15)

$$A = \int_{\delta_o}^{\delta_{cl}} [P_m - P_{e3}^{max} \sin\delta]\, d\delta \tag{2.15}$$

and decelerating area by Eq. (2.16)

$$D = \int_{\delta_{cl}}^{\delta_{max}} [P_{e3}^{max} \sin\delta - P_m]\, d\delta \tag{2.16}$$

as mentioned earlier as per *equal-area stability criterion* necessary inequality for system to be transient stable is area $A <$ area D_{max} shown the same in Fig. 2.11. D_{max} is the area when upper limit for δ is δ_{max}, substituting this in Eq. (2.16) to yield

$$D_{max} = \int_{\delta_{cl}}^{\delta_u} [P_{e3}^{max} \sin\delta - P_m]\, d\delta$$

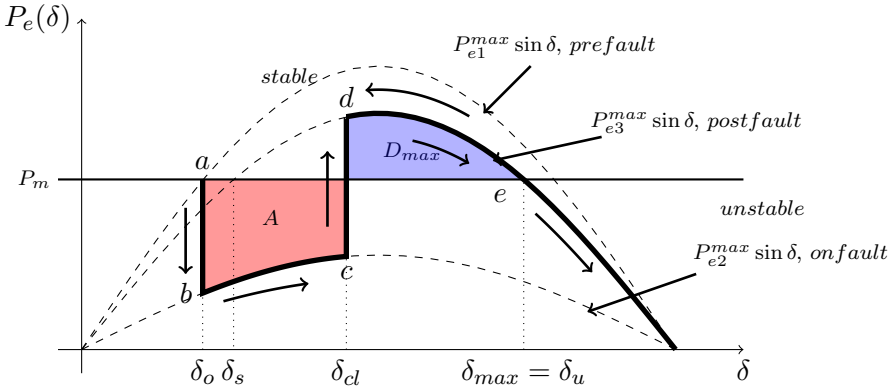

FIGURE 2.11: Critically stable condition

When $\delta_{max} = \delta_u$, area D is maximum such that system is critically stable, it can be seen from Fig. 2.11, we know that beyond point δ_u the system is unstable.

With the help of Fig. 2.12 the critical condition can be proved using areas under curve, that upon clearing of fault the net injected KE is are $A + C$ and PE is area post-fault area $(C + D_{max})$ which has got an upper limit for transient PE. From equal-area critical stability criterion we have $A < D_{max}$, adding area C on both sides will retain the same inequality condition

$$A + C < C + D_{max} \tag{2.17}$$

The accelerating area A is transient kinetic energy given by

$$A = \frac{1}{2} M \omega_{cl}^2 = V_{ke}(\omega_{cl})$$

ω_{cl} is the speed gained upon clearing fault. The transient PE at clearing time can be written from Eq. (2.14)

$$C = \int_{\delta_s}^{\delta_{cl}} -[P_m - P_{e3}^{max} \sin\delta]\, d\delta$$

$C = V_{pe}(\delta_{cl})$ and sum of areas $C + D_{max}$ is the transient PE at δ_u,$V_{pe}(\delta_u)$ for the post-fault configuration, giving rise to

$$C + D_{max} = \int_{\delta_s}^{\delta_u} -[P_m - P_{e3}^{max} \sin\delta]\, d\delta$$

from the inequality Eq. (2.17) we obtain the necessary condition for transient stability using energy function method

$$V_{ke}(\omega_{cl}) + V_{pe}(\delta_{cl}) < V_{pe}(\delta_u)$$

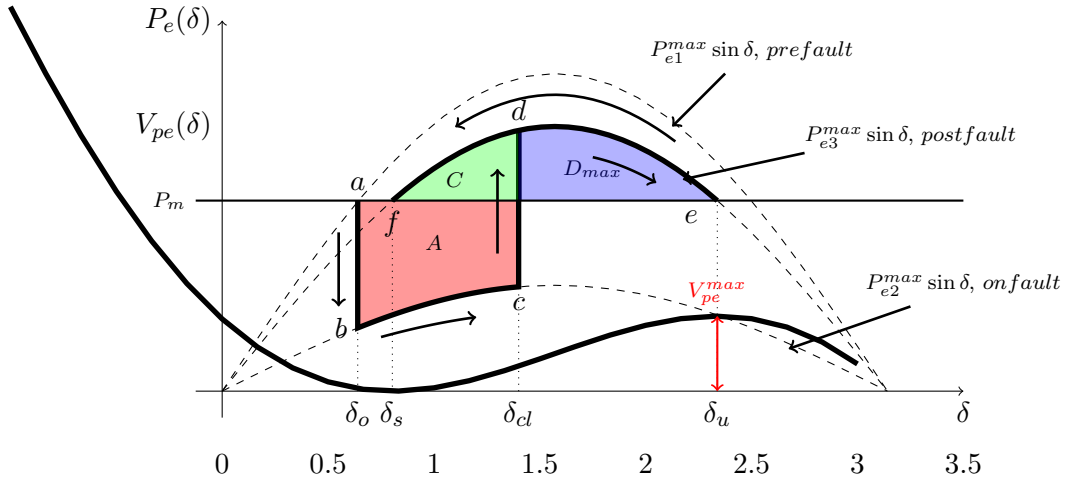

FIGURE 2.12: Power angle and Potential energy of SMIB

and this condition is satisfied during all period of post-fault duration.

2.4.7 Plotting phase plane trajectories

Figure 2.12 shows potential energy V_{pe} vs δ pertaining to Eq. (2.14) and superimposed on power angle-curves. The parameters (pu) of the system used to obtain this are the following: $P_{e1}^{max} = 3$ pre-fault, $P_{e2}^{max} = 1$ on-fault and $P_{e3}^{max} = 2.5$ post-fault

$P_m = 1.8$ p.u, $M = 0.2\text{MW s}^2/\text{MVA rad}$

using these parameters and $P_e(\delta) = P_{e3}^{max}\sin\delta$ from Eq. (2.12), we get $\delta_s = \sin^{-1}(1.8/2.5)$ and $\delta_u = \pi - \delta_s$

$$V_{pe}(\delta) = -\int_{\delta_s}^{\delta}[P_m - 2.5\sin\delta]d\delta, \frac{\text{MW rad}}{\text{MVA}} \tag{2.18}$$

$$V_{pe}(\delta)\Big|_{\delta_s}^{\delta} = -P_m(\delta - \delta_s) - P_{e3}^{max}(\cos\delta - \cos\delta_s)$$

Figure 2.12 shows V_{pe} projected over power angle curve, further computing for $\delta_s = 0.8038$ rad, $\delta_u = 2.3378$ rad and $V_{pe}(\delta_u)$ is $V_{pe}^{max} = 0.7087\,(\text{MW rad/MVA})$ being the local energy maxima, the second neighbouring energy maxima is found at angle $\delta_u - 2\pi = \delta_U$ (not shown in figure) with $V_{pe}(\delta_u - 2\pi) = 11.3097\,(\text{MW rad/MVA})$. Figure 2.13 shows family of trajectories of system with increment of fault duration by $0.4s$, the corresponding (δ, ω) for each fault duration is projected on equi-potential energy contour space provided by Eq. (2.14). Figure also shows the pre-fault SEP, fault and post-fault trajectories projected on transient energy contour map, it has increments of V_{pe} , the inner-most contour represents a level of 0.01, the second contour represents 0.2. the contour close to 0.7 energy level is the post-fault trajectory corresponding to critically

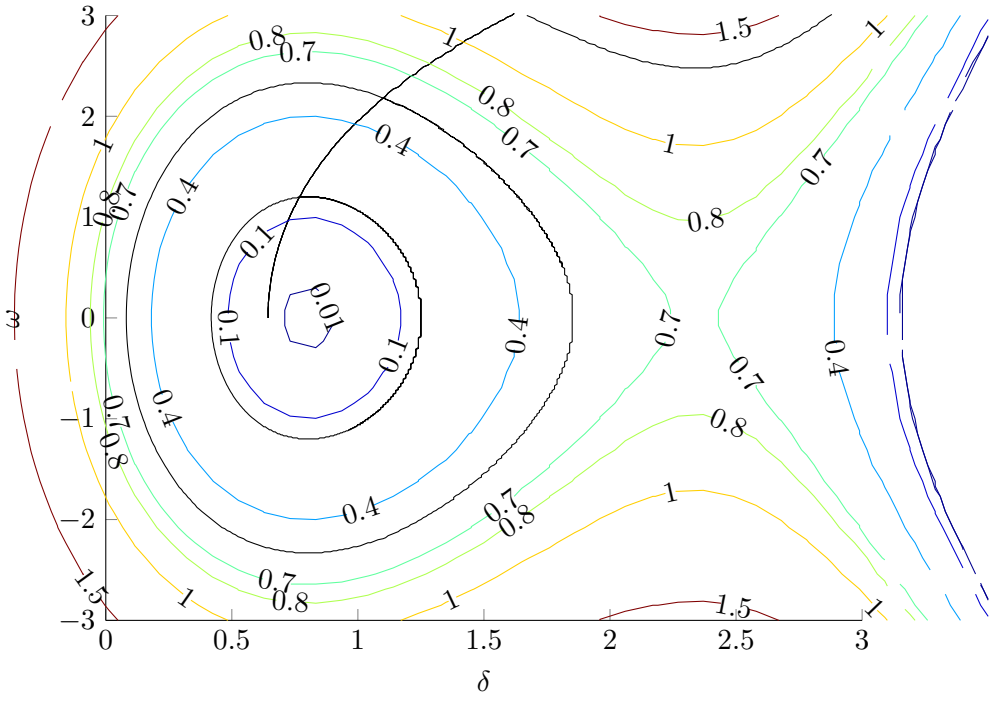

FIGURE 2.13: Phase plane trajectory with energy contour 2D

stable case, hypothetically this state moves towards $(\delta_u, 0)$ as $t^+ \to \infty$. An energy little less than this critical energy the system remains to be stable, little more will let the system go unstable. So a fault has to be cleared while total energy is less than $V_{pe}(\delta_u)$. Figure 2.14 is 3-D plot of the same Eq. (2.13) on δ and ω (phase plane). This equi-energy contour level plot is visualised as a energy well. It can be observed that the system has a local minima and when the system trajectory crosses the rim of the potential well the system will not return to SEP.

2.5 Energy function of multi-machine System

2.5.1 Power system representation

- The input power, P_m to all the machines in the system remains constant during the entire transient period. Time constants of the governors are considered large with respect to the period under study, damping power is neglected.
- Each machine is represented by direct axis transient reactance X'_d in series with a constant EMF, E_a.
- The rotor angles are measured with respect to axis rotating at synchronous speed ω_s or in COA formulation.
- Loads are represented as constant impedance, X_L.

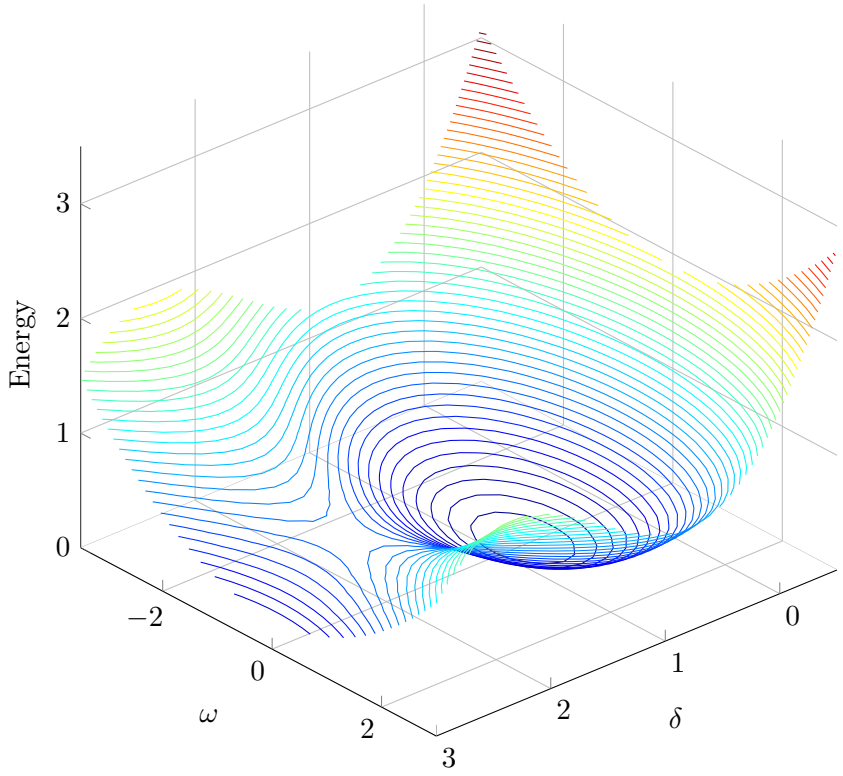

FIGURE 2.14: Energy well of SMIB

2.5.2 Network reduction to internal nodes

To obtain expression for electrical output at the machines internal nodes, the network has to be reduced to internal nodes[9, 29]. Following are few steps to reach an internal matrix Y_{int}.

1. consider a network with m machines, n buses and Y_{bus} is admittance matrix between buses. Initially a load flow solution is performed to obtain voltage information, this voltage information is required to create load admittance matrix Y_L.

$$Y_L(i) = -\frac{P_{load}(i) - jQ_{load}(i)}{V(i)^2}$$

2. Load Y_L is a diagonal matrix added to corresponding load bus locations and transient admittance at corresponding generator location of network bus matrix, giving rise to new bus matrix.

$$Y_{bus}^{new} = Y_{bus}(i,i) + Y_L(i) + y(i)$$

3. Y_{bus}^{new} is appended with machine transient admittance matrix y along with matrices Y_b, Y_c and Y_d to give rise to an augmented matrix Y_{aug} of order $(n+m) \times (n+m)$.

Y_{aug} includes all the original buses and the internal nodes. Y_{aug} is partitioned as following matrix:

$$Y_{aug} = \begin{bmatrix} Y_a & Y_b \\ Y_c & Y_{bus}^{new} \end{bmatrix}$$

Y_a is of order $(m \times m)$, Y_b is of order $(n \times m)$ and Y_c is of order $(m \times n)$

4. For a system reduced to generator nodes as shown in Fig. 2.15 with E as machine voltage, V internal bus voltages, following system of equations are formulated to obtain current from machines (I_{int})

$$\begin{bmatrix} I_{int} \\ 0 \end{bmatrix} = \begin{bmatrix} Y_a & Y_b \\ Y_c & Y_{bus}^{new} \end{bmatrix} \begin{bmatrix} E \\ V \end{bmatrix}$$

The augment matrix from above can be reduced further to internal nodes with "Kron reduction".

$$Y_{ij}^{new} = Y_{ij}^{old} - \frac{Y_{ik}Y_{kj}}{Y_{kk}}$$

This reduction technique eliminates all external nodes and network matrix is now reduced to internal nodes, the reduced matrix Y_{int} is of order $(n \times n)$. The new system equation is $\bar{I}_{int} = \bar{Y}_{int}\bar{E}$, an example in section 2.6 will help in understanding these steps

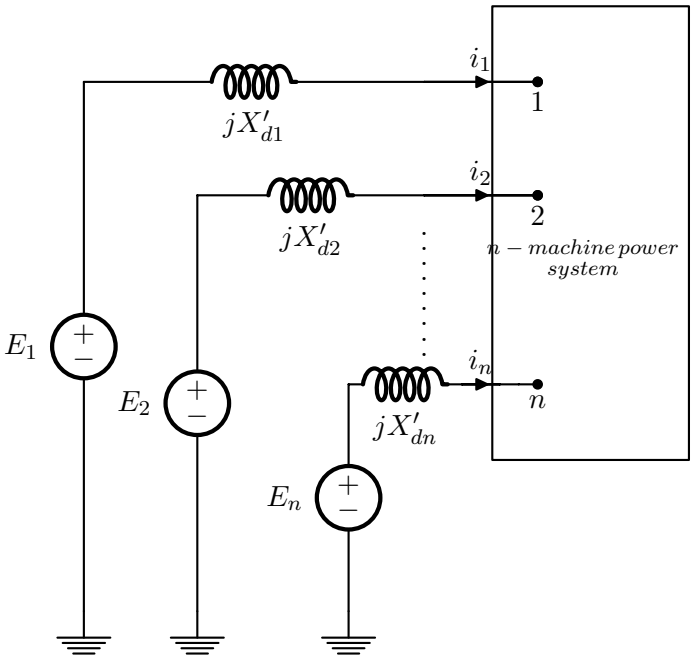

FIGURE 2.15: n-machine power system reduced to generator nodes

2.5.3 Electrical power of a machine in multi-machine system

An expression for electrical power at internal node i of a machine is obtained from the equation of complex power at node i, and is given by

$$P_{gi} + jQ_{gi} = E_i I_i^*, \text{pu} \tag{2.19}$$

I_i is current from machine i, is given by

$$I_i = \sum_{k=1}^{n} [G_{ik} + jB_{ik}E_k] \tag{2.20}$$

$G_{ik} + jB_{ik}$ is admittance between node i and k in reduced admittance matrix. Upon submitting Eq. (2.19) into Eq. (2.20) we obtain the apparent power from generator i as below

$$P_{gi} + jQ_{gi} = \sum_{k=1}^{n} (G_{ik} - jB_{ik})E_i E_k e^{j(\delta_i - \delta_k)} \tag{2.21}$$

separating above equation for real power from generator i gives rise to

$$P_{gi} = \sum_{k=1}^{n} \Big[B_{ik}E_i E_k \sin(\delta_i - \delta_k) + G_{ik}E_i E_k \cos(\delta_i - \delta_k) \Big] \tag{2.22}$$

or

$$P_{gi} = G_{ii}E_i^2 + \sum_{k=1,\neq i}^{n} \Big[B_{ik}E_i E_k \sin(\delta_i - \delta_k) + G_{ik}E_i E_k \cos(\delta_i - \delta_k) \Big] \tag{2.23}$$

$$\begin{aligned} C_{ik} &= B_{ik}E_i E_k, \quad D_{ik} = G_{ik}E_i E_k \\ P_{ei} &= \sum_{k=1,\neq i}^{n} \Big[C_{ik} \sin(\delta_i - \delta_k) + D_{ik} \cos(\delta_i - \delta_k) \Big] \end{aligned} \tag{2.24}$$

real power from generator i can also be written as

$$P_{gi} = G_{ii}E_i^2 + P_{ei} \tag{2.25}$$

2.5.4 Differential equations

The acceleration equation of machine i (2.10) written here for convenience

$$M_i \frac{d^2\delta_i}{dt^2} = P_{mi} - P_{gi},$$

replacing the sum of constant parameter P_{mi} and $G_{ii}E_i^2$ with $P_i = P_{mi} - G_{ii}E_i^2$ in above equation yields to

$$M_i \frac{d^2\delta_i}{dt^2} = P_{mi} - G_{ii}E_i^2 - P_{ei},$$

so the new swing equations for the system is

$$M_i \frac{d^2\delta_i}{dt^2} = P_i - P_{ei},\ i = 1, \dots n \tag{2.26}$$

Eq. (2.26) has n second-order differential equations, that can be split into a system with $2n$ first-order differential equations:

$$\begin{aligned} \frac{d\delta_i}{dt} &= \omega_i, \text{ rad/s} \\ \frac{d\omega_i}{dt} &= \frac{P_i - P_{ei}}{M_i}, \text{ rad/s}^2, \text{ for } i = 1, \dots n \end{aligned} \tag{2.27}$$

In the swing equations, angle differences are used instead of angles in respect to synchronous rotating frame, so $\delta_i - \delta_k$ is preferred, instead of using only δ_i. The number of state variables are now $2(n-1)$ instead of $2n$. In general there two formulations, in one formulation angles are in respect to a large machine as reference, and the other is centre of angle formulation [32]. COA is used from here on as it is convenient to perform transient stability assessment in relative to movement of group of generators, by subtracting the acceleration gained by weighted average of all machine from each machine.

2.5.5 Centre of angle formulation

Centre of angle (δ_o) of the system is the weighted average of the n machine angles corresponding to total inertia of the system [33].

$$M_T \delta_o = \sum_{i=1}^{n} M_i \delta_i \tag{2.28}$$

total inertia (M_T) is given my

$$M_T = \sum_{i=1}^{n} M_i$$

also centre of angle velocity as sum of weighted average

$$\dot{\delta}_o = \omega_o = \frac{1}{M_T} \sum_{i=1}^{n} M_i \omega_i$$

Thus the new angles with respect to centre of angle are

$$\tilde{\delta}_i = \delta_i - \delta_o = \theta_i$$

similarly angular velocity in COA frame is $\tilde{\omega}_i = \omega_i - \omega_o$. Dynamics of COA is obtained from Eq. (2.28) and so the power of COA is given as

$$M_T.\ddot{\delta}_o = \sum_{i=1}^{n} M_i.\ddot{\delta}_i$$

RHS of above is the sum of all n swing equations, which gives rise to

$$M_T.\ddot{\delta}_o = \sum_{i=1}^{n} P_i - \sum_{i=1}^{n} P_{ei} \tag{2.29}$$

or simply as

$$M_T.\ddot{\delta}_o = \sum_{i=1}^{n} P_{mi} - \sum_{i=1}^{n} P_{gi}$$

which is equal to sum of mechanical input power minus sum of electrical power output of each generator. Simplification of Eq. 2.29 gives rise to power of COA as shown below

$$P_{COA} = \sum_{i=1}^{n} P_i - 2\sum_{i=1}^{n-1}\sum_{j=i+1}^{n} D_{ij}\cos\tilde{\delta}_{ij} \tag{2.30}$$

using above condition, state equations written in COA as below

$$\begin{aligned} \frac{d\theta_i}{dt} = \frac{d\tilde{\delta}_i}{dt} &= \tilde{\omega}_i, \text{ rad/s} \\ \frac{d\tilde{\omega}_i}{dt} &= \frac{P_i - P_{ei}}{M_i} - \frac{P_{COA}}{M_T}, \text{ rad/s}^2, \text{ for } i = 1, \ldots n-1 \end{aligned} \tag{2.31}$$

from COA relation of Eq. (2.28) and angles with respect to COA we obtain the following identity

$$\begin{aligned} M_i\theta_i &= M_i\delta_i - M_i\delta_o \\ \sum_{i=1}^{n} M_i\theta_i &= \sum_{i=1}^{n} M_i\delta_i - \sum_{i=1}^{n} M_i\delta_o = 0 \end{aligned} \tag{2.32}$$

from identity Eq. (2.32) we can get n^{th} machine θ_n and ω_n from following equations

$$\theta_n = -\frac{1}{M_n}\sum_{i=1}^{n-1} M_i\theta_i, \quad \omega_n = -\frac{1}{M_n}\sum_{i=1}^{n-1} M_i\omega_i$$

redefining the angle subspace as

$$\hat{\theta} = \begin{bmatrix} \theta_1 & \theta_2 & \dots & \theta_{n-1} \end{bmatrix}^T$$

and the angular velocity subspace as

$$\hat{\tilde{\omega}} = \begin{bmatrix} \omega_1 & \omega_2 & \dots & \omega_{n-1} \end{bmatrix}^T$$

the new state vector in COA is the following vector:

$$\hat{x} = \begin{bmatrix} \hat{\theta} \\ \hat{\tilde{\omega}} \end{bmatrix}$$

2.5.6 Transient energy in centre of angle formulation

Acceleration equation in COA, given by Eq. 2.31 can be rewritten for acceleration power as

$$M_i \dot{\tilde{\omega}}_i = P_i - P_{ei} - \frac{M_i}{M_T} P_{COA} = f_i(\theta) \tag{2.33}$$

Similar to derivation of energy of a machine in Eq. 2.14, The transient energy V_i for a machine defined for post-fault system can be obtained by multiplying relative acceleration ($M_i \dot{\tilde{\omega}}$) or f_i to its corresponding velocity ($\tilde{\omega}_i$) and integrating with respect to time from a lower limit SEP (θ_i^s) to a variable upper limit as follows

$$\dot{V}_i = [M_i \dot{\tilde{\omega}}_i - f_i(\theta)]\tilde{\omega}_i$$

$$\int \frac{dV_i}{dt} dt = \int_0^{\tilde{\omega}_i} M_i \frac{d\tilde{\omega}_i}{dt} \tilde{\omega}_i dt - \int_{\theta_i^s}^{\theta_i} f_i(\theta) \frac{d\theta_i}{dt} dt$$

$$V_i(\theta, \tilde{\omega}) = \frac{1}{2} M_i \tilde{\omega}_i^2 - \int_{\theta_i^s}^{\theta_i} f_i(\theta) d\theta_i \, , \; i = 1, \dots, n \tag{2.34}$$

Summing up of these individual machine energy function, will provide the total system energy function [34].

$$\begin{aligned} V(\theta, \tilde{\omega}) &= \frac{1}{2} \sum_{i=1}^{n} M_i \tilde{\omega}_i^2 - \sum_{i=1}^{n} \int_{\theta_i^s}^{\theta_i} f_i(\theta) d\theta_i \\ &= \frac{1}{2} \sum_{i=1}^{n} M_i \tilde{\omega}_i^2 - \sum_{i=1}^{n} P_i(\theta_i - \theta_i^s) \\ &- \sum_{i=1}^{n-1} \sum_{j=i+1}^{n} \left[C_{ij}(\cos\theta_{ij} - \cos\theta_{ij}^s) - \int_{\theta_i^s + \theta_j^s}^{\theta_i + \theta_j} D_{ij} \cos\theta_{ij} \, d(\theta_i + \theta_j) \right] \\ V(\theta, \tilde{\omega}) &= V_{ke}(\tilde{\omega}) + V_{pe}(\theta) \end{aligned} \tag{2.35}$$

$$V_d(\theta) = \sum_{i=1}^{n-1} \sum_{j=i+1}^{n} \int_{\theta_i^s+\theta_j^s}^{\theta_i+\theta_j} D_{ij} \cos\theta_{ij} d(\theta_i + \theta_j)$$

The last term of (2.35) denoted by $V_d(\theta)$ is a path dependent term. Which can be evaluated using trapezoidal integration as

$$V_d(\theta) = \sum_{i=1}^{n-1} \sum_{j=i+1}^{n} I_{ij}$$

where at k^{th} step

$$I_{ij}(k) = I_{ij}(k-1) + \tfrac{1}{2} D_{ij} \left[\begin{array}{l} \cos\Big(\theta_i(k) - \theta_j(k)\Big) + \\ \cos\Big(\theta_i(k-1) - \theta_j(k-1)\Big) \end{array} \right] \times [\theta_i(k) + \theta_j(k) - \theta_i(k-1) - \theta_j(k-1)]$$

If the post-fault network is the same as the pre-fault network then $V_{pe}(\theta^o) = 0$, else this value has to be subtracted from the energy function,

$$V(\theta, \tilde{\omega}) = V_{ke}(\tilde{\omega}) + V_{pe}(\theta) - V_{pe}(\theta^o)$$

2.5.7 Network decomposition and aggregation

The concept of decomposition-aggregation method for stability analysis can be carried out when the system separates into more than two parts, based on the accelerations of the machines at $t = 0^+$ relative to the inertial accelerations, the machines are grouped in three categories: Machines with large relative acceleration, machines with little acceleration or deceleration and machines with large relative deceleration. Thus, we get three groups of machines. Each group can be combined into an equivalent machine resulting in a 3-machine 9-bus system. Sometimes, depending on the nature of the fault, one may not have either the accelerating or the decelerating machines so that we have just a 2-machine equivalent, reference [35] illustrates the method on a 7-machine system. A 2-machine equivalent with time varying parameters study is provided in reference [36]. The system reduction is explored in this chapter by identifying coherent generator groups on 39-bus 10-machine system. Literature on coherent generator groups and dynamic aggregation can be found in [37–40]. In the following section TSA on 3-machine 9-bus system, a fundamental network for multi-machine system is performed.

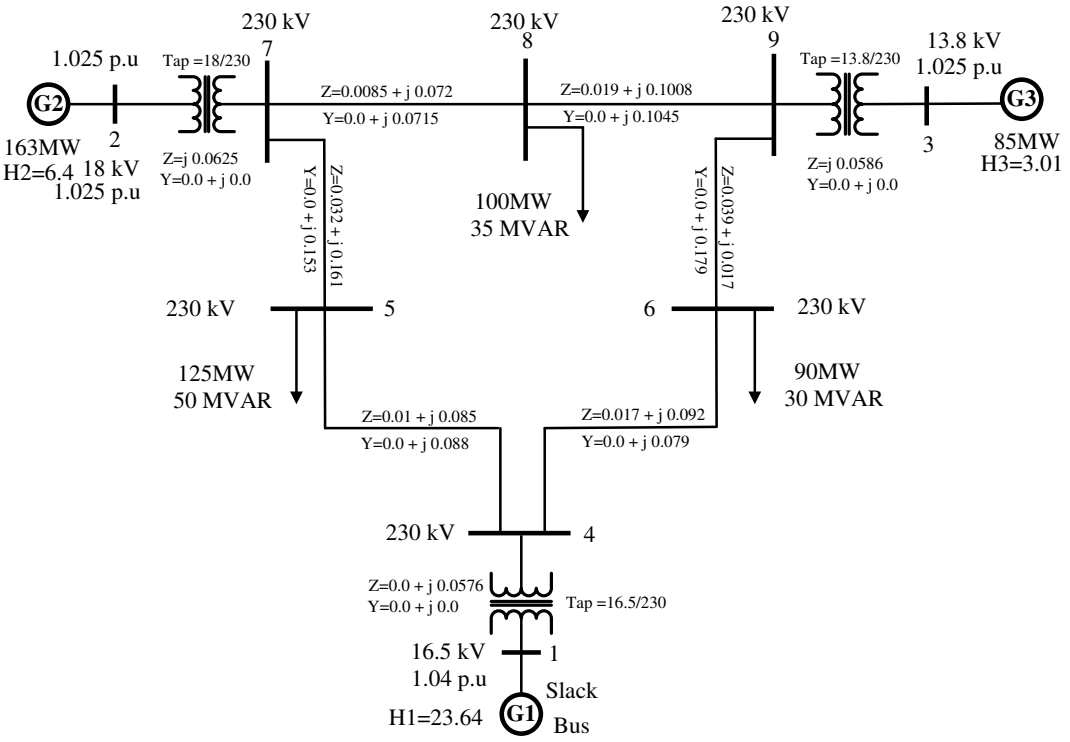

FIGURE 2.16: Three machine nine bus system

2.6 Analysis of three machine system

Figure 2.16 is the single line diagram of system on 100MVA base. It is a WSCC 3-machine, 9-bus system, following parameters of the system are used in time domain simulation performed by a program developed in MATLAB environment. Inertia H(in sec) of the three generators 1,2 and 3 are 23.64, 6.4 and 3.01 respectively. Direct axis transient reactance X'_d of the generators are 0.0608, 0.1198 and 0.1813 respectively. following are steps for TSA

1. Load flow solution for the pre-fault system.
2. For a specific contingency. Determination of transfer admittance matrix (Y_{int}), between internal buses of machines both for faulted and post-fault systems.
3. Determination of stable equilibrium state of post-fault system.
4. Forward step-by-step integration (swing curves) during pre-fault, on-fault and post-fault period.
5. Construct an Lyapunov function 'V', Eq. (2.35) for the post-fault system and derive its kinetic, potential and total energy components.
6. repeat from step 4 while incrementing the fault duration.

An example from [41] is re-investigated with MATLAB programs, this is based on the steps for obtaining critical switching time and $V_{pe}^{max}(\theta)$

TABLE 2.1: Load-Flow results for the WSCC 3-machine, 9-bus system

	bus	**Voltage (pu)**	P_g**(pu)**	Q_g**(pu)**	**-**P_l**(pu)**	**-**Q_l**(pu)**
1	Slack	$1.04\ \angle 0^o$	0.716	0.27	-	-
2	P-V	$1.025\ \angle 9.3^o$	1.63	0.067	-	-
3	P-Q	$1.025\ \angle 4.7^o$	0.85	-0.109	-	-
4	P-Q	$1.026\ \angle -2.2^o$	-	-	-	-
5	P-Q	$0.996\ \angle -4.0^o$	-	-	1.25	0.5
6	P-Q	$1.013\angle -3.7^o$	-	-	0.9	0.3
7	P-Q	$1.026\ \angle 3.7^o$	-	-	-	-
8	P-Q	$1.016\ \angle 0.7^o$	-	-	1.00	0.35
9	P-Q	$1.032\ \angle 2.0^o$	-	-	-	-

step 1: Obtain the load flow (Table 2.1)

step 2: Compute $\bar{I}_i = I_{di} + jI_{qi}$ as $\bar{I}_i = \frac{P_{gi} - jQ_{gi}}{V_i e^{-j\theta_i}}$

step 3: Compute $E_i\angle\delta_i (i = 1, 2, 3)$ as $E_i\angle\delta_i = V_i e^{j\theta_i} + jX'_{di}(I_{Di} + jI_{Qi})$

$$I_1 = \frac{0.716 - j0.27}{1.04\angle 0^\circ}, \quad E_1\angle\delta_1 = 1.04\angle 0^\circ + j0.068 \cdot I_1$$
$$I_2 = \frac{1.63 - j0.067}{1.025\angle -9.3^\circ}, \quad E_2\angle\delta_2 = 1.025\angle 9.3^\circ + j0.1198 \cdot I_2$$
$$I_3 = \frac{0.85 + j0.109}{1.025\angle -4.7^\circ}, \quad E_3\angle\delta_3 = 1.025\angle 4.7^\circ + j0.1813 \cdot I_3$$

step 4: After computation of initial conditions to obtain Y_{int}, an admittance matrix reduced to internal nodes. We start with forming a machine transient reactance admittance matrix

$$y = diag\left[\frac{1}{jX'_{di}}\right] i = 1, 2, 3$$

$$y = \begin{bmatrix} -j16.45 & 0 & 0 \\ 0 & -j8.35 & 0 \\ 0 & 0 & -j5.52 \end{bmatrix}$$

above matrix is added to load admittance matrix and bus admittance matrix to give rise to a new matrix

$$Y_{bus}^{new} = Y_{bus} + \begin{bmatrix} y & 0 \\ 0 & 0 \end{bmatrix} + \begin{bmatrix} y_{L1} & 0 & 0 \\ 0 & y_{L2} & 0 \\ 0 & 0 & y_{L3} \end{bmatrix}$$

Y_{bus} is the system matrix (9×9) with only line admittance between buses. The above matrix Y_{bus}^{new} is augmented with transient admittance to give rise to an augmented Y

matrix of structure preserving classical model

$$
Y_{aug} = \begin{array}{c} \\ 10 \\ 11 \\ 12 \\ \\ 1 \\ 2 \\ 3 \\ \\ 4 \\ \vdots \\ 9 \end{array}
\begin{array}{c}
\begin{array}{ccc} 10,11,12 & & 1,2,3 \end{array} \\
\left(\begin{array}{c|c|c}
 & & \\
y & -y & 0 \\
 & & \\
\hline
 & & \\
-y & & \\
 & & \\
\hline
 & & \\
0 & & \\
 & &
\end{array}\right.
\begin{array}{c} \\ \\ \\ \\ \\ \\ \\ \\ Y_{N2} \\ \\ \\ \end{array}
\left.\begin{array}{c} \\ \\ \\ \\ \\ \\ \\ \\ \\ \\ \\ \end{array}\right)
\end{array}
\begin{array}{c} 4\ldots 9 \\ \\ \\ \\ \\ \\ \\ \\ \\ \\ \\ \end{array}
$$

Y_{int} is obtained by eliminating nodes $1\ldots 9$

$$
Y_{int} = \begin{bmatrix} 0.8455 - j2.9883 & 0.2871 + j1.5129 & 0.2096 + j1.2256 \\ 0.2871 + j1.5129 & 0.4200 - j2.7239 & 0.2133 + j1.0879 \\ 0.2096 + j1.2256 & 0.2133 + j1.0879 & 0.2770 - j2.3681 \end{bmatrix}
$$

The initial rotor angles from *step 3* are $\delta_1(0) = 0.0442$ rad, $\delta_2(0) = 0.3447$ rad and $\delta_3(0) = 0.2304$ rad. The COA is calculated as $\delta_o = \frac{1}{M_T}\sum_{i=1}^{3} M_i\delta_i(0) = 0.1194$ rad, where $M_T = M_1 + M_2 + M_3$, Hence, we have $\theta_1(0) = \delta_1(0) - \delta_o = -0.0761$ rad, $\theta_2(0) = \delta_2(0) - \delta_o = 0.2278$ rad.

step 5: For a fault applied on bus 4, $V_4 = 0$. In Y^{new}_{aug} corresponding row and column are deleted and matrix is reduced to nodes $(10, 11, 12)$, this will obtain Y_{int} a matrix reduced to machine internal nodes for faulted system.

step 6: For a post-fault system Y_N is obtained by eliminating line 5-4, this Y_N is used to obtain Y_{int} as demonstrated in *step 4*.

step 7: As there is no loss of generation or power, Eq. (2.22) in COA is sufficient to arrive at post-fault SEP$(\theta_i, i = 1, 2)$ as $\theta_3 = -(1/M_3) \cdot (M_1 \cdot \theta_1 + M_2 \cdot \theta_2)$ and pre-fault rotor angles are used as initial guess.

step 8: Plot the rotor angle trajectory for this contingency of fault duration less than $0.31s$

step 9: Above step is repeated with an increment in fault duration until the system goes unstable.

It can be seen that, rotor angles and speed at end of fault duration are the initial angles and speed for post-fault system equations.

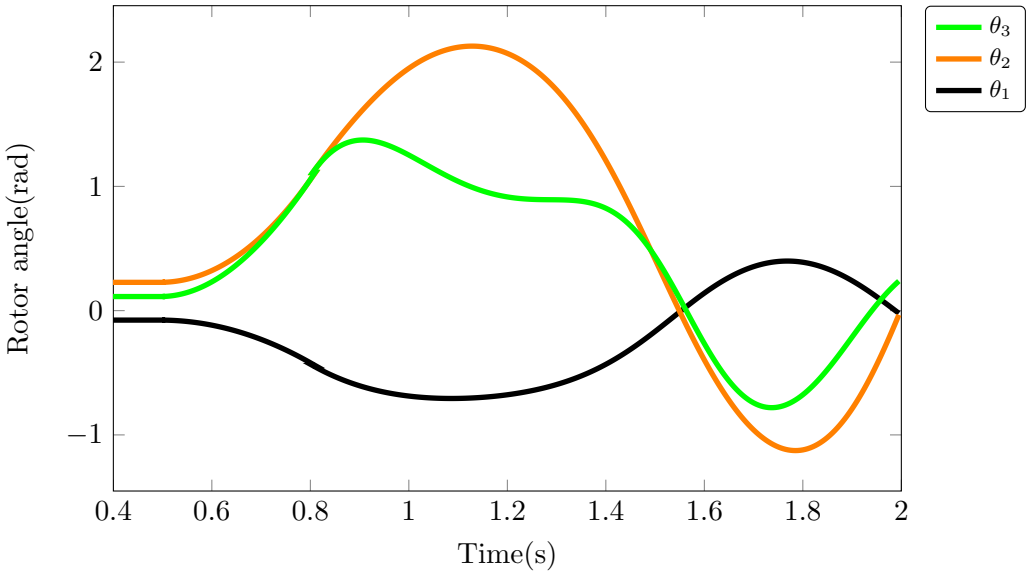

FIGURE 2.17: Rotor angle deviation for a fault on bus 4 for 0.31s and line 5-4 removed to clear fault

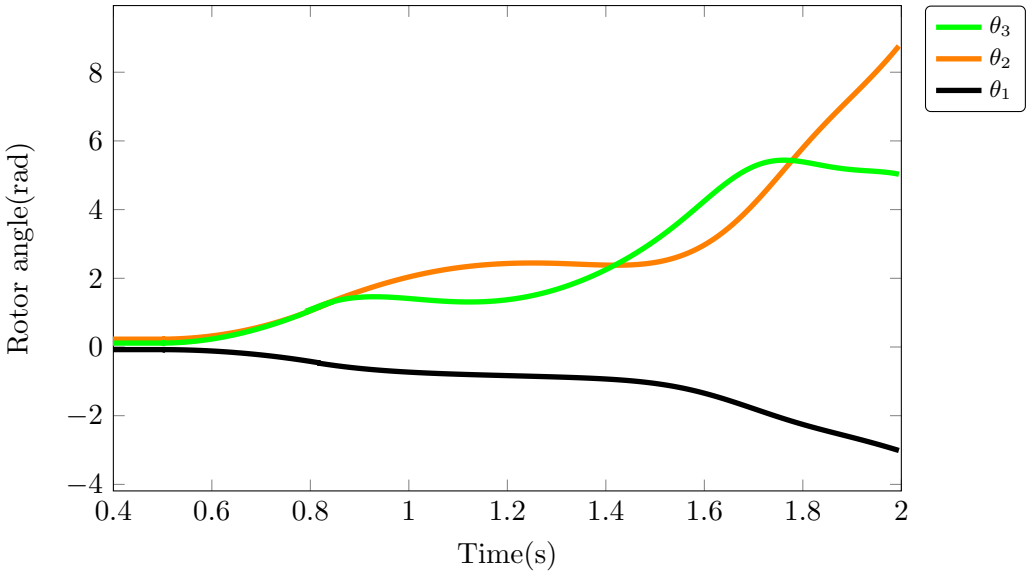

FIGURE 2.18: Rotor angle deviation for a fault on bus 4 for 0.32s and line 5-4 removed to clear fault

Critical clearing time is 0.31s for this fault scenario. Fig. 2.18 is unstable case and Fig. 2.19 is transient energy gained for clearing time of 0.31s.

Note: Energy function is not utilised here in finding the critical clearing time and energy function is always a derived quantity obtained from solved values of θ and $\tilde{\omega}$.

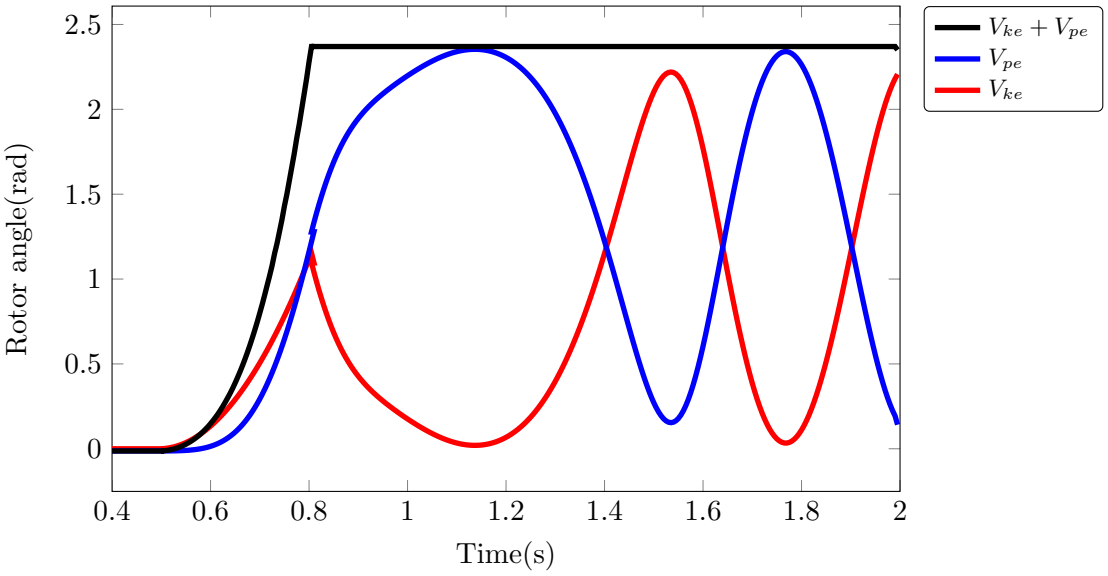

FIGURE 2.19: Transient energy gained by system from the fault

2.7 Coherent generator group identification

Extending the knowledge about "Network Decomposition and Aggregation" from section 2.5.7, in this section coherent generator groups are identified for certain contingencies. New England or 39-bus 10-machine system is the test system with 60 Hz synchronous frequency. The network consists of 10 synchronous generators, 46 transmission lines and is shown in Fig. 2.20. All the generators, lines and load parameters are provided in Appendix A[28]. This network has two bus voltage levels 345 kV and 13.8 kV. All generation (P-V) buses are at 13.8 kV except for bus 39 and bus 20 which are at 110 kV, bus 31 is considered 'Slack bus'. This network is subjected to various fault scenarios and for each fault scenario coherent group of generators are identified.

2.7.1 Test scenarios and results

The network shown in Fig. 2.20 is developed in DIgSILENT- Powerfactory. Simulations were carried to capture dynamic fault studies. Table 2.2 provides five fault conditions. Coherent groups are identified through graphical approach by observing the trajectory of rotor angle response when the system is subjected to a fault. In each case, the system exhibits critical unstable condition. The faults are three-phase short circuit faults. The fault location and fault duration are standard parameters to identify coherent groups. The coherent groups obtained from this study are compared with an established study [42]. Rotor angles are plotted for pre and post-fault duration of few seconds. However, only first swing curves of the generators are considered in identifying coherent generator groups. The generator labels in rotor angle response plot shown in Figure 2.21 are

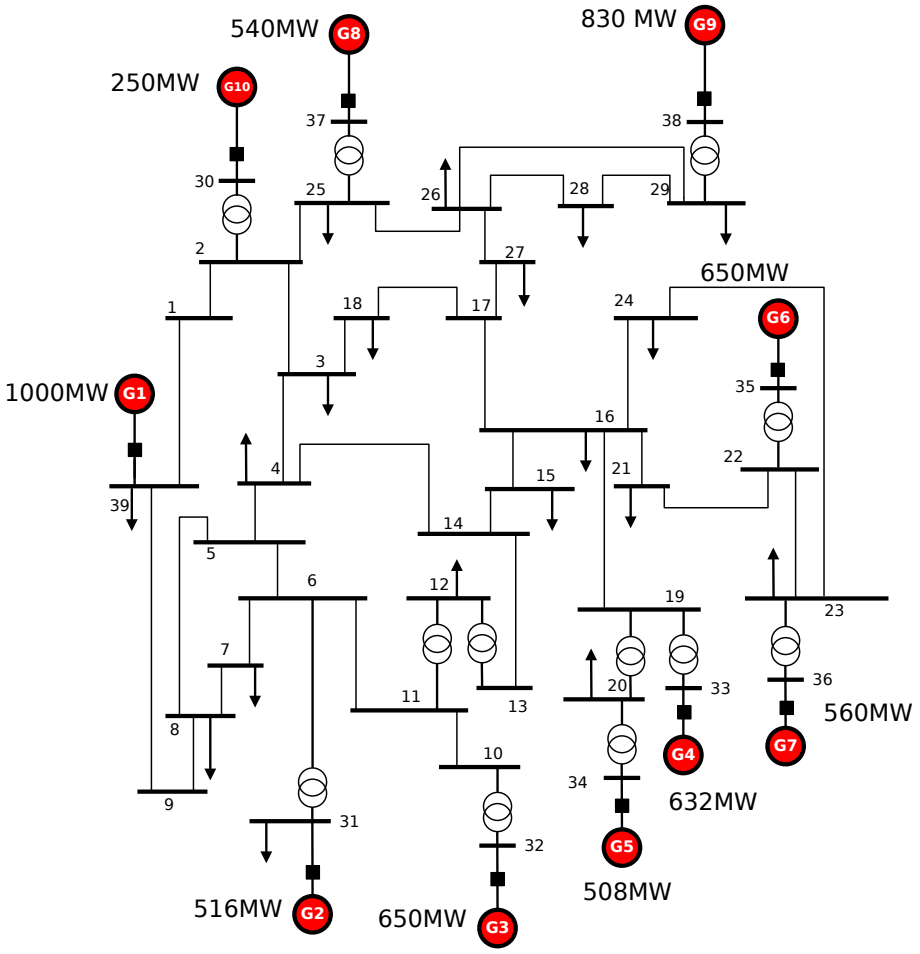

FIGURE 2.20: IEEE 10 generator 39 bus System

TABLE 2.2: Fault cases and coherent generator groups

Fault location bus	**Fault duration (ms)**	**Line removed**	**Coherent generator groups**
29	80	29-26	(33,34,35,36)
25	140	25-2	(33,34,35,36)
20	200	no line removed	(32,38)and(35,36)
31	240	no line removed	(30,32,33,34,35,36,37,38,39)
10	230	10-13	(30,33,36,37,38)

replaced with their bus numbers for convenience. For the first fault case, shown in Table 2.2 a three phase-short circuit fault is applied on bus 29 and fault is cleared after 0.08s along with removing line 29-26. Rotor angle responses obtained from simulations have different initial angular positions from reference in steady state, it is general practice to observe rotor angle deviations from large generator or slack bus, generator 2 at bus 31 here is considered as reference. Angle deviations are plotted in Fig. 2.21. It is observed that generator $33, 34, 35, 36$ form a coherent group. Table 2.2 summarizes coherent groups for other five fault contingencies applied.

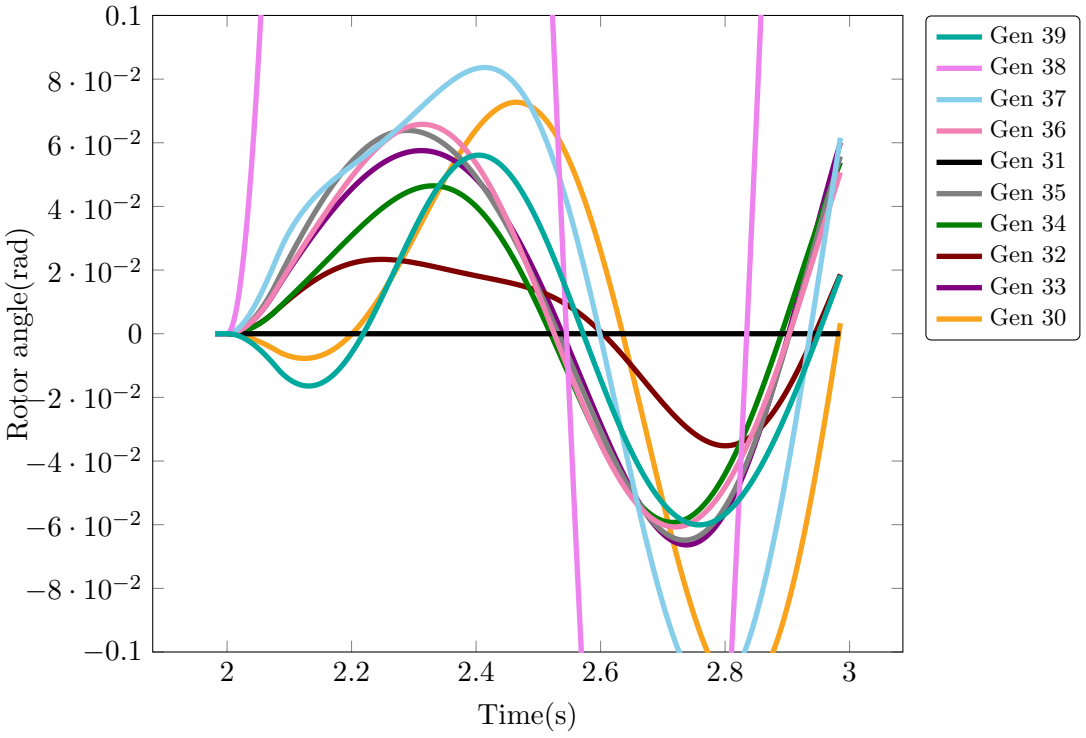

FIGURE 2.21: Swing curves for fault on bus 29, line 29-26 removed

2.8 Summary

In this chapter transient stability methods and analysis is comprehensively reviewed. General algorithm of obtaining CCT using energy function was provided. Disadvantages and challenges of direct methods were identified. Electrical output was derived for SMIB and its energy function was derived with the help of equal area criterion under power-angle curve which has also been demonstrated. Energy function for multi-machine system was derived in center of angle formulation. A brief introduction was provided for large network reduction and generation aggregation methods to support the scope of reducing large network into smaller set of machines and interconnecting buses. A 3-machine 9-bus system was analysed to obtain CCT using trial and error time-domain method and coherent generator groups were identified for a 39-bus 10-machine system.

The energy function derived in this chapter is extended in the sense of Lyapunov stability in the next chapter with the significance of equilibrium point and region of attraction being investigated.

Chapter 3

Stability theory applied to transient energy function method

3.1 Stability in the sense of Lyapunov

Lyapunov stability theory was named after Lyapunov, who laid foundation to the most important theorem in stability theory. The theory asserts the properties of equilibrium point without explicitly solving the ordinary differential equations describing the system [43–45], and this is commonly referred as "Spirit of Lyapunov". Lyapunov stability theorem provides sufficient conditions for Lyapunov stability and asymptotic stability. This theorem is been attractive for power system transient stability as it avoids time consuming complete time-domain simulation[46, 47]. Following sections provides an overview of fundamental Lyapunov function theorem.

Theorem 3.1: Lyapunov's stability [48, 49]

Let $\hat{x}$ be an equilibrium point of a non-linear dynamical system

$$\dot{x} = f(x) \tag{3.1}$$

where $f : \mathbb{R}^n \to \mathbb{R}^n$. Let $V : U \to \mathbb{R}$ be a continuous function defined in the neighbourhood of $\hat{x}$, differentiable on $U \to \hat{x}$ such that

(a) $V(\hat{x}) = 0$ and $V(x) > 0$ if $x \neq \hat{x}$, and $x \in U$.
(b) $\dot{V}(x) \leq 0$ in $U - \hat{x}$. then, $\hat{x}$ is stable, and if
(c) $\dot{V}(x) < 0$ in $U - \hat{x}$, then $\hat{x}$ is asymptotically stable.

As stated before Lyapunov function theory not only asserts the stability property of local equilibrium point. It also asserts that trajectories does not have any oscillatory

behaviour, complicated or bounded chaotic motion in the subset of the state space where Lyapunov function is defined. Lyapunov function theory only furnishes sufficient conditions, if for a particular Lyapunov function candidate V, if the required conditions of its derivative $\dot{V}$ are not met, stability condition of the equilibrium point cannot be determined.

Lyapunov stability can be defined as follows: If for a real number ϵ, there exists a positive real number $\delta(\epsilon)$ such that $||X_e - X_0|| < \delta$, implying $||X(t) - X_e|| < \epsilon$ for all $t \geq 0$ then point X_e is stable in the sense of Lyapunov. From theorem 3.1 a function $V(\hat{x})$ is called Lyapunov function if it satisfies both conditions (a) and (b), if it also satisfies condition (c), then it is strictly Lyapunov [50].

The fundamental drawback of Lyapunov direct method is that no systematic procedures exist to construct Lyapunov functions for non-linear systems. Therefore given a non-linear dynamical system for example a electrical or mechanical system, one has to rely upon intuition, trial and error, physical insight and some experience to arrive at an appropriate Lyapunov function. A number of methods and techniques facilitating the search of Lyapunov functions have been proposed in the literature [51–55]. The primary advantage of Lyapunov's method is, it avoids solving of post-fault differential equations in checking stability, in addition to determination of stability of equilibrium point, it is also possible to estimate the size of "basin of attraction" of an asymptotically stable equilibrium point.

A stable limit set L is said to be *Lyapunov stable* if, for each open neighbourhood A of L, there exists an open neighbourhood B of L, such that for all $x \in B$ and for all $t > 0$, $\phi(x) \in A$, else L is unstable. Similarly, a stable limit set L is *Asymptotically stable* if there exists an open neighbourhood B of L such that limit set of every point in B is L. Precisely, $\phi_t(x) \in B$ for $t > 0$ and $\phi_t(x) \to L$ as $t \to \infty$.

3.2 Region of stability

Considering a stable equilibrium point x_s, there exists a positive real number δ such that every point in the set is $||x_0 - x_s|| < \delta$, i.e., trajectories starting from x_0 converge to SEP x_s. $\phi_t(x_0) \to \hat{x}$ as $(t \to \infty)$. If δ is large, then $\hat{x}$ is a *global SEP*. There could be more then one SEP for physical system that are not global SEPs, to understand more on these SEPs a more useful concept *stability region* also called as *region of attraction* is helpful[48, 49]. Therefore stability region of a SEP x_s can be defined for all points x such that $\lim_{t\to\infty} \phi_t(x) \to x_s$ denoting stability region of x_s by $A(x_s)$

$$A(x_s) := \{x \in \mathbb{R}^n : \lim_{t\to\infty} \phi_t(x) = x_s\} \tag{3.2}$$

Stability region $A(x_s)$ is an invariant, open and connected set. *stability boundary*(also called as *separatrix*) of point x_s denoted as $\partial A(x_s)$ is boundary of stability region $A(x_s)$. An equilibrium point is hyperbolic if corresponding Jacobian matrix has no eigenvalues with a zero real part. In the next section unstable and stable manifold theorem for a hyperbolic equilibrium point is presented.

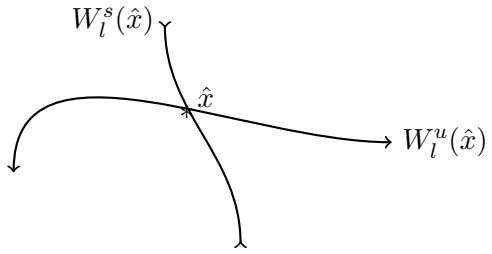

FIGURE 3.1: Stable and unstable manifolds of a local equilibrium point

3.2.1 Characterization of stability boundary

Concept of stable and unstable manifolds of limit sets is reviewed here. We start from the simplest limit set — the equilibrium point as shown in Fig. 3.1. Let $\hat{x}$ be an equilibrium point and $U \subset \mathbb{R}^n$ be a neighbourhood of $\hat{x}$. We define the local stable manifold of $\hat{x}$ as follows:

$$W_l^s(\hat{x}) := \{x \in U : \phi_t(x) \to \hat{x} \quad \text{as} \quad t \to \infty\}$$

The local unstable manifold of $\hat{x}$ is defined as

$$W_l^u(\hat{x}) := \{x \in U : \phi_t(x) \to \hat{x} \quad \text{as} \quad t \to -\infty\}$$

Note that $W_l^s(\hat{x})$ is a positive invariant set, while $W_l^u(\hat{x})$is a negative invariant set. They may not be manifolds when $\hat{x}$ is non-hyperbolic.

So stability boundary can be characterized for non-linear dynamic systems (3.1), where they have non-zero stability boundary, while the following three assumptions are made about its vector field:

1. On the stability boundary, all equilibrium points are hyperbolic in nature.
2. Transversality condition is satisfied by stable and unstable manifolds coming from these equilibrium points.
3. Trajectories originating on the stability boundary will approach towards one of the equilibrium points as $t \to \infty$.

Theorem 3.2: Characterization of the stability boundary [50] A non-linear dynamic system given by Eq. (3.1) satisfying above assumptions, where $x_i, i = 1, 2, \ldots$ are

the system unstable equilibrium points on stability boundary ∂A surrounding a SEP, and the SEP is described as $x_i \in \partial A$ if and only if $W^u(x_i) \cap A \neq \phi$ and $\partial A \supseteq \underset{i}{\cup} W^s(x_i)$, thus providing conditions for existence of equilibrium points on stability boundary ∂A. The theorem states the stability boundary is defined by union of stable manifolds of the UEPs that lie on the boundary.

3.2.2 Procedure to obtain stability boundary

A procedure to determine stability boundary $\partial A(x_s)$ of SEP belonging to a dynamic system of Eq. (3.1) satisfying above three assumptions, this procedure is arrived on *Theorem* 3.2 [56, 57]

1. Find all the equilibrium points of system, solution of $f(x) = 0$.
2. Identify the equilibrium points, whose unstable manifolds have trajectories which approach to SEP x_s. Next steps will walk through in identifying these equilibrium points.
3. Find the Jacobian at equilibrium point $\hat{x}$.
4. Find all the normalised, generalised unstable eigenvector of unit length from the Jacobian.
5. Find intersection of each of those normalized, generalized unstable eigenvectors (say, y_i) with in the boundary of ϵ. ϵ is like a ball of radius ϵ around the equilibrium point, the intersection points are $\hat{x} + \epsilon y_i$ and $\hat{x} - \epsilon y_i$.
6. Perform backward integration of this vector field from each of these intersection points for a specified time. If this trajectory remains inside the ball-ϵ, then proceed to next step. Else we repeat this step by reducing the value ϵ by $\alpha\epsilon$ and now the intersection points $\hat{x} \pm \epsilon y_i$ become $\hat{x} \pm \alpha\epsilon y_i$, and value of α is $0 < \alpha < 1$.
7. Again integrate backwards the vector field beginning from all the new intersection points.
8. Repeat above steps from 3 to 5. If any of the trajectories approach SEP x_s, then the EP point $\hat{x}$ is on stability boundary.
9. Finally, stability boundary of SEP x_s is the union of stable manifolds of equilibrium points identified in *step 2* above.

A one-dimensional stable manifold of EP, $\hat{x}$ can be found using above procedure. In a planar system, the equilibrium point on stability boundary is either a type-one equilibrium point or a type-two equilibrium point.

Definition: Type of equilibrium point (EP)
For a general non-linear system Eq. (3.1), having an EP 'p' is said hyperbolic, if the Jacobian of 'p' has no eigenvalues with zero real part. If all the eigenvalues of its Jacobian have negative real parts it is asymptotically SEP, else it is an UEP. The type

of hyperbolic EP 'p' is defined as the number of eigenvalues of ($\partial f/\partial x$, Jacobian) of (p) with positive real parts. If $J_f(p)$ has to have only '1' eigenvalue with a positive real part, we call 'p' as type-1 EP. Similarly, 'p' is called type 'k' EP if $J_f(p)$ has to be exactly 'k' eigenvalues with a positive real parts. Type-1 EPs play a dominant role in characterization of a stability boundary and a quasi-stability boundary, Type-1 EPs and SEPs are important equilibrium points.

3.3 Potential energy boundary surface method

In section-2.4.7, we found that two UEP points δ_u and $\pi - \delta_u$ surround a SEP δ_s, thus becoming zero-dimensional PEBS for a SMIB system. Also in section -2.4.7, it is found that for a SMIB critical energy $V_{cr} = V_{pe}(\delta_u)$ is the energy $V(\delta, \omega)$ evaluated at nearest equilibrium point $(\delta_u, 0)$. If the machine loses synchronism due to acceleration, equilibrium point δ_u is not only the nearest but also the relevant or controlling UEP for the system.

In multi-machine case, system may lose synchronism with one or more machines going unstable and it is dependent upon nature and location of fault. So each disturbance gives rise to a mode of instability (MOI), associated with each MOI is an UEP called the controlling UEP for that particular disturbance. In the case of multi-machine systems, the PEBS is quite complex in the rotor-angle space. Much theory and details on characterization of PEBS is provided in greater detail in references [27, 28, 32, 58–61].

Similar to SMIB, the concept of computing V_{cr} using PEBS method can be extended to multi-machine systems as follows, A number of UEPs surround a SEP of post-fault system, we know these points are mathematical solutions of system equation Eq. (3.3), starting from pre-fault SEP, if the faulted system is integrated and cleared critically then the post-fault trajectory approaches a particular UEP depending on the mode of instability. That UEP becomes the controlling UEP for that particular disturbance. The potential energy boundary surface therefore constitutes a multidimensional surface passing through the UEPs. PEBS method derived are based on heuristic arguments, complete theoretical justifications for PEBS method are still lacking except for SMIB.

In a multi-machine system PEBS can be visualised as a boundary of a multi-machine potential "well", analogous to the Fig. 2.14 belonging to SMIB case. For a 3-machine 9-bus system, one such "well" is shown in Fig. 3.3 where two axes being rotor angles θ_1 and θ_2 of two machines in COA frame. On vertical axis is the potential energy $V_{PE}(\theta)$ presented along with Equi-potential contours forming a surface and a a SEP surrounded by three UEP's U1,U2,U3 can also be seen. The line connecting these UEP's

is orthogonal to equi-potential curves and this line is the Potential energy boundary of surface. The system will be unstable if at the instant of fault-clearing the system state in angle space has crossed the PEBS, and if the fault is cleared early enough, then the post-fault trajectory in angle space will tend to return to equilibrium subsequently due to damping in the system. Thus T_{cr} is the maximum fault duration that can be sustained by the system such that the post-fault trajectory stays within the energy "well". The post-fault trajectory of the system for fault cleared at T_{cr} passes close to controlling UEPs and this condition is called "first swing" stable phenomenon.

Critical value of $V(\delta, \omega)$, is obtained by monitoring fault-on trajectory until it crosses PEBS at a point θ^*. In most cases the controlling UEP θ^u, is close to θ^*, such that $V_{pe}(\theta^u) and V_{pe} = V_{cr}$, thus providing an essence for use of PEBS method there by detection of PEBS crossing is essential. Also this point of crossing is approximately the point along which the faulted trajectory has $V_{pe}(\theta)$ maximum. Hence, V_{cr} can be taken to be equal to $V_{pe}^{max}(\theta)$ along the faulted trajectory. The PEBS crossing is also the point at which $f^T(\theta).(\theta - \theta^s) = 0$ [59]. $f_i(\theta)$ is at which $V_{pe}(\theta)$ is maximum has been shown to be true for a conservative system, an algorithm to determine PEBS is explained in following section.

PEBS method is a fast direct method as it avoids the need of determining controlling UEP[28]. For a given fault-on trajectory PEBS method is used to find a local approximation of relevant stability boundary of the original system model helping to perform direct transient stability analysis, Therefore PEBS method cannot always give conservative stability assessments results like controlling UEP method, it gives either overestimated or underestimated stability assessments. In this thesis focus is on understanding the effect of reduced inertia on power system transient stability not determining accurate critical clearing time, essentially PEBS is the tool for fast direct method for stability assessment.

3.3.1 PEBS derived by solving directional derivative of potential energy

As previously stated and derived, swing equation of machine i is given by the following equation

$$\begin{aligned} M_i\dot{\tilde{\omega}}_i &= P_i - P_{ei} - \frac{M_i}{M_T}P_{COA} = f_i(\theta) \\ \dot{\theta}_i &= \tilde{\omega}_i, \quad i = 1, ...n \end{aligned} \tag{3.3}$$

and transient energy function 'V' defined for the system (usually with post-fault system parameters) where all the changes are with respect to stable equilibrium point $(\theta^s, 0)$

$$\begin{aligned} V(\theta,\tilde{\omega}) &= \frac{1}{2}\sum_{i=1}^{n} M_i\tilde{\omega}_i^2 - \sum_{i=1}^{n} P_i(\theta_i - \theta_i^s) \\ &\quad - \sum_{i=1}^{n-1}\sum_{j=i+1}^{n}\left[C_{ij}(\cos\theta_{ij} - \cos\theta_{ij}^s) - \int_{\theta_i^s+\theta_j^s}^{\theta_i+\theta_j} D_{ij}\cos\theta_{ij}\, d(\theta_i+\theta_j)\right] \\ &= V_{KE}(\tilde{\omega}) + V_{PE}(\theta) \end{aligned} \tag{3.4}$$

where θ_i and $\tilde{\omega}_i$ are rotor angle and speed of i^{th} machine in COA formulation.

PEBS is obtained by setting the directional derivative of potential energy (ray emanating from the SEP) equal to zero. Further details of characterization of PEBS is provided in [62]. PEBS crossing is also an important aspect of procedure, it is approximately the point when V_{PE} is maximum along the faulted trajectory. With $f_i(\theta)$ accelerating power in the post-fault system PEBS crossing is the point at which

$$\sum_{i=1}^{n}\left[f_i^T(\theta)\cdot(\theta_i - \theta_i^s)\right] = 0 \tag{3.5}$$

Following are steps to compute T_{cr} and V_{cr} using PEBS method

1. Solve for post-fault SEP (θ_i^s) by solving Eq. (3.3) where $\tilde{\omega}_i = 0$
2. Compute fault–on trajectory with faulted system equations similar as Eq. (3.3)
3. Derive quantities

$$\sum_{i=1}^{n}\left[f_i^T(\theta)\cdot(\theta_i - \theta_i^s)\right] = f^T(\theta)\cdot(\theta - \theta^s)$$

   and $V_{pe}(\theta)$ at each time step. The parameters involved in obtaining $f_i(\theta)$ and $V_{pe}(\theta)$ are from post-fault system.

4. Continue steps 2 and 3 until $f^T(\theta)\cdot(\theta - \theta^s) \simeq 0$, this is the PEBS crossing and also $f^T(\theta)\cdot(\theta - \theta^s) < 0$ inside potential "well". At PEBS crossing, note the value $(t^*, \theta^*, \tilde{\omega}^*)$ and derive net $V_{PE}(\theta^*)$, this will provide an estimate of V_{cr} for the fault.
5. Finally from fault-on trajectory find when Eq. (3.4), $V(\theta,\tilde{\omega})$ is equal to above V_{cr}, this gives time is T_{cr}.

As mentioned before the PEBS is obtained by setting the directional derivative equal to zero. Therefore, PEBS is the angle subspace which satisfies

$$\sum_{i=1}^{n} f_i(\theta) \cdot (\theta - \theta_i^s) = 0$$

or the zero level contour of energy Eq. (3.6).

$$\sum_{i=1}^{n} \left[P_i - P_{ei}(\theta) - \frac{M_i}{M_T} P_{COA}(\theta) \right] \cdot (\theta - \theta_i^s) = 0 \tag{3.6}$$

3.3.2 PEBS represented as stability boundary of gradient System

PEBS is redefined as stability boundary of gradient system in infinite bus formulation [56]. State equation is rewritten as negative of potential energy gradient, following is state equation of the gradient system in reference to COA formulation

$$\frac{d\theta_i}{dt} = (P_i - P_{ei}) - \frac{M_i}{M_n}(P_n - P_{en}) \quad i = 1, 2, \ldots, n-1 \tag{3.7}$$

same as negative of potential energy gradient as below

$$-\frac{\partial V_{pe}(\theta)}{\partial \theta_i} = P_i - P_{ei}(\theta) - \frac{M_i}{M_n}[P_n - P_{en}(\theta)]$$

If the reference machine is an infinite bus, then

$$-\frac{\partial V_{pe}(\theta)}{\partial \theta_i} = P_i - P_{ei}(\theta)$$

In summary the stability boundary of the gradient system of n machines is the PEBS given by Eq. (3.7).

3.3.3 Athay's three machine system example

In this section, Athay's 3-machine system is used to illustrate the energy function approach to a multi-machine system [59]. Chapter 2 already provides details about the simulation. Athay 3-machine system shown in bit modified in parameters compared to 3-machine 9-bus system analysed so far. Table 3.1 provides system parameters.

The SEP angles, machine powers P_i, and voltages E_i of system are given below

i	j	C_{ij}	D_{ij}	H
1	2	1.3023	0.2180	10
1	3	3.0004	0.8052	15
2	3	7.2806	1.4865	60

TABLE 3.1: Athay Three machine system

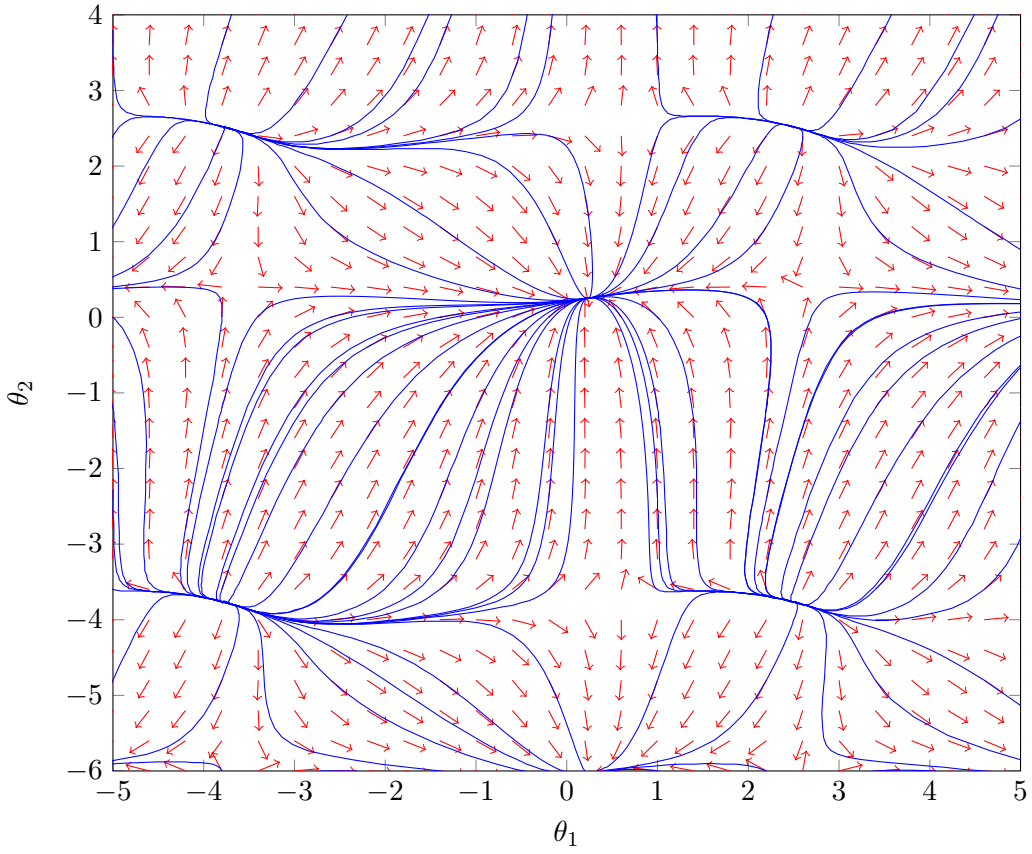

FIGURE 3.2: Vector field presentation of region of attraction-Athay three machine system

i	SEP	P_i	E_i
1	12.7827	1.6510	1.0736
2	13.4473	3.6167	1.0573
3	-5.4947	-2.6751	1.0530

3.3.4 Region of attraction of three machine system

Region of attraction of system can be understood by observing the energy surface and contours shown in three figures, Figure 3.3 is potential energy surface of Athay's model of three machine system, Figure 3.2 is phase portrait of region of attraction indicated

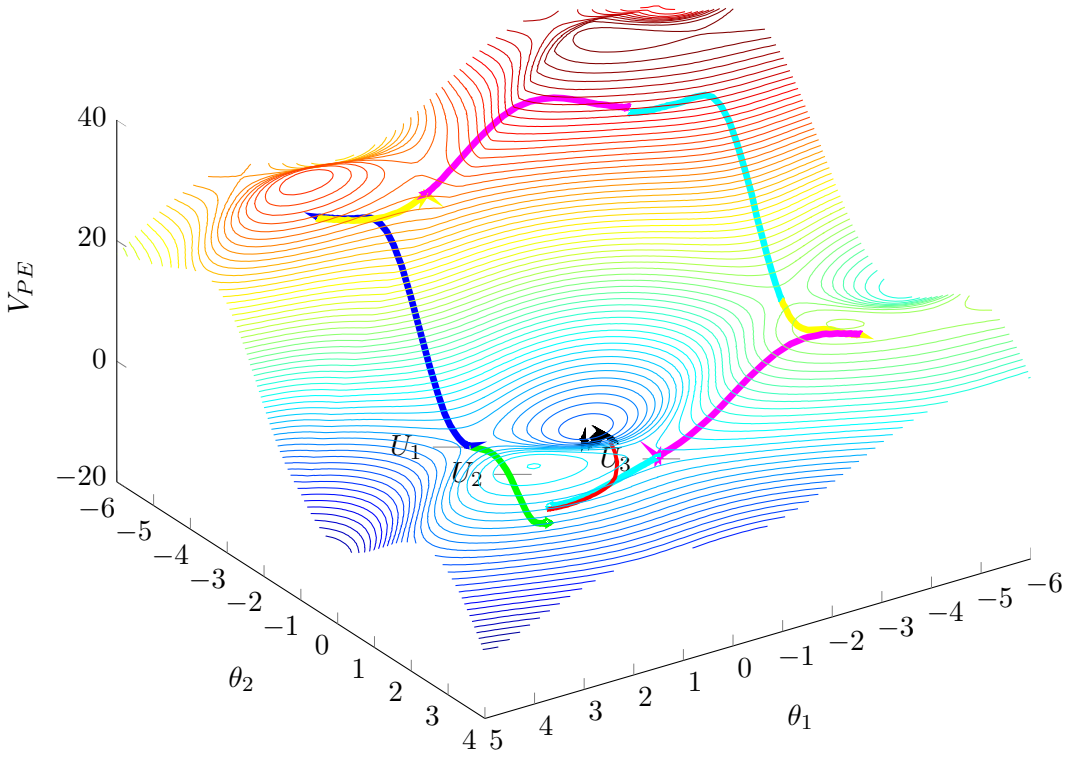

FIGURE 3.3: PEBS crossing plotted on potential energy surface

by vector fields and Fig. 3.4[1] provides information about stability boundary around a SEP. In section 3.2 we learned that stable manifold are set of state points, such that all trajectories starting from these states tend to approach EP on boundary upon forward integration, and similarly unstable manifolds trajectories approach towards EP upon backward integration[59].

Points on PEBS are actually the trace of trajectory in angle space until a local potential peak is encountered. Several peak points can be obtained form different trace directions, at the peak, trace of the tangent is orthogonal to surface. The contour map of the potential energy is shown in Fig. 3.4 and the region of attraction of reduced system given by Eq. 3.7. In three machine example we have seen that region of attraction of gradient system is orthogonal to equi-potential lines, and PEBS intersects the level surface $\delta : V_p(\delta) = c$ orthogonally [47].

Stability of a multi-machine system can be explained in simple terms using an analogy of rolling ball on potential energy surface, and the surface can be visualised as a multi-dimensional bowl[41]. A ball initially at rest and at the bottom of the bowl is said to be at SEP state and at this state PE is minimum or zero. Upon disturbance, Kinetic energy is imparted on the ball resulting in the ball to move upwards and gain PE as

[1]Fig. 3.4 is different from Fig. 2.13 there axis were δ and ω

moving towards the edge of the bowl to escape the surface. The rim of the bowl can be considered as PEBS. The rim of the bowl need not be even and can have several saddle points on structure as type-1 UEPs, hence all UEPs have different PE levels. The UEP with lowest energy is called the closest UEP with respect to SEP, closest UEP is considered to define the region of stability and this consideration can offer conservative results, calculation of all UEPs is challenging and oftern few approximations are often made in estimating UEP.

3.3.5 Transient stability analysis with Controlling UEP method

In Controlling UEP method, critical energy is determined at controlling UEP x_{co}, $V_{cr} = V(x_{co})$ where x_{co} is the type-1 UEP with respect to a fault-on trajectory, this UEP is lying on the stability boundary and whose stable manifold is intersected by fault-on trajectory. If energy V at the time of fault clearing is less than $V(x_{co})$, the post fault system is stable. Determination of correct CUEP for a fault-on trajectory is important to avoid over estimate or under estimate of stability and its determination is complex.

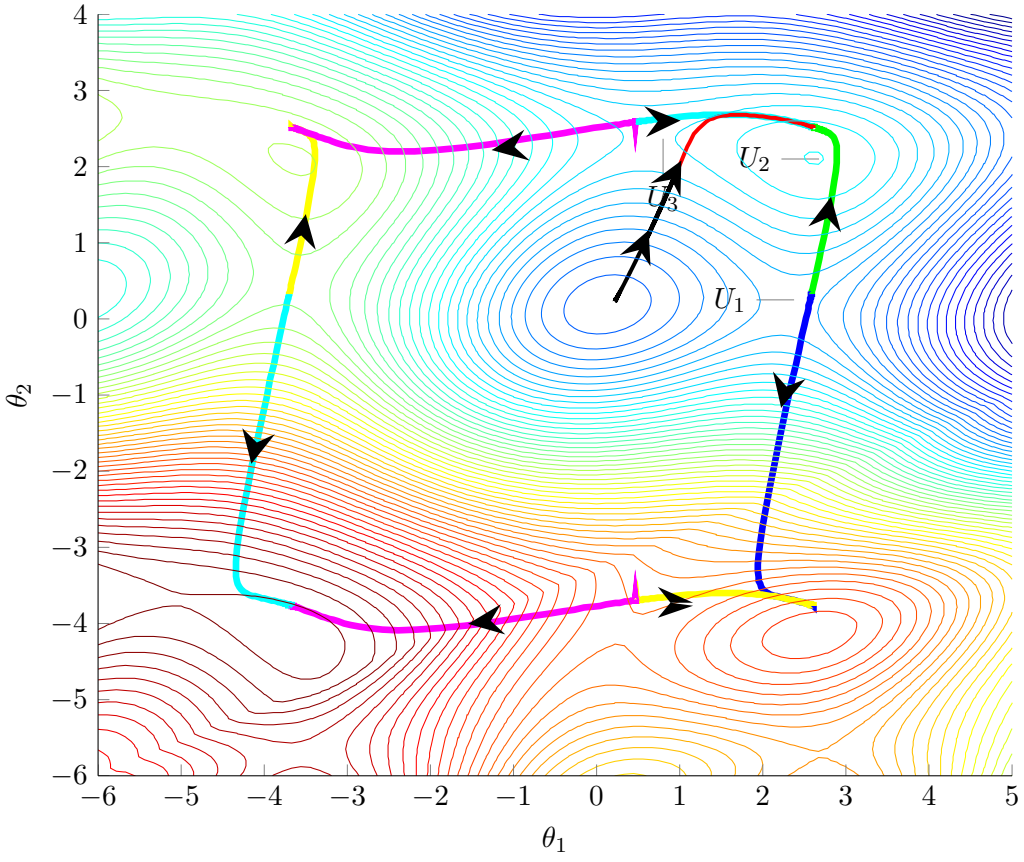

FIGURE 3.4: PEBS as intersection of stable manifolds on energy contour

Mode of disturbance (MOD)[27] and BCU method sometimes also called exit point method are two prominent methods to determine Controlling UEP.

3.3.6 BCU method to find controlling UEP

Boundary of stability region-based controlling unstable equilibrium point - BCU method was proposed by Chiang et al. [57]. This method explores the relationship defined between the stability boundary of post-fault classical system model and stability boundary of post-fault reduced system model as given below

$$\dot{\theta} = f(\theta) \tag{3.8}$$

The state variables of this reduced system are only rotor angles thus it is only has n dimensions, while the original system is of $2n$ dimension (n angle and n speed). $(\hat{\theta})$ is an EP on boundary of the reduced system defined by Eq .3.8 if and only if EP $(\hat{\theta}, 0)$ is on stability boundary of the original system. BCU method involves following steps to determine controlling UEP:

step 1 From fault-on trajectory $(\theta(t), \omega(t))$ detect the exit point θ^*, point where the projected trajectory $\theta(t)$ exits the stability boundary of reduced system. This exit point corresponds to the point at which first local maximum of V_{PE} is reached.

step 2 Using point θ^* as initial condition integrate the post-fault reduced system of Eq. (3.8) to determine first local minimum of

$$\sum_{i=1}^{n} |f_i(\theta)|$$

say it gives θ_o^*

step 3 Using point θ_o^* as initial guess solve

$$\sum_{i=1}^{n} |f_i(\theta)|$$

say it gives θ_{co}^*

Controlling UEP of the original system can now be given by $x_u = (\theta_{co}^*, 0)$. It can be seen that BCU method tries to relate the controlling UEP of the reduced system to controlling UEP of original system relative to a fault-on trajectory. Controlling UEP of the reduced system is easy to compute as it is defined only in angle space.

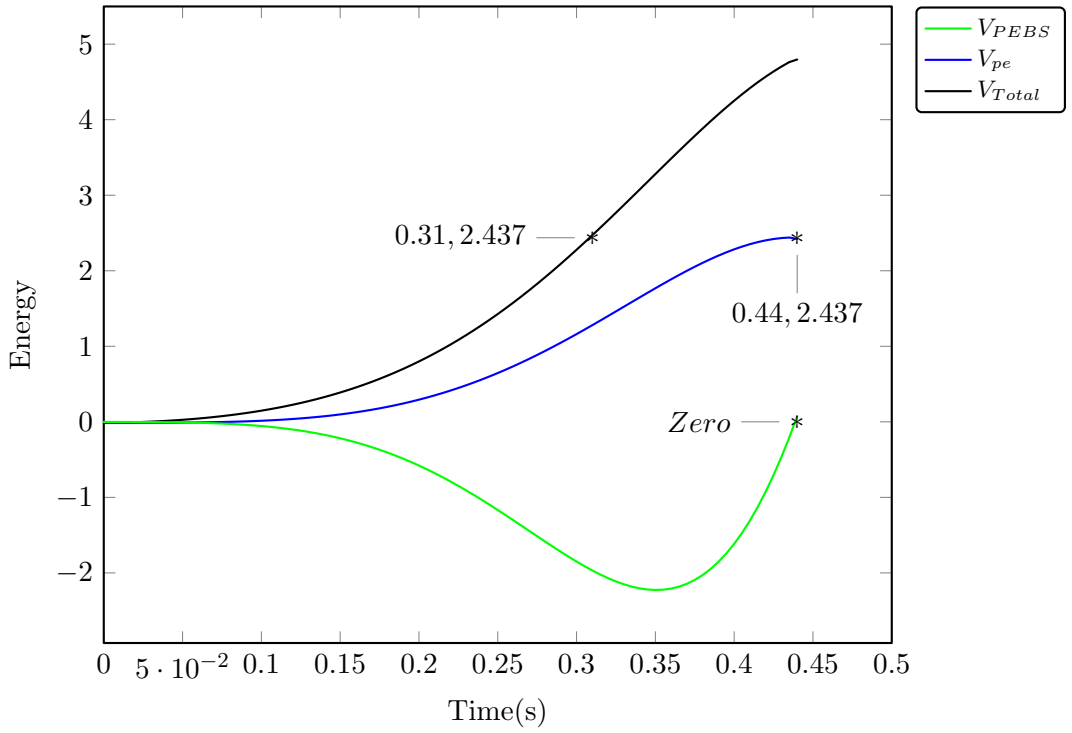

FIGURE 3.5: PEBS method for determination of CCT and critical energy for fault applied on bus 4 and line 5-4 removed

3.4 Critical clearing time and critical energy using PEBS method

Figure 3.5 shows the energy (p.u) of the system when a fault is applied on bus 4 and is cleared by removing line 5-4. Note that the fault is applied until PEBS zero crossing is achieved. The potential energy at zero crossing is 2.4705, this is the critical energy of the system, and the system total energy reaches this critical energy at $0.31s$, this obtained CCT validates the time-domain based result shown in Fig. 2.17 and 2.18. Table 3.2 summarizes all the contingencies run on the system along with CCTs and V_{cr} values obtained using this PEBS method.

3.5 Summary

In this chapter stability was explained in the sense of Lyapunov function theory. Theorem and algorithm to obtain stability boundary as intersection of manifolds is provided. Algorithm for obtaining CCT and critical energy using PEBS method has been developed. Region of attraction is demonstrated on Athay 3- machine system. Algorithm to obtain EP using CUEP and BCU methods was also provided. It is shown that PEBS

TABLE 3.2: CCT and critical energy using PEBS method for various fault scenarios

Faulted bus	**Line removed**	**CCT(s)**	**Critical energy**
7	7-5	0.1800	1.2478
7	8-7	0.2000	1.8480
5	7-5	0.3150	1.0276
5	5-4	0.4050	2.3819
4	4-6	0.3100	2.4734
4	5-4	0.3100	2.4705
9	6-9	0.2400	2.1020
9	9-8	0.2400	2.7247
8	9-8	0.3200	2.9796
8	8-7	0.3150	2.8198
6	4-6	0.4450	2.4317
6	6-9	0.3850	1.3426

is a stability boundary of gradient system. PEBS method was explored on 3-machine 9-bus system to obtain CCT and critical energy for nine type of contingencies.

3-machine 9-bus system based analysis using PEBS method demonstrated in this chapter will be performed over a wide range of inertia values of machine 2 and 3 to obtain a family of CCT curves in next chapter.

Chapter 4

PEBS method with reduced inertia

Time domain method to obtain CCT for SMIB and multi-machine has been discussed in Chapter 2. These outputs have been verified using PEBS in chapter 3. In this chapter we will provide the analysis which has never been attempted before i.e. towards focusing on inertia parameter using time-domain and PEBS method.

In this chapter, using PEBS method TSA is performed on several inertia combinations to understand the impact of reduced inertia of machines in TSA, with SMIB and 3-machine 9-bus system. A new method is introduced which represents CCT contour lines projected on inertia space. The inertia space is the neighboring inertia values of the two machines in 3-machine 9-bus network with one machine anchored. Similarly critical energy is obtained using PEBS method and projected as equi-potential contour lines over inertia space.

4.1 Effects of varying inertia on transient stability of SMIB system

The effects of variations of inertia on transient stability is studied considering an example of SMIB system. Mechanical power input $P_m = 1$, moment of inertia $M = 0.2$, pre-fault maximum electrical output is $P_e^{max} = 2$ and on-fault electrical output is $P_{e-fault}^{max} = 1$. pre-fault and post-fault electrical output is same.

As CCT (T_{cr}) of the system is the duration of fault applied, upon which the system would gain energy $V(\delta, \omega) = V_{cr}$, given by Eq. 4.2. t is the fault duration variable

and T_{cl} denotes the time when the fault is cleared just before the system goes unstable. If $t \leq T_{cl}$, the energy along the faulted trajectory is less than the critical energy i.e., $V(\delta, \omega) \leq V_{cr}$ and T_{cl} can be obtained from double integrating acceleration equation is given below [29].

$$t_{cl} = \sqrt{\frac{2M}{P_a}(\delta - \delta_0)} \tag{4.1}$$

δ is δ_{cl} the machine angle when fault is cleared and $\delta_0 = \delta_s$(post-fault SEP). Clearing angle δ_{cl} can also be obtained from equal area criterion identity [9].

Configuration of post-fault system is assumed to be same as pre-fault. Critical energy V_{cr} for the post-fault configuration beyond which system goes unstable, is obtained from Eq. 4.2 value is 1.3697 and $\delta_s = \sin^{-1}(1/2) = 0.5236$. This critical energy (1.3697) is reached when fault lasts for $1.4850s$, then $\delta = (3.14 - 0.5235)rad = \delta_u$. Fig. 4.1 provides an illustration of pre-fault, on-fault and post-fault speed deviation against angle for a fault applied for $1.40s$ and $1.5s$ with $M = 0.2$.

$$V_{cr} = -P_m(\pi - 2\delta_s) + 2P_e^{max}\cos\delta_s \tag{4.2}$$

In Fig. 4.3 is the angle deviation for a fault applied for 1.40 and $1.5s$ with inertia

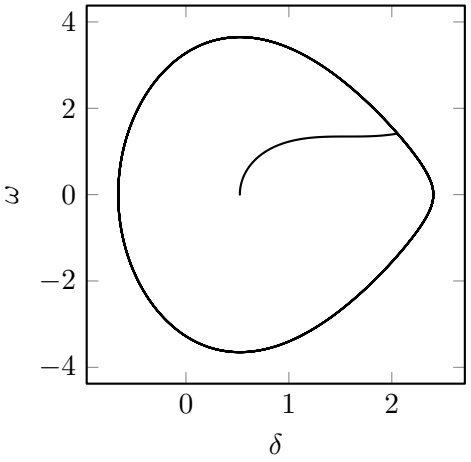

FIGURE 4.1: Angle and speed deviation when $M = 0.2$, fault of 1.45s

$M = 0.5$. We can see system is stable for $1.50s$ fault duration, with much less speed deviation compered to when $M = 0.2$. To demonstrate further, the effect of inertia on T_{cr}, it is computed for range of values of inertia, as shown in Fig. 4.5 it is observed that as inertia increases so does the T_{cr} increase. It can be inferred that, the fault duration could be increased without letting system go unstable if the machine has higher inertia.

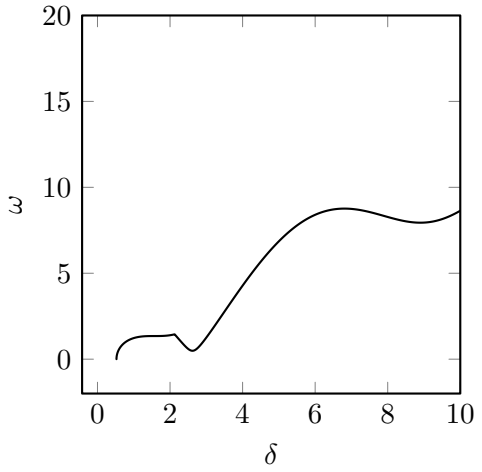

FIGURE 4.2: Angle and speed deviation when $M = 0.2$, fault of 1.50s

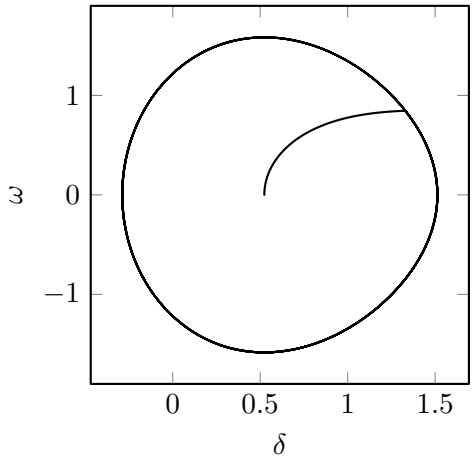

FIGURE 4.3: Angle and speed deviation when $M = 0.5$, fault of 1.45s

4.2 Three machine nine bus system PEBS case study with varying inertia

Note that in earlier studies of load flow, the windfarms are assumed to be present at load bus. This assumption is valid for low level of penetration. However, this assumption often give misleading results with increasing level of penetration, further details on this is provided in section 5.3.1. In this thesis, the windfarms are represented as conventional synchronous machines (can be referred as pseudo synchronous machine) at the generation buses, much details provides in next chapter, The effects of increasing wind energy penetration are factored by reducing the inertia of the pseudo synchronous machines. Simulations are carried by fixing inertia of machine 1 at 23.64s and varying inertia of other two machines 2&3 for a range of values of inertia to reflect penetration levels of wind energy. T_{cr} and corresponding V_{cr} are calculated as given in section 3.3.1.

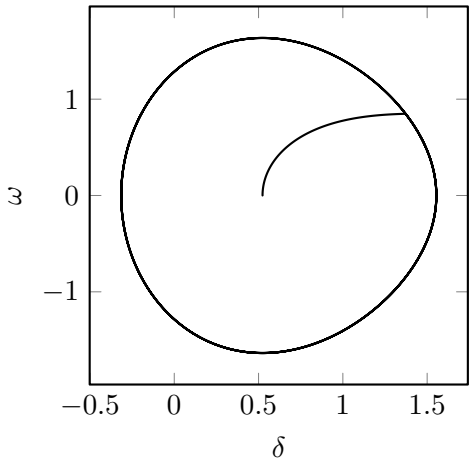

FIGURE 4.4: Angle and speed deviation when $M = 0.5$, fault of 1.50s

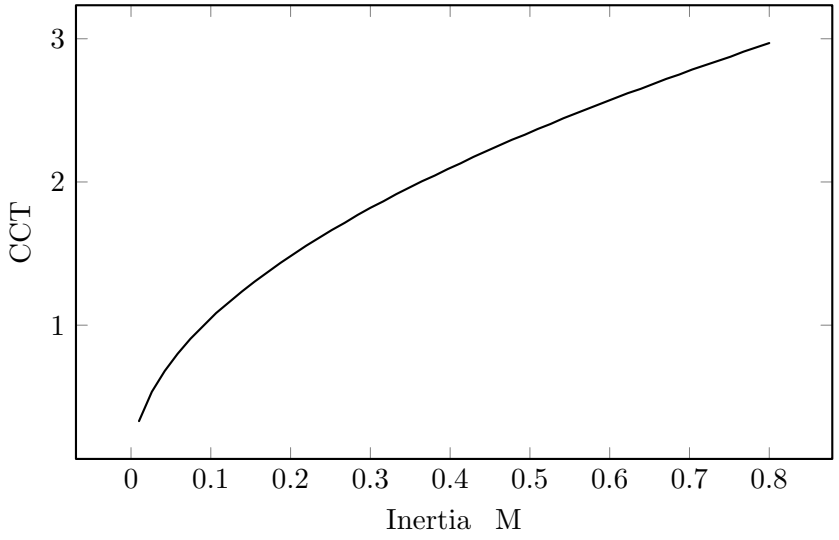

FIGURE 4.5: CCT of a SMIB against varying inertia, at $V_{cr} = 1.3697$

Results of this investigation on varying inertia of two machines are presented by plotting equi-CCT contours over inertia space. Note that this plot essentially shows the set of combinations of inertias (H2 and H3) that return the same CCT, with inertia of machine 1 fixed to 23.64. CCT contours are computed for various fault scenarios, Fig. 4.6[2] shows results for a typical scenario i.e., when a three phase short circuit fault is applied at bus 6 and cleared by removing line $6-9$. In Fig. 4.6, inertia of machine 2 and 3 of original system are marked with thick lines. Fig. 4.7 shows equi-critical energy contours for this fault scenario. Fig. 4.6 are the neighboring lines of $T_{cr} = 0.385$s (Table 5.4). At 'A' T_{cr} is 0.385s. If the inertia of machine 2 is reduced to a value corresponding to point 'B' while keeping the inertia of machine 3 unchanged, T_{cr} will reduce to 0.350s. To maintain T_{cr} of 0.385s of the system, inertia of machine 3 has to be increased to a value corresponding to point 'C'. This suggests that reducing inertia of one of the machines

[2]Fig. 4.6 different from Fig. 3.4, there axis are angles θ_2 and θ_3

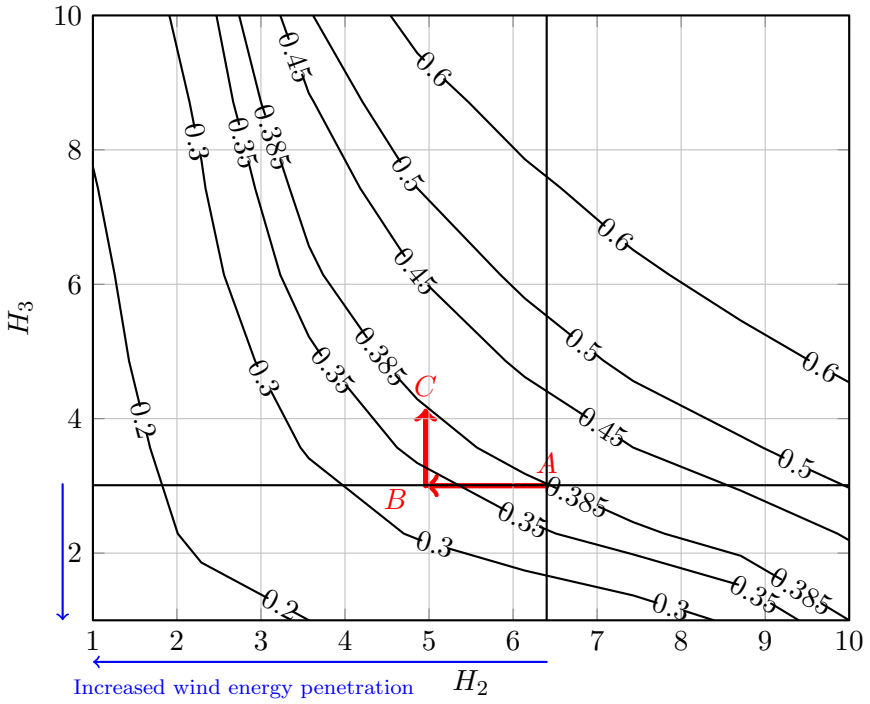

FIGURE 4.6: CCT lines for a fault applied on bus 6 and line 6-9 removed

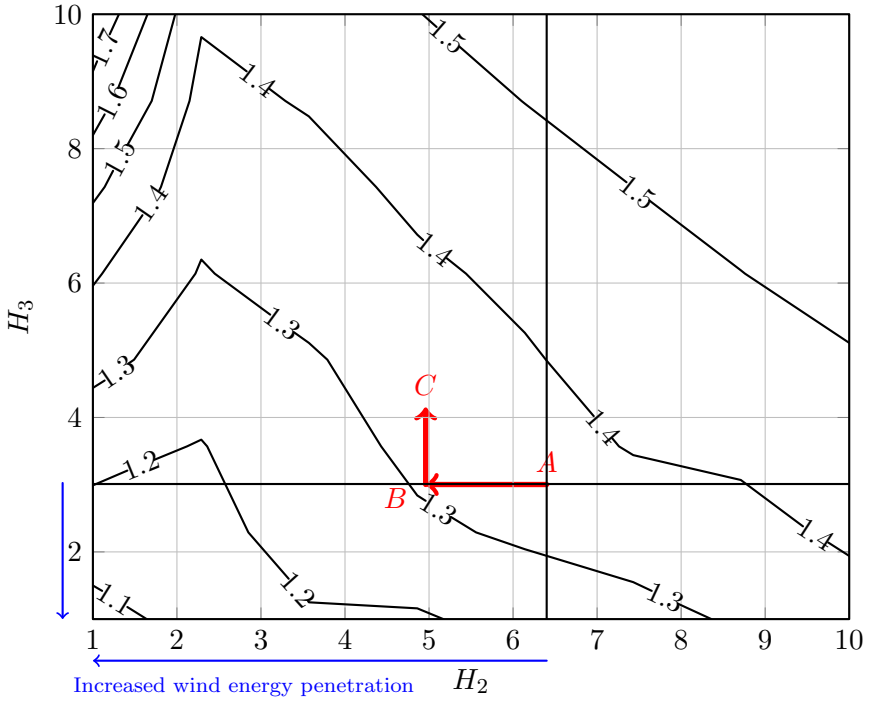

FIGURE 4.7: V_{cr} lines for a fault applied on bus 6 cleared by removing line 6-9

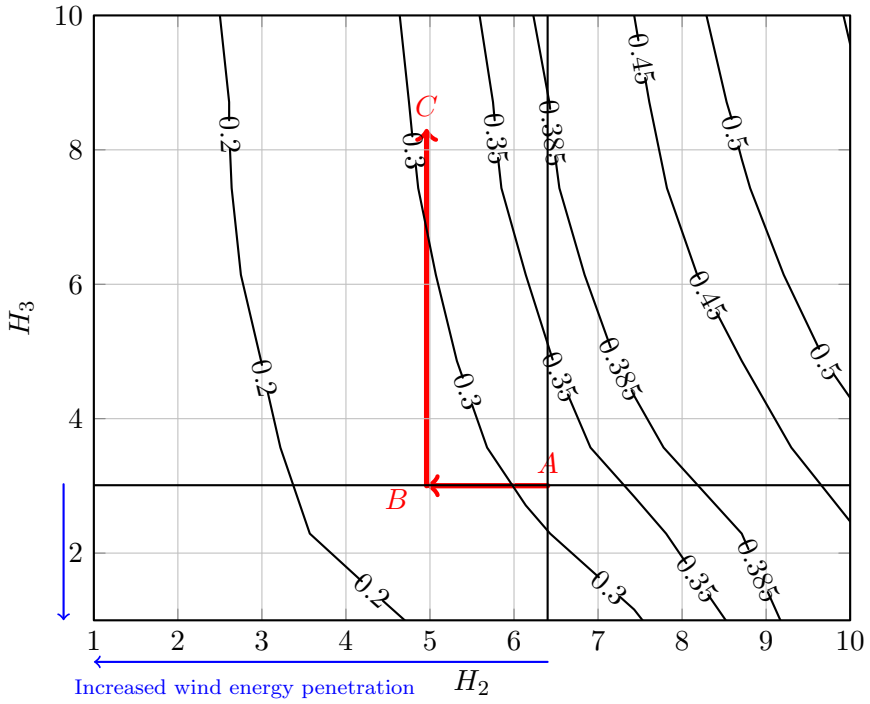

FIGURE 4.8: CCT lines of a fault applied on bus 5 with line 7-5 removed

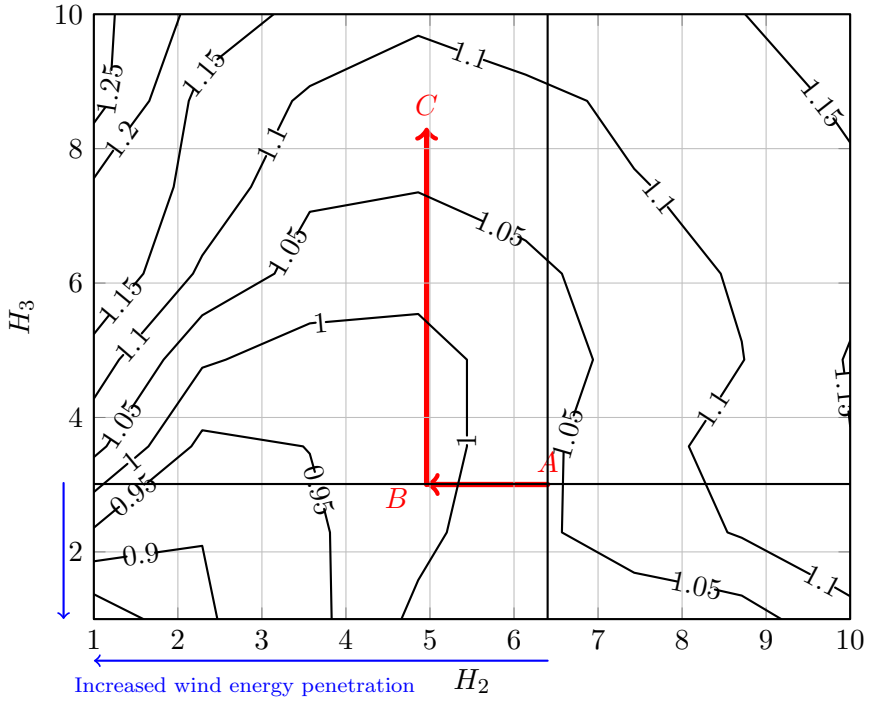

FIGURE 4.9: V_{cr} lines for a fault applied on bus 5 cleared by removing line 7-5

reduces the critical clearing time and transient stability margin. To maintain or improve the stability margin, inertia of other machine should be increased.

Similar illustration is provided for a fault applied on bus 5 and fault is cleared by removing line $7-5$. Fig. 4.8 provides the CCT contour lines on inertia space. If the inertia combination of (H2-H3) reduced from (6.4-3.01: 'A') to (5.0-3.01: 'B'). CCT would drop close to 0.25s. In order to keep CCT of 0.315s, machine 3 inertia has to be increased from 3.01s to 9.5s i.e., $H_2 = 5.0$ and $H_3 = 9.5$: 'C'. The increased penetration of wind generation is indicated with blue directional arrows along the inertia axes. Fig. 4.9 shows the equi-potential lines of critical energy for this fault, where the critical energy of system reduce with reduced inertia of machine 2(point B), but with increase in inertia of machine 3 to restore the critical energy of point 'C=A' does not improve CCT. This can be understood from the observation made in earlier section that reduction in inertia of a machine leads to much speed deviation, machine spins faster acquiring significant kinetic energy, thus critical energy is quickly attained which corresponds to lower clearing time.

4.3 Summary

We were able to demonstrate that reducing inertia of a SMIB will reduce CCT. We contributed a new mode of representing equi-CCT contour lines in inertia space of two machines. This helped to prove that in a three machine system fixing the inertia of a large machine(1) and reducing inertia of one machine(3/2) will reduce CCT. To retain or maintain same CCT, we need to increase inertia of the second machine(2/3).

In the next chapter we will provide the basis of understanding reduced inertia of wind-farm using pseudo synchronous generation, and also with the help of network reduction and coherent generators aggregation techniques.

Chapter 5

Asynchronous generation in power system networks

In this chapter we discuss about the analysis and assumption made towards integrating wind generation into a traditional power system network of synchronous machines.

5.1 Modeling aspects of wind generators

Generally, wind generators are classified on the basis of speed. They can operate on fixed speed operation or variable speed operation based on the generator technology used.

5.1.1 Fixed-speed wind generators

Although the wind speed is variable in nature, the rotor speed of wind generators is constant in operation, they aim to gain optimal efficiency for a fixed speed. As the fixed speed generator is supposed to operate at fixed speed any variation in wind speed will lead to voltage and power fluctuations when connected to a weak grid. Fixed speed generators are typically squirrel cage or wound rotor induction generators. They are connected directly to grid with a soft stator, along with units providing reactive power compensation. These generators come with disadvantage like issues with power quality, lack of reactive power control and mechanical stress, but they still offer an advantage being simple at operation, low maintenance and robust at operation.

5.1.2 Variable-speed wind turbines

Due to variable nature of speed, variable speed wind turbines are designed to attain maximum efficiency at a fairly constant machine torque. This is done by accelerating and decelerating turbine with changing wind speed conditions to attain maximum efficiency. As turbine sizes increased, new generation technologies moved from fixed speed to variable speed, along with ability to comply grid code requirements.

Variable speed generator types can be conventional induction generator or a doubly fed induction generation or a synchronous generator type, all are connected to grid via power electronic converters. These converters come with an advantage of voltage ride through capability and a certain level of reactive power compensation.

DFIG is a variable speed wind generator, it can deliver power while rotating about synchronous speed and absorb power when rotating below synchronous speed, the frequency converter is about 30% of generation capacity[3, 63]. On converter end of DFIG, the inverter unit and point of common coupling decouples the inertia of rotating mass, unlike a synchronous machine, rotor winding is mounted on the shaft.

DFIG wind turbine has a wound-rotor induction generator, through slip rings current is taken in and out from rotor winding and the variable-speed operation is achieved by injecting voltage across rotor terminals at slip frequency [64, 65]. The variable-frequency power converter on rotor is generally a AC-DC and DC-AC IGBT based voltage source converters linked via DC bus. The power converter decouples the grid electrical frequency from the turbine frequency and inertia so is the decrease of synchronising forces, while enabling variable-speed operation of the wind turbine[12].

Table 5.1 provides significant differences in general between synchronous generation and asynchronous wind generation [19]. These differences cause wind generators to interact differently with the network. Wind generation impact on operation of system are local at windfarm level and also at network level, local level impact is due to turbine characteristics.

5.2 Coherent generator groups with windfarm in 39-bus 10-generator network

39-bus 10-machine network model is modified here by replacing a generator with a windfarm. Fig. 5.1 is the modified network model with windfarm (DFIG technology) replacing synchronous generators at bus 33. Net power generation capacity is unaltered when synchronous generator is replaced by windfarm, DFIG parameters are provided in

TABLE 5.1: Differences between synchronous and asynchronous generation[1]

Synchronous	**Asynchronous**
• Generation at grid frequency (3 phase, 50/60 hz) and rotor at same frequency.	• Variable frequency of generation and operation on rotor side.
• Machine mechanical angle is equal to electrical output angle.	• Machine mechanical angle is variable, also different to point of common coupling, phase angle is determined by converter terminal voltage.
• No converters are generally involved to rectify and invert to match and synchronise with grid.	• Rotor side and Grid side converters are involved to synchronise with grid.
• For transient stability purpose all synchronous machines can be modelled as constant electrical output behind transient reactance.	• For transient stability purpose it is complex to model individual machines, an aggregate model will be easy to model and simulate. For dynamic studies (short time frame) the key participation is from machine mass, which is decoupled in here.

table 5.2, windfarm at bus 33 has a generation capacity of 632 MW with 316 induction generators of 2 MW connected in parallel. Similarly for another case the network has got windfarm at bus 35, so the P-V at bus remains unchanged. Same set of fault scenarios as applied in section-2.7.1 are applied on this network to identify coherent generator groups.

TABLE 5.2: DFIG model and rotor-side converter parameters

Parameters	**Value**
Rated voltage	0.69 kV
Inertia	75 Kg-m^2
Rotor type	Single cage
Rotor reactance X_r	0.0312 pu
Rotor resistance R_r	0.056 pu
Stator reactance X_s	0.1 pu
Stator resistance R_s	0.01 pu
Mag. reactance X_m	3.5 pu
PQ control	
Kp Active power control gain	4 pu
Tp Active power control time constant	0.1 pu
Kq Reactive power control gain	4 pu
Tq Reactive power control time constant	0.1 pu

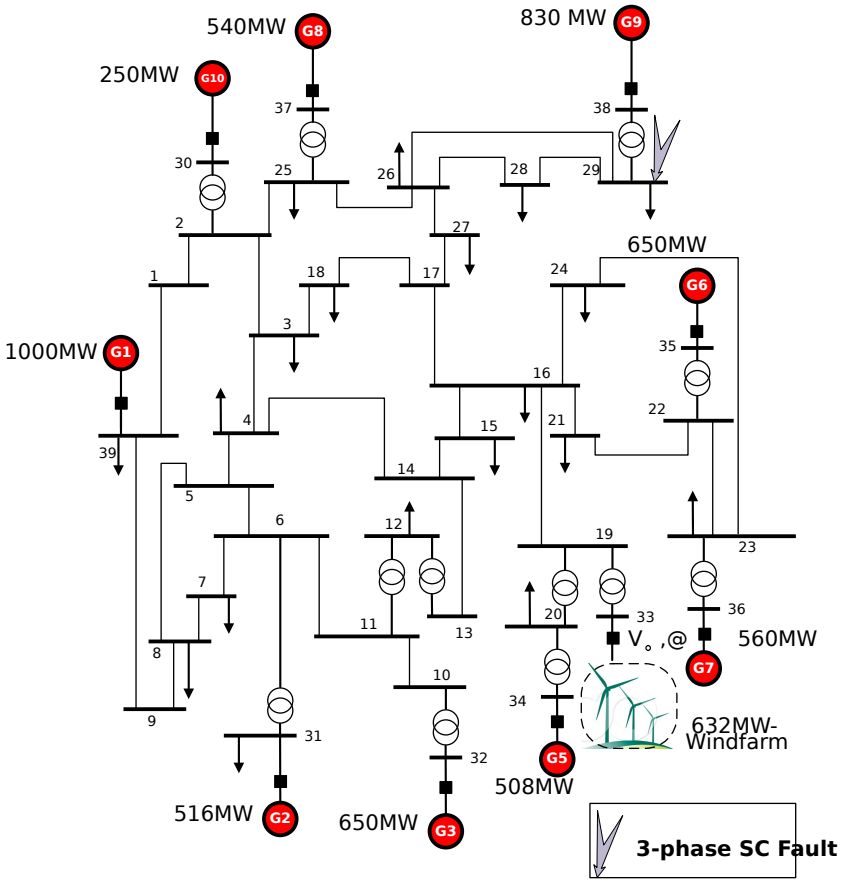

FIGURE 5.1: Modified 10-generator 39-bus network, windfarms at bus 33 with fault on bus 29

TABLE 5.3: Coherent group of generators indicated by bus locations for different fault scenarios

Fault bus	**duration (ms)**	**Line removed**	**Coherent groups without windfarms**	**Coherent groups-windfarm at bus 33**	**Coherent groups-windfarm at bus 35**
29	80	29-26	(33,34,35,36)	(34,35,36)	(33,34,36)
25	140	25-2	(33,34,35,36)	(33,35,36)	(33,34,36)
20	200	no line removed	(32,38)and(35,36)	(32,38) and (35,36)	(32,38)
31	240	no line removed	(30,32,33,34, 35,36,37,38,39)	(30,32,34,35, 36,37,38)	(30,32,33,34, 36,37,38,39)
10	230	10-13	(30,33,36,37,38)	(30,35,36,37,38)	(30,33,36,37,38)

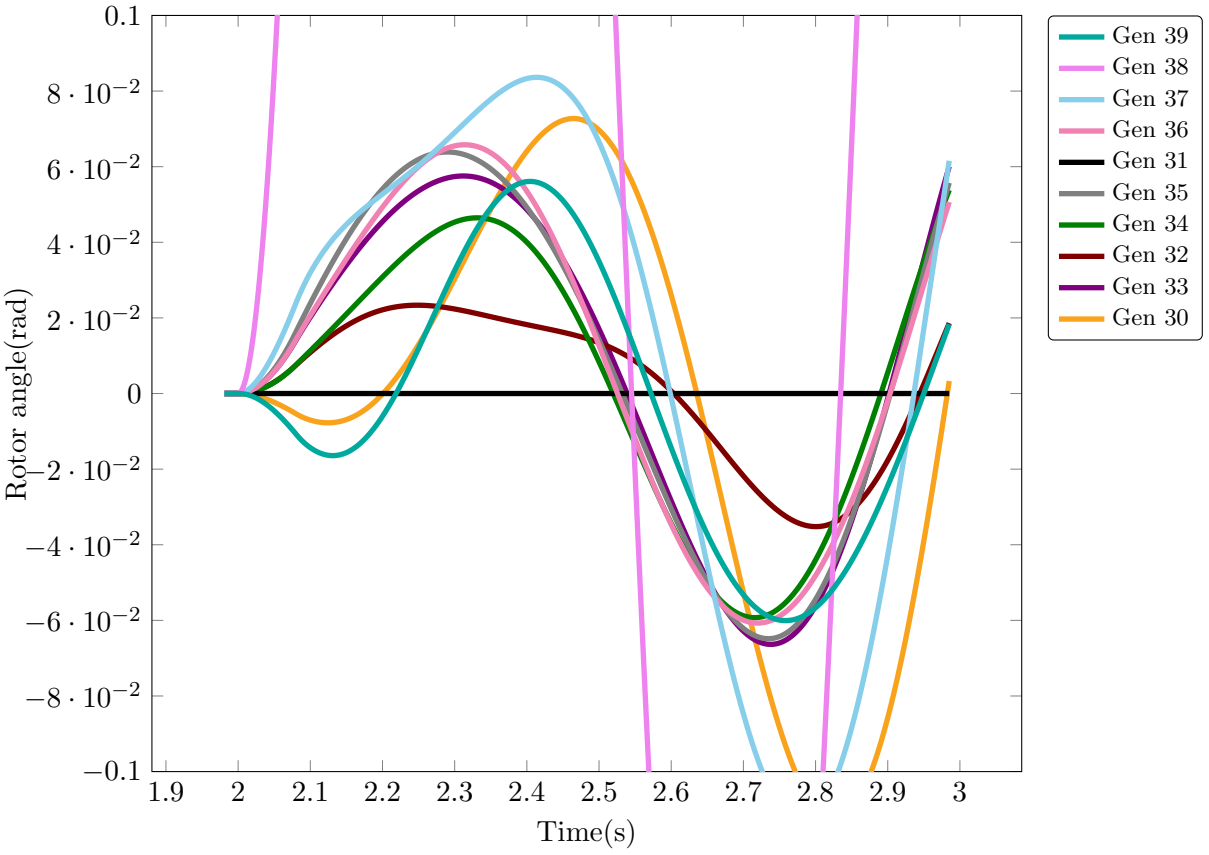

FIGURE 5.2: Swing curves for fault on bus29 with no windfarm in the network

5.3 Test scenarios and results

Network shown in Fig. 5.1 developed in DIgSILENT- PowerFactory. Coherent generator groups are identified as before using time domain graphical approach of observing rotor angle trajectory. In each case, the system exhibits critical unstable condition. Key disadvantage here we cannot obtain the rotor angle of DFIG plant like traditional synchronous machine at bus 33 (bus 35) and this generator does not appear in coherent groups. The generator labels in the Fig. 5.2 to Fig. 5.4 are replaced with their bus numbers for convenience. The protection of DFIG converters are a significant consideration for any particular fault level, for all the faults being considered, the currents and voltages for grid side convector during the fault are within the limits of the converter protection settings and the wind power generators are able to ride through the faults.

From Table 5.3 it is inferred that the coherent group of generators did not change with introduction of windfarm, but there has been a change in the tolerance level on coherent angle within the group. It is found that coherent generators rotor angle deviation increases for fault scenarios on bus 20 and deviation decreases for fault on bus 29. As windfarm generators not having significant inertia do not bring significant change to

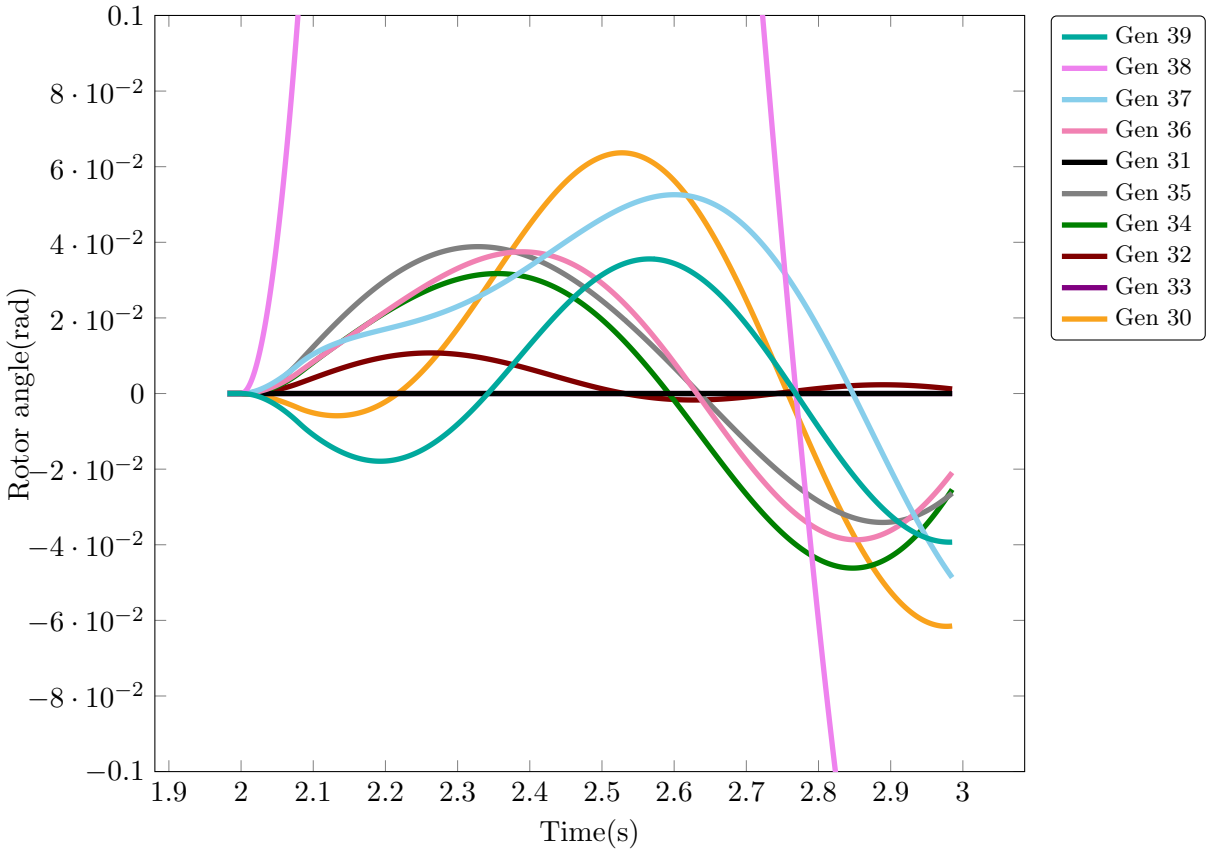

FIGURE 5.3: Swing curves for fault on bus 29, with windfarm at bus 33

the coherent groups, the coherent generator groups still remain same. Thus, network reduction methods used for conventional synchronous machine systems can be applied without much modification, although detailed investigation is required to validate this statement. Future directions can include increasing number of windfarms and penetration level in the same network to identify level of penetration margins and locations which may change the coherent groups. Windfarm at bus 33 and bus 35 were chosen randomly for this investigation, in future more windfarm bus locations could be studied, provided able to overcome PowerFactory modelling and simulation limitations that avoid the simulation to proceed to post-fault duration. These limitations could be like voltage saturation limits pre-set at converter side of DFIG. In this thesis few results are presented as the simulation was unable to proceed satisfactorily at some windfarm and fault locations.

The rotor angle deviation with and with out windfarm at bus 33 is plotted in Fig. 5.5. This deviation plot suggests that introduction of windfarms offers angle deviation, which can be attributed to net reduction of synchronizing forces provided by inertia, deviation is much significant for the machines close to windfarm bus location. Results shown in Fig. 5.5 doesn't contribute much information about effect of inertia on angular

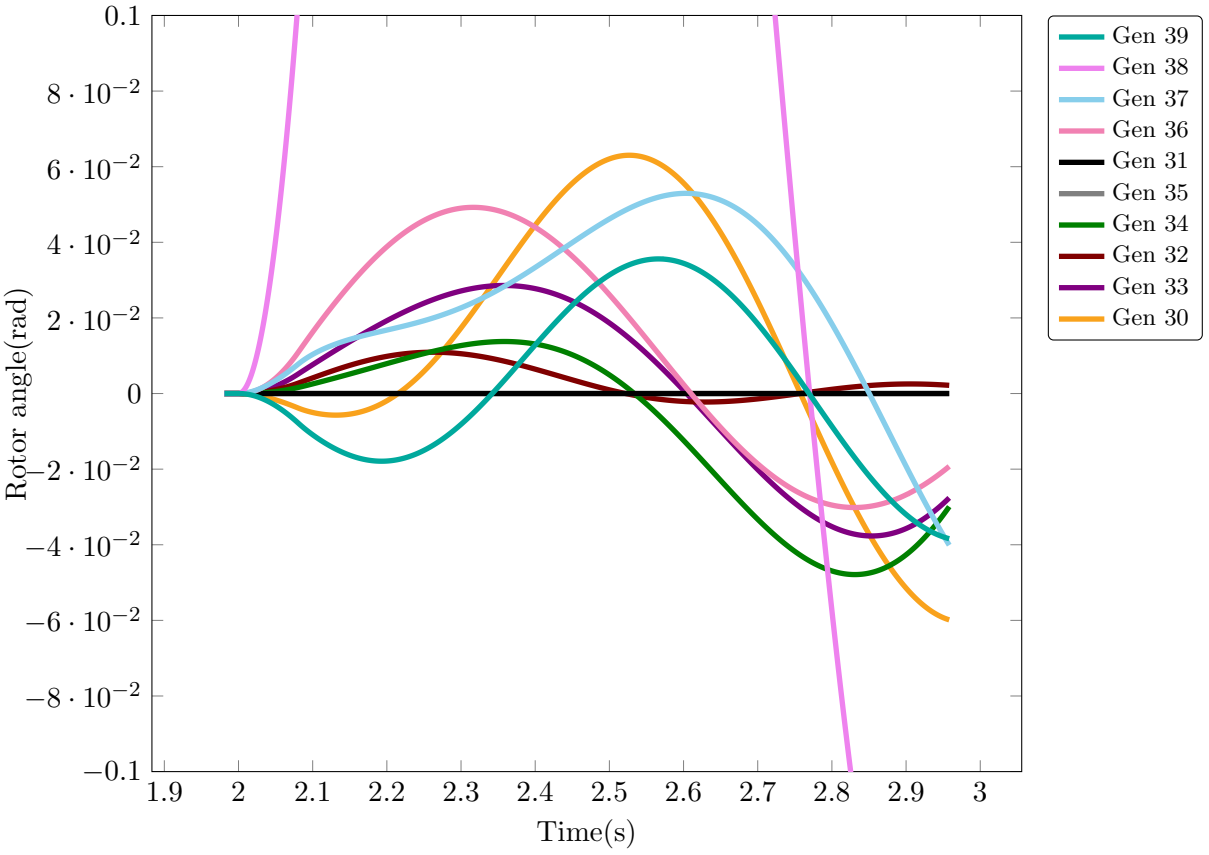

FIGURE 5.4: Swing curves for fault on bus 29, with windfarm at bus 35

deviation, much understanding of interaction of wind generator converter is required. Angle deviation of machines 32 and 35 which are close to bus 33 (windfarm) has large angular deviations suggests the effect of inertia-less effect on swing. This cannot be told affirmatively as the PowerFactory program doesn't offer much transparent reasoning to justify this angle deviation. This leaves with a choice for much detailed understanding can be inferred from 3-machine 9-bus system analysis.

5.3.1 Windfarm modeled as negative load

Transmission grid operators often consider wind generation as negative load while performing load flow studies and operational scheduling. The results of their investigation are valid, only with low amount of wind energy penetration. However, the transient stability of the system with high wind energy penetration has not received much attention from researchers and this thesis focuses this aspect. An exercise is performed here to check the effects of windfarm on the transient stability, with windfarms assumed as negative load by changing the load at P-V bus 8 from $100 + j35$ to $80 + j55 MVA$. This change in load can factor a decrease in active power injection from bus 8 and increase in reactive power drawn by the windfarm. The critical energy V_{cr} and corresponding

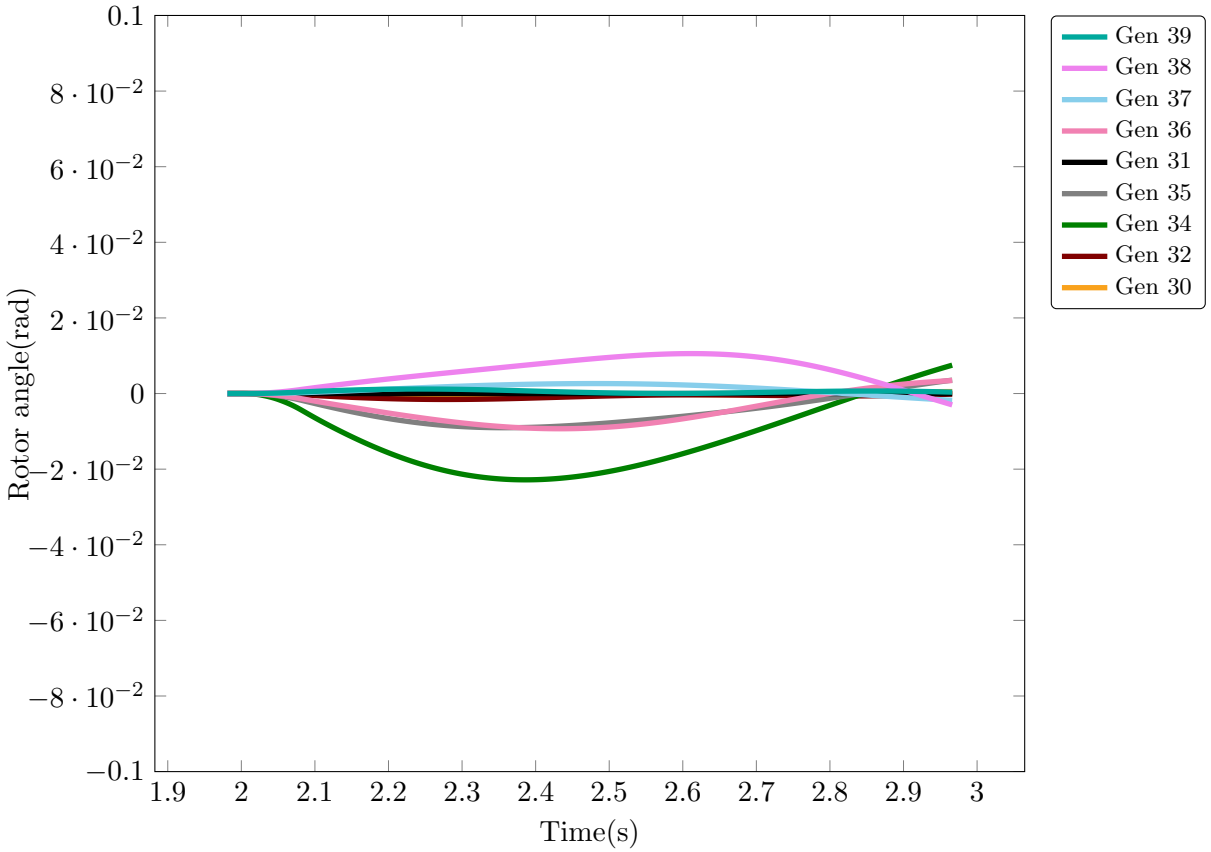

FIGURE 5.5: Rotor angle deviation with windfarm at bus 33 from normal network for a fault on bus 29

critical clearing time T_{cr} for negative load configuration are computed and shown in Table-5.4. From the results shown in Table-5.4, it is observed that the values of V_{cr} and T_{cr} are less compared to the case when the windfarm is absent. This implies that transient stability margin(T_{cr}) of this test system with presence of windfarm is less compared to the system without the windfarm. The key network change here is new active power flow and change in load modifying admittance matrix offering altogether different SEP and UEPs for the system, thus providing a different network parameters and state equations.

To over come this configuration change and retain the steady state values, only the dynamic behavior is addressed in event of disturbance, which is the underlying motivation of TSA. Therefore in this thesis windfarms are represented as conventional synchronous machines (can be referred as pseudo-synchronous machine) at the generation buses. The effects of increasing wind energy penetration are factored by reducing the inertia of these pseudo-synchronous machines.

TABLE 5.4: CCT and critical energy for various fault scenarios. Last 2 columns are for the system where the windfarm is represented as negative load at bus 8

Critical clearing time and Critical energy					
		Existing system		**Negative load**	
Faulted bus	**Line removed**	**CCT**	**Critical energy**	**CCT**	**Critical energy**
7	7-5	0.1800	1.2478	0.1600	1.0330
7	8-7	0.2000	1.8480	0.1900	1.7235
5	7-5	0.3150	1.0276	0.2600	0.7919
5	5-4	0.4050	2.3819	0.3600	2.0545
4	4-6	0.3100	2.4734	0.2750	2.1135
4	5-4	0.3100	2.4705	0.2800	2.2141
9	6-9	0.2400	2.1020	0.2300	1.9156
9	9-8	0.2400	2.7247	0.2300	2.5798
8	9-8	0.3200	2.9796	0.3050	2.6719
8	8-7	0.3150	2.8198	0.3000	2.5427
6	4-6	0.4450	2.4317	0.3950	2.1520
6	6-9	0.3850	1.3426	0.3300	1.3333

5.3.2 Induction generator in 3-machine 9-bus system

From 39-bus 10-machine coherent generator group identification study one can reduce a network to a system of three machines as analysed before, each machine is equivalent generator aggregate of few generators[66, 67]. Generator aggregation can be made using classical aggregation (CA) where an equivalent generator model with an equivalent inertia is, the sum of inertia of all generators in the coherent group, the equivalent transient reactance is parallel sum of all the generators transient reactance in the group. Much details about aggregation techniques are available in reference [68–71]. Once the reduced equivalent generators are determined, network is reduced to remain the same steady state power flow conditions as earlier. Windfarm participation at generation bus location is equivalent to a conventional generator except with negligible inertia. So the net inertia is reduced of equivalent generator model. Thus the analysis done with reducing inertia in chapter 4 imparts same effect with windfarms connected to one generation bus location in 3-machine 9-bus system. As mentioned in section 5.4 Fig. 4.6 to Fig. 4.9 in studying dynamics with increased amount of wind energy penetration can be factored as decreasing inertia of each machine under a generation bus which is aggregated generation equivalent of group of coherent generators.

Following assumptions are made for modelling asynchronous generators as 'synchronous generators with negligible inertia and reduction in over all inertia upon aggregation'.

- In a large network this assumption of asynchronous windfarm generation as a synchronous generator with negligible inertia, is valid when the synchronous and

asynchronous generators are aggregated along at transmission level not at distribution level.

- So that for a synchronous generator at a farther bus location can see the power flow, equivalent swing, and impact on its angular deviation are like an effect form a synchronous generator.
- Use of traditional techniques of network reduction, where reduction is carried on coherency basis.
- The model verification can only be performed if the initial state of Simpower system or commercial software with complete converter based windfarm model network has same initial states as of a network with reduced inertia synchronous machine models. Provided the commercial model can also ride through voltage and frequency limits.

5.4 Backward method to estimate inertia of a generator

The graphical representation of CCT for several inertia combinations shown in Fig. 4.6 offers a quantifiable amount of inertia required in maintaining desired stability margin. This representation also offers an index in proceeding with a backward method of calculating inertia. From the critical clearing time contour lines, we can observe that this is a unique solution problem. Say two Nine bus systems provided with information as listed below

- Same contingency states and also with same pre-fault conditions
- Inertia values of any two machines
- and provided with CCT information, CCT can be obtained from any energy function method or time domain method

With these information one can estimate inertia of third machine. Implies that one can estimate the pseudo inertia offered by aggregated asynchronous generator or from a generation bus. To be noted here in this analysis synchronous machine are still a constant voltage behind transient reactance model. This backward method can be of special interest in windfarm integration and system planning to incorporate the lack of inertial ability. Fig. 4.6 and Fig. 4.8 mode of representation in inertia space can be used as reference guide for planning, operation/control of windfarms, especially in the motivation towards participating in ancillary services like providing inertial support.

5.5 Summary

In this chapter we were able to provide necessary preliminaries of DFIG. Coherent generator groups were identified when a windfarm displaced a synchronous generator in a 39-bus 10-machine system. From 3-machine 9-bus system case study, we demonstrated that assuming windfarm as negative load is unsuitable for TSA in network with high wind energy penetration, this is because of inconsistent values compared to system with no windfarm. Equi-CCT contour lines provide enough information about the amount of additional inertia need to be added to neighbouring generator to maintain stability margin.

The technique of obtaining equi-CCT contour lines demonstrated in this chapter, will be used in next chapter to calculate the necessary series compensation required when inertia reduces.

Chapter 6

Transient stability enhancement of power system with reduced inertia

In this chapter dynamic series compensation using bang-bang control of FACT devices is proposed to improve transient stability limit. We utilize PEBS method to obtain CCT. Simulations on SMIB and 3-machine 9-bus system are carried out to illustrate the effects of proposed dynamic compensation on CCT.

6.1 Modern power system monitoring and security

In most grids computer based supervisory control and data acquisition systems (SCADA) are at the heart of energy and control centres for monitoring and security assessments. SCADA helps managing and controlling grid. The SCADA systems at control centers receive tele-metered measurements about real and reactive power flowing between substations, from the voltage magnitudes and breaker statuses and other data gathered and sent by remote terminal units (RTU). This voluminous data can offer preliminary security check if various system equipments are operating with-in feasible operation limits. SCADA systems filter data and from the available data they compute supplementary power flow information in lines where the measurements are not available.

Active power and reactive power data at all load buses and lines is derived from state estimation (SE) where states are defined by voltage magnitudes and phase angles at individual buses. SE information does not completely capture system dynamics as information relayed is not updated sufficiently fast that can accommodate sudden changes

caused by large disturbances, thus unable to perform dynamic security analysis. On-line based transient stability programs are available for addressing dynamic security problem. These programs perform high speed parallel computations to get security assessment results, still the results take long time making them unattractive [72]. Transient Energy function based dynamic security assessment (DSA) and preventive control are employed in grids of US, Canada and Japan and they seem to give desirable results [73–75].

6.2 Application of FACTS devices and controllers for emergency control

It is general practice to quickly detect emergency state of a system and apply emergency control, so the system can move in an alert state and slowly be restored to normal state of operation, this avoids preventive control. Synchronized phaser measurement units aided with SE offer direct and fast measurement of phase angles for real-time transient stability prediction [76, 77]. Synchronous optical networking (SONET) are capable of delivering messages between nodes in less then 6ms [78].

Transient stability is traditionally handled by employing few of the following primary and discrete supplementary control strategies

(a) Braking resistors in hydro generators and fast valving of thermal generation [79].

(b) Reducing system reactance between stations by inserting switch-able reactance.

(c) Series capacitor insertion in transmission line.

(d) Fast response capacity of excitation system.

(e) High speed fault clearing within 2-power cycles and high speed re-closure of circuit breakers typically in 1-cycle.

Power electronic based converter controls used in **F**lexible **A**lternating **C**urrent **t**ransmission **S**ystem (FACTS) and HVDC controllers can also be applied during transient events to provide emergency control, basically moderating the reactance between stations. The capability of FACTS is not just limited to achieve first swing stability, the control actions can also damp out large size oscillations [80–82].

As demonstrated in earlier chapters Lyapunov's method investigates the transient stability margin by determining the maximum duration of sustaining the fault before the system loses synchronism. This energy function approach is useful in determining accurately the optimum locations and control laws to operate FACTS devices, enabling towards enhancement of system stability and therefore it is pursued in this chapter[83–85].

Small disturbances cause small oscillations and are investigated under small signal stability study. We know in practice that system equations are linearised to design controllers for series and shunt FACTS devices to damp out these small oscillations. However FACTS controllers are applied here for improving dynamic security for severe fault situations, it is therefore necessary to retain the non-linear system models and develop control strategies around it. The controllers then switch the FACTS devices that can operate in their spare capacity, so as to ensure first swing stability. With suitable control strategies, system trajectory can be steered towards an equilibrium point attaining multi-swing stability.

The corrective actions listed in the beginning of this section are designed to attain first swing stability on application, on application they either increase the electrical power output demand or decrease the mechanical power input of the advanced generators [86]. These corrective actions to maintain transient stability are initiated only upon detection and clearing of large disturbance. Bang-bang type controller algorithm for FACTS devices is detailed in next section[87–90], and this control strategy is illustrated on SMIB and 3-machine 9-bus system.

In general, small signal stability controls developed around steady-state condition are applied and maintained continuously all times, where as the transient stability problem being a function of disturbance where the primary objective is towards preventing loss of synchronism. The control actions here are initiated following a disturbance and can be stopped when the system reaches close to desired equilibrium point. With an assumption that the post-fault equilibrium is stable and the control actions are also temporary.

FACTS devices with high-power semiconductor switches such as Thyristor, GTO and IGBT are programmable to deliver desired discrete control action [91]. FACTS device controllers for transient stability enhancement are discrete supplementary controllers where as speed governor, excitation systems and protective relaying action stated in beginning of this section act as primary controllers [92].

6.3 Bang-bang type control strategy

Time optimal discrete control based on Pontryagin's maximum or minimum principle is used here to arrive with a control strategy that can not only ensure first swing stability but can also steer the system trajectory towards stable equilibrium point, this forms a basis for multi-swing stability. The control strategy used here is bang-bang control[93, 94]. The control action is achieved via thyristor controlled series compensator(TCSC) to vary series line capacitance between two extreme limits. The series compensation is

provided only at the time of fault, and the value is varied such that the and compensation is removed after few cycles.

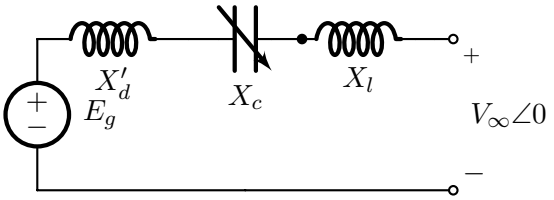

FIGURE 6.1: Series capacitive compensation of SMIB for stability study

The bang-bang control based on time-optimal control strategy is implemented here on SMIB. The machine is connected in series to capacitor as shown in Fig. 6.1 . Natural damping factor is neglected here in this case, while giving rise to system equations as below

$$\begin{aligned} \dot{\delta} &= \omega \\ \dot{\omega} &= \frac{1}{M}\left[P_m - \frac{E_g E_b}{X - X_C}\sin\delta\right] \end{aligned} \tag{6.1}$$

In above equation E_g is generators internal voltage, $E_b = V_\infty \angle 0$ is the infinite bus voltage, X_l is transmission line reactance, X'_d is transient reactance of generator, this reactance is in series with a switchable capacitor of reactance X_C. Note, this series generator reactance is only for transient stability studies. The reactance has got a nominal value of X_{Co} and is varied with in limits $X_{Cmin} \leq X_C \leq X_{Cmax}$. Therefore net reactance in series to X_C is $X = X'_d + X_l$ Energy function of SMIB derived in earlier chapters is presented here for convenience, the energy function of interest around stable equilibrium point as a sum of kinetic and potential energy is given by

$$V(\delta, \omega) = \frac{1}{2}M\omega^2 - P_m(\delta - \delta_s) - P_e^{max}(\cos\delta - \cos\delta_s) \tag{6.2}$$

A fault causes a mismatch of 'mechanical power input' to 'electrical power output demand', this leading the machine to accelerate if $P_m > P_e$ the machine gains kinetic energy as the machine spins above synchronous speed. After the fault is cleared, the machine can remain stable only if the speed gained becomes zero and returns to synchronous speed, and this can be possible by natural damping of machine after many cycles. It is also possible that after the fault is cleared, the kinetic energy gained can be quickly converted to potential energy [28]. PE of the system is greater with a capacitor and this fact is utilised in developing discrete switching strategy, that can be applied to TCSC, and this strategy is explained below[95].

1. Upon detection of fault and followed by clearing, the control variables are chosen such that the maximum power transfers ($P_t = P_m - P_e$) to the infinite bus. At this instant maximum electrical output demand is increased by the capacitor (TCSC), which is in series and of nominal value X_{C0}, is now increased to value X_{Cmax}.

2. When $(\delta - \delta_s) \geq \mu$ and $\omega \leq \eta$ the switch-able capacitor X_C is switched back to nominal operating value X_{C0} .

3. When $(\delta - \delta_s) \leq \mu$ and $\omega \leq \eta$ at negative maximum, capacitor X_C is reduced to X_{Cmin}, this will minimize the power flow P_t and also minimise angle undershoot.

4. When $(\delta - \delta_s) \leq \mu$ and $\omega \geq \eta$, control variable is chosen such that capacitor X_C is back switched back to nominal operating value X_{C0}.

5. Above steps are repeated until $(\delta - \delta_s) \leq \mu$ and $\omega \leq \eta$.

This control scheme is disabled when $|d\delta/dt| < \eta$ and $\delta \simeq \delta_s$, η is the stability region where system equations can be linearised, so that small signal control schemes can take over.

This scheme is explained elaborately with the help of power angle curves of Fig. 6.2 and in [92, 95]. It can be seen that after occurrence of disturbance and followed by clearing, the system is switched between two extremities of power angle curves. Intermittently it is switched to a power-angle curve corresponding to desired post-fault stable system (i.e., $X_C = X_{C0}$). The two extremities curves correspond to X_{Cmax} and X_{Cmin} mentioned in steps earlier.

A fault causes machine angle to advance forward from δ_0 to an angle when fault is cleared δ_{cl}. Acceleration area under power-angle curve is '**abcd**' where $P_m \neq P_e$. The area under the curve is the KE stored in the high speed rotating mass, beyond point '**d**' machine starts decelerating until area '**defg**' is equal to area '**abcd**'. Validating equal-area criteria and rotor angle reaches a peak of δ_{max}, this part is also explained elaborately earlier in second chapter.

1. With an assumption that $\delta_{max} \leq \delta_u$, angle δ_{max} can be minimized by maximising the power flow P_t. i.e., electrical power demand is made more than the mechanical power input which will decelerate the machine.

2. When system crosses point '**a**' where machine speed is above synchronous speed but negative, the control variables are selected to switch such that power flow is minimum here ($X_C = X_{Co}$) reducing rotor angle undershoot. The rotor angle now reaches a minimum value of δ_{min} such that accelerating area '**aijk**' is equal to decelerating area '**gfa**'.

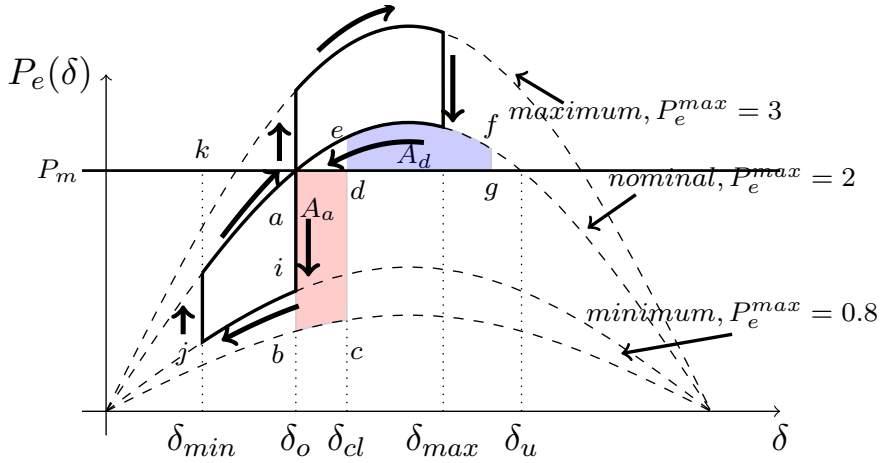

FIGURE 6.2: Discrete control demonstrated on power-angle curves

3. When δ is equal to δ_{min}, ω is 0, switch control variable is now selected to nominal operating value ($X_C = X_{C0}$) this will steer rotor towards δ_0.

4. Again while $\delta = \delta_0$ and ω is maximum, the control variables are selected for ($X_C = X_{Cmax}$) such that maximum power transfer occurs in the line, this will reduce angle overshoot.

It can be seen that the control strategy attempts to minimise both overshoot and undershoot the rotor angles over few cycles until δ reaches close to SEP, i.e., maximise power flow when $\delta > \delta_0$ and $\omega > 0$, minimise power flow when $\delta < \delta_0$ and $\omega > 0$.

6.3.1 Single machine discrete control

In Fig. 6.3 is rotor angle deviation for a fault applied at $2.5s$ after start of the simulation, the fault is applied and cleared within 1.35s. The initial states of the system are as follows, pre-fault $P_e^{max} = 2$, $P_m = 1$, $M = 0.2$ and SEP $\delta_s = 0.523$ rad. Post-fault maximum electrical output power demand denoted by (P_e^{max}). The acceleration Eq. 6.1 is varied by hard switching series compensator X_C. This switching is based upon the discrete control strategy discussed (in section 6.3). The maximum electrical output P_e^{max} against time is plotted in Fig. 6.3 along with accelerating power $P_a = P_m - P_e$i and $P_e = P_e^{max} \sin\delta$. Fig. 6.5 is the power angle trace over the switching duration. Fig. 6.4 is the phase-plane of rotor angle deviation from δ_0. P_e^{max} of the post-fault trajectory is decided by the quadrant on $\omega - \delta$ plane i.e., state of machine at that moment. In first quadrant P_e^{max}=3 this will reduce the angle overshoot. In the third quadrant P_e^{max}=1.5 this will reduce the undershoot and the nominal power in fourth and second quadrants is $P_e^{max} = 2$. Angle and speed deviation shown in 6.4 can be used to explain the control strategy implemented here, assuming that post-fault SEP is close to pre-fault SEP .

Remarks on Fig. 6.4:

- The faulted trajectory starts immediately in the first quadrant, after the fault is cleared and $\delta > 0$, the control variable is changed to u_{Cmax} so the capacitive TCSC shifts to maximum value X_{Cmax}, this ensures the machine to decrease its speed and enter into fourth quadrant by crossing δ-axis.

- At the δ-axis crossing $\omega = 0$, the control parameter is switched to u_{Co} corresponding to capacitor nominal value X_{Co}, causing ω to decrease below synchronous speed. When ω is negative and minimum, switchable control parameter is made to $u_c = u_{cmin}$ corresponding to X_{Cmin}, this ensures trajectory move into third quadrant. ω(negative) will increase until it becomes zero and crosses δ-axis.

- Now the system is in second quadrant, X_C is made to X_{Co} by $u_c = u_{Co}$, this ensures the machine to advance towards δ_s. When ω reaches positive maximum, switching u_c to u_{Cmax} will increase PE demand thus decreasing the net transient energy.

- It is easy to observe that total energy decays while system is in first (X_{Cmin}) and third quadrant (X_{Cmax}), and remains unchanged in second and fourth quadrants (X_{Co}).

- Variables δ and ω continue to oscillate and the energy associated continues to decay until system trajectory approaches close to post-fault SEP, at which the control actions can be disabled, there on suitable damping controllers can take over to ensure post-fault stable equilibrium.

In Fig. 6.6 shown is the transient energy gained by the system and its decay over time due to varying accelerating power. Fig. 6.7 is the rotor angle deviation for the same fault and duration, just as shown in Fig. 6.3 but for range of inertia (0.1 to 1) in steps of 0.1. Fig. 6.8 is similar to Fig. 6.7 except for the maximum electric power output is inversely proportional to inertia in first quadrant i.e., (P_{em1}^{max}/M) to minimise overshoot and directly proportional to inertia $(P_{em1}^{max} \times M)$ in third quadrant to minimise undershoot. The value of $P_{em1}^{max} = 2$, the maximum electrical output when $M = 0.2$. Fig. 6.9 provides the trend of electric power output made dependent of machine inertia.

6.3.2 Three machine nine bus system discrete control

The discrete control strategy described before is applied to a multi-machine system with equations in COA formulation[33]. The energy function derived in second chapter is

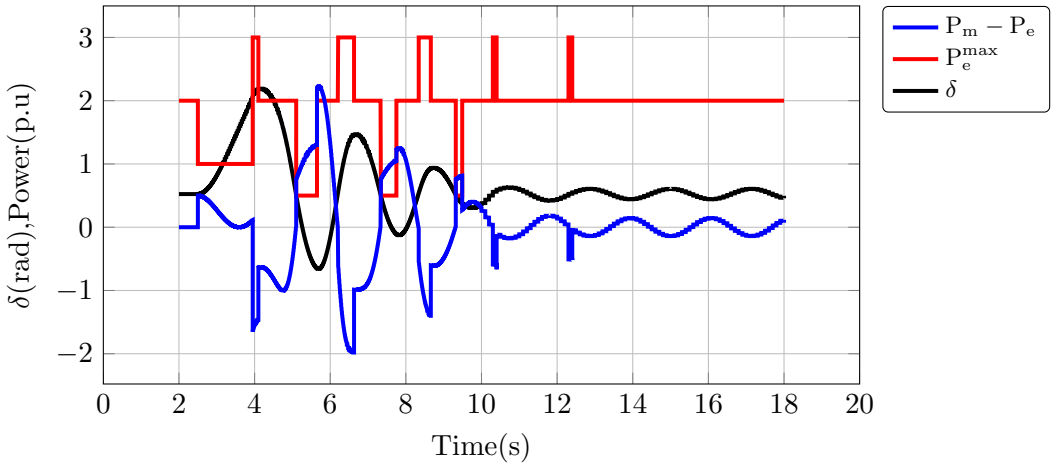

FIGURE 6.3: Rotor angle deviation, accelerating power and maximum electrical power output over time

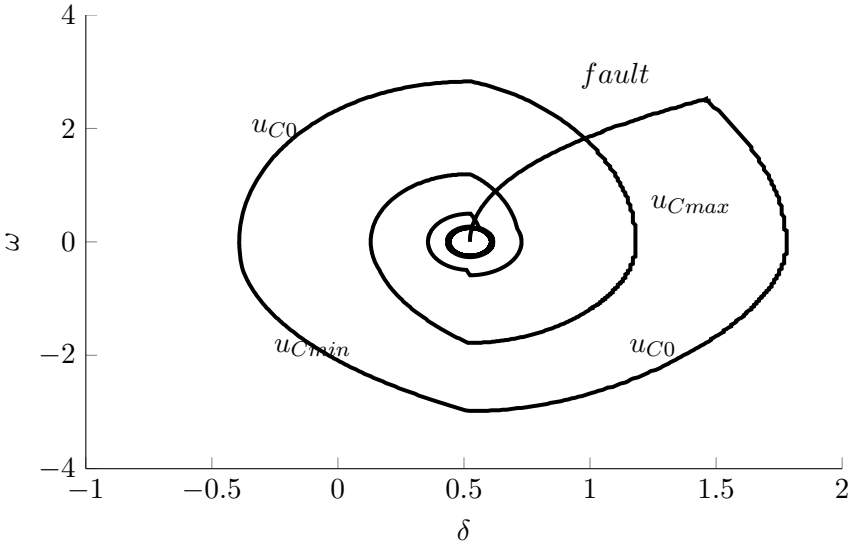

FIGURE 6.4: Speed deviation upon discrete control

presented here for convenience, and the control strategy is applied to machine 2 of 3 machine 9 bus system.

$$\begin{aligned} V(\theta,\tilde{\omega}) &= \frac{1}{2}\sum_{i=1}^{n} M_i {\tilde{\omega}_i}^2 - \sum_{i=1}^{n} P_i(\theta_i - \theta_i^s) \\ &- \sum_{i=1}^{n-1}\sum_{j=i+1}^{n}\left[C_{ij}(\cos\theta_{ij} - \cos\theta_{ij}^s) - \int_{\theta_i^s+\theta_j^s}^{\theta_i+\theta_j} D_{ij}\cos\theta_{ij} d(\theta_i+\theta_j)\right] \\ &= V_{KE}(\tilde{\omega}) + V_{PE}(\theta) \end{aligned} \tag{6.3}$$

In Eq. 6.3, θ_i and $\tilde{\omega}_i$ are i^{th} machine rotor angle and speed in COA. Network parameters of system are provided in Fig. 6.10. Inertia H(in sec) of the three generators 1, 2 and 3 are 23.64, 6.4 and 3.01 respectively. The transient reactance X'_d of these machines are

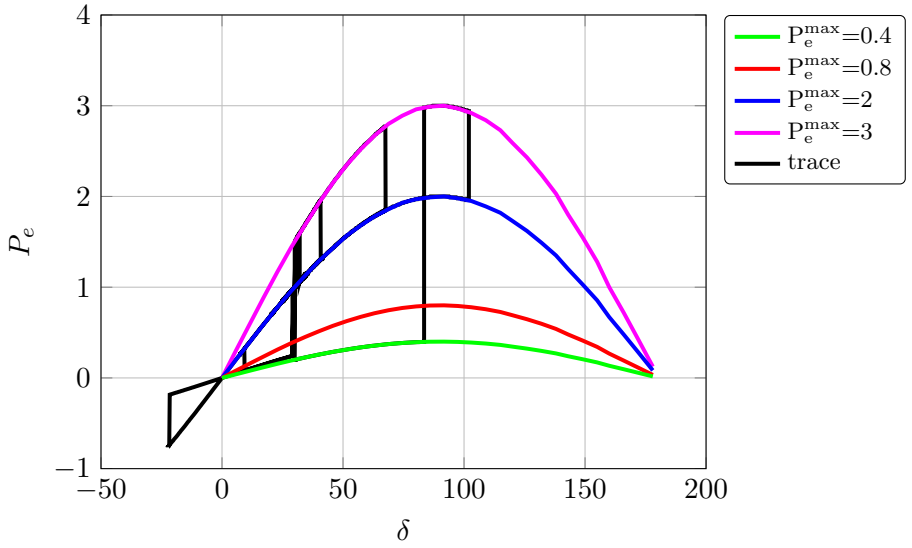

FIGURE 6.5: Power-angle trace

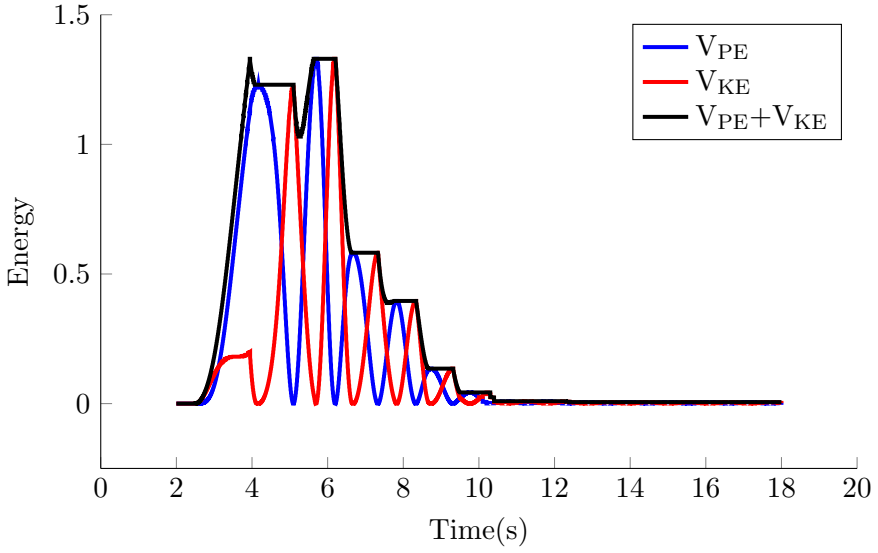

FIGURE 6.6: Energy deviation of SMIB on discrete control

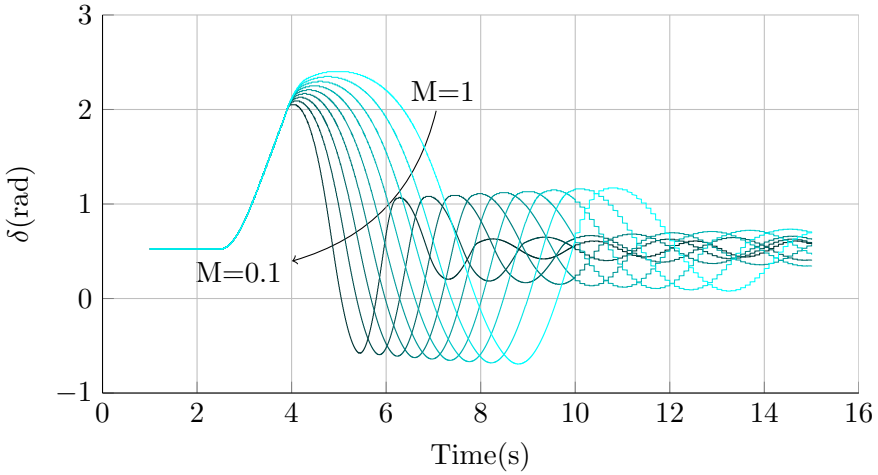

FIGURE 6.7: Angle deviation with changing inertia for a fault of 1.4s

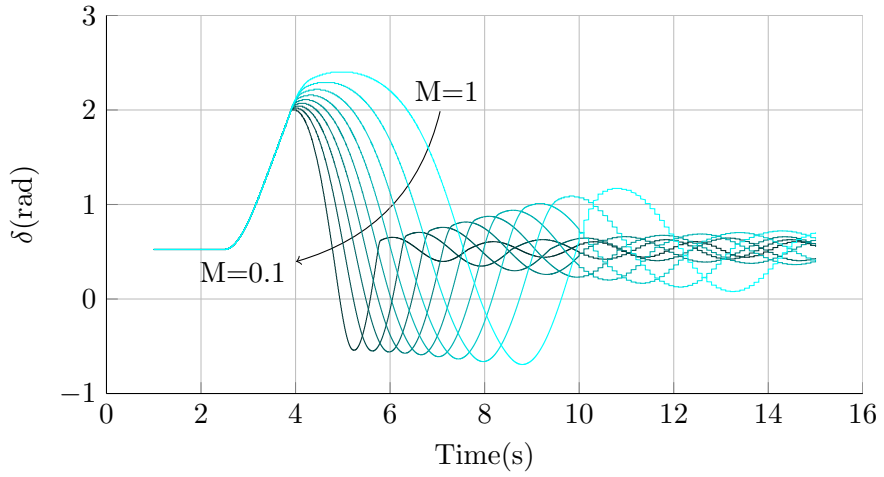

FIGURE 6.8: Angle deviation, Electrical output is P_e^{max}/M

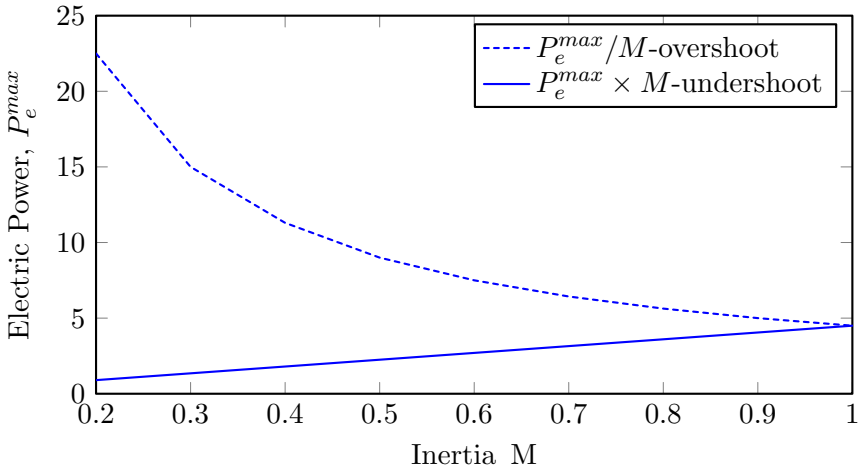

FIGURE 6.9: Maximum power output to varying inertia

0.0608, 0.1198 and 0.1813 respectively. The procedure to perform load flow analysis and arrival of initial machine angles, bus voltages are omitted here and can be referred to chapter 2.

For a fault applied on bus 4 for 0.25s and cleared by removing line 6. Discrete control strategy is applied for post-fault system i.e., switching the compensator inserted in series of the line between 5-7. The effective switch-able reactance is $X = X_{5-7} - X_{Co} = 0.161$ such that nominal capacitor reactance value is $X_{Co} = 0$. Conditions of switching are when $\omega > 0$ and $\theta > 0$(first quadrant), $X = X_{57} - X_{Cmax} = 0.161 - (0.161 \times 0.8)$, i.e., the line is compensated with 80% of its line capacity(rating MVA), this will minimize the system overshoot and when $\omega < 0$ and $\theta < 0$ (third quadrant), $X = 0.161 - (0.161 \times -0.2)$ this will minimize undershoot. In all other cases (quadrant 4 and 2) with nominal value of 0 such that $X = 0.161$. Similarly compensation can be carried on more lines and the most effective compensation is assessed, which is discussed in detail in section 6.4. The

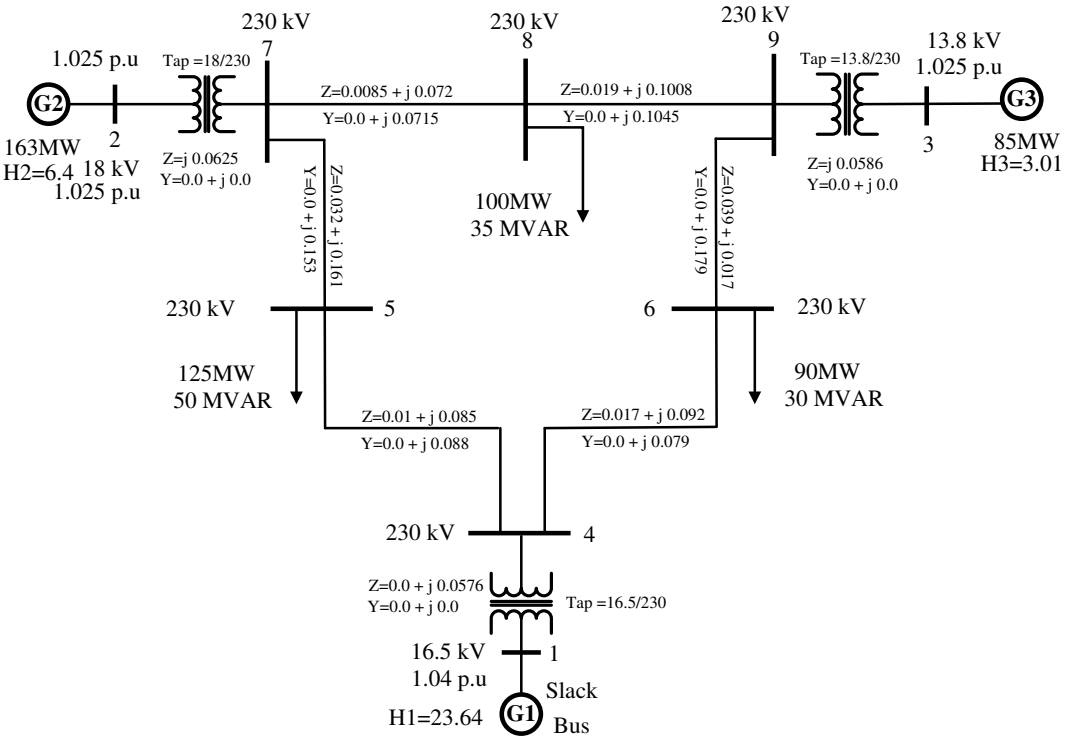

FIGURE 6.10: Three machine nine bus system, value of Y is half the line charging

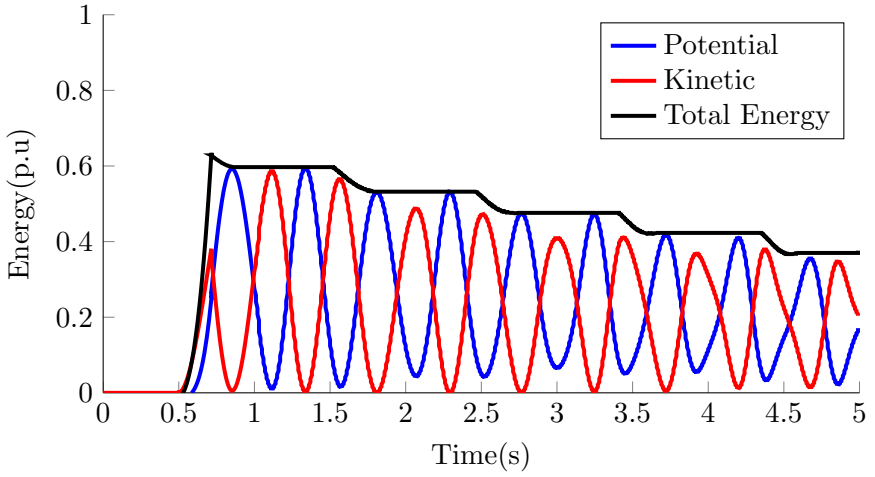

FIGURE 6.11: Potential Energy, kinetic Energy and total energy for a fault of 0.22s fault at bus 5

current case study is to investigate the discrete control strategy applied to asynchronous generation(windfarms) at bus 2. Fig. 6.11 is the transient energy (6.3) gained upon fault and it decays over time due to varying electrical power output and is provided with constant mechanical power input, this leads to attaining multi-swing stability. Series compensation of generator reactance using TCSC is the only control strategy applied here while several other literature on methods to attain transient stability can be found in [29, 96].

6.3.3 First swing stability assessment with asynchronous generation

The system with 3-machines and 9-bus analysed before is investigated here, where each machine can be an equivalent generator aggregate. As explained in section 5.3.2, here an equivalent classical generator model is in its simplest form with equivalent inertia as sum of inertia of all generators in the group, and the equivalent transient reactance is obtained by paralleling the transient reactance of all generators under the generation bus[66, 68]. This assumption is utilised to factor windfarm penetration. So windfarm is equivalent to a conventional synchronous generator except with a negligible inertia. Further stability assessment by obtaining CCT using PEBS method is performed on 3-machine 9-bus system to investigate the impact of decreasing inertia at machine 2 on CCT. Bus 2 is where asynchronous generation is in mix with synchronous generation, thus net inertia is reduced.

For a fault on bus 4 the following observation are made. From Fig. 6.12 [3] it is observed that there is relative drop in CCT with decrease in inertia which is at 0% compensation of the line. Here, the drop in CCT from 0.31s to 0.27s occurs for an inertia decrease from 6.5 to 5.2. To improve the CCT from 0.27 to 0.31 , line 5-7 need to be compensated by 80% of line reactance X i.e., $X = 0.161 - 0.161 \times 0.8 = 0.0322$, this will increase CCT to 0.31s. In summary, decreasing the line reactance X_{57} from 0.1610 to 0.0322 in post-fault system will return a desired CCT of 0.31s, when its inertia is reduced from 6.5 to 5.2.

This is also verified in time domain, where Fig. 6.13 is the rotor angle swing of machine 2 at clearing time for three inertia and compensation combination. It demonstrates that line series compensation $X_{57} - X_c$ of post-fault network can help in maintaining CCT even when the inertia of machine is reduced. This will achieve first swing stability. Subsequently appropriate compensation of $X_{57} - X_{ca}$ during overshoot period and $X_{57} + X_{cb}$ during undershoot will decay oscillation similar to Fig. 6.11.

6.4 Series compensation location in 3-machine 9-bus system

It is observed from Fig. 6.14 that for a fault similar to Fig. 6.12 by providing series compensation on line 8-7, CCT (and hence stability) cannot be improved for the reduced inertia. Similarly even by providing compensation on line 6-9, 8-9 and 5-4. Table-6.1 provides a summary of lines that can participate in line series compensation if the inertia

[3] Fig. 6.12 different from Fig. 4.6, there axis are inertia H_2 and H_3

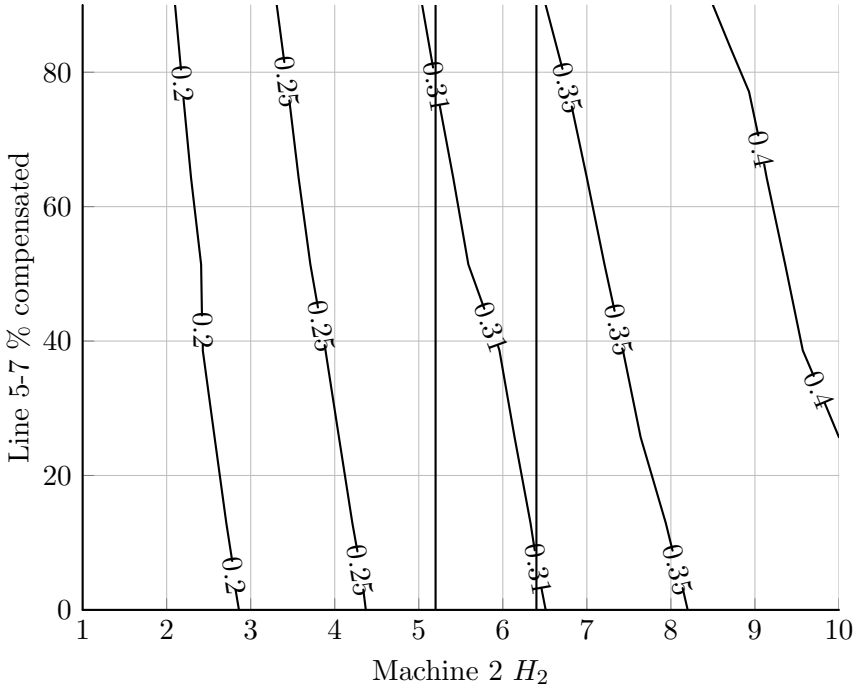

FIGURE 6.12: CCT lines of machine 2 over X_c and inertia for fault on bus 4 with line 6-4 removed and line 5-7 compensated

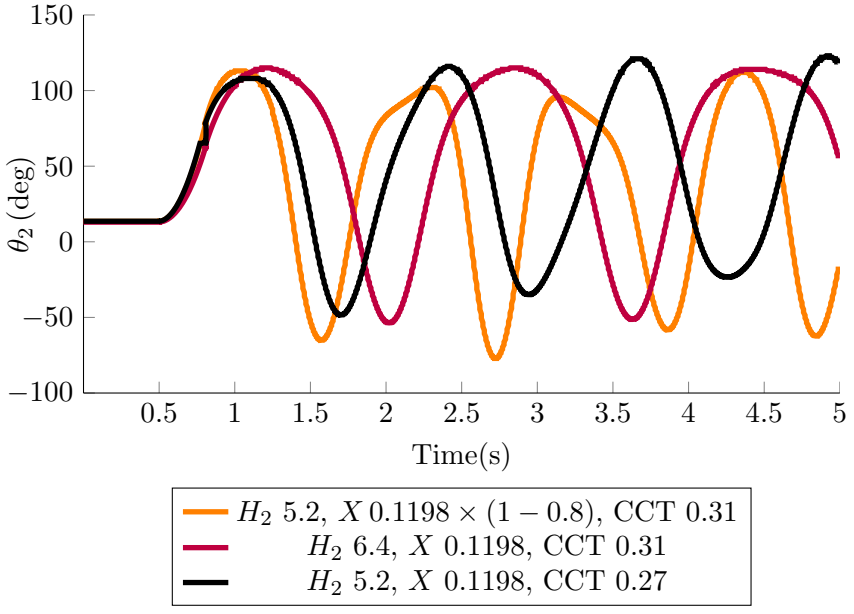

FIGURE 6.13: Machine 2 angle deviation for a fault critically cleared on bus 4 with line 6-4 removed and line 5-7 is compensated

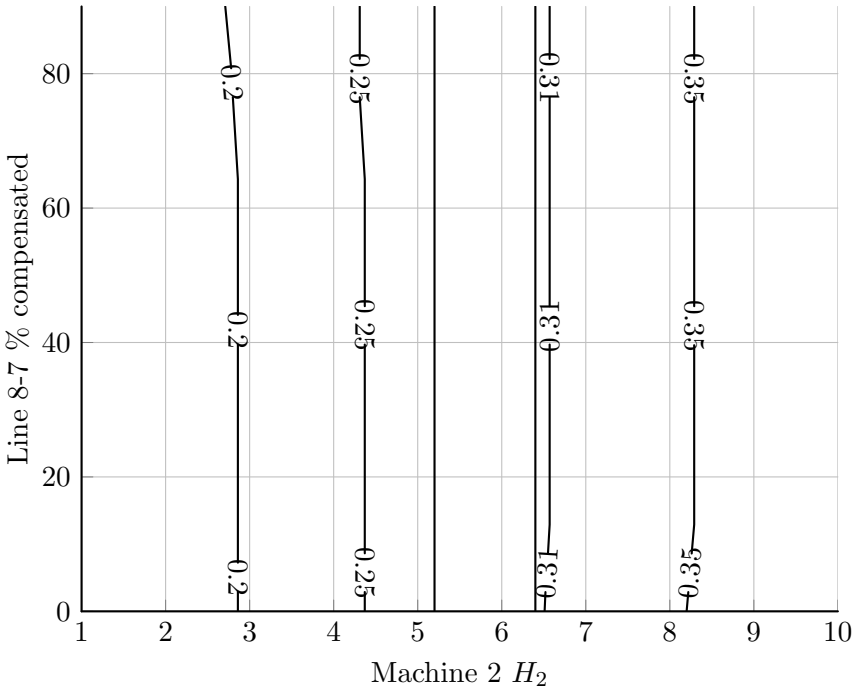

FIGURE 6.14: CCT lines of machine 2 over X_c and inertia for fault on bus 4 line 6-4 removed, line 8-7 value is % compensated in series

TABLE 6.1: Lines that can participate in compensation

Fault line removed	**Bus**	Line compensated					
		6-4	5-7	6-9	8-7	8-9	5-4
6-4	4 6		√ √				
5-7	5 7		√	√	√	√	
6-9	6 9		√				
8-7	8 7		√ √				
8-9	8 9		√				
5-4	5 4			√ √			

of machine 2 drops from 6.4 to 5.2 only, as this compensation is within 80% limit of the line capacity. This limit can be varied as desired, this table is prepared from observing the plots like Fig. 6.12. Table-6.1 can be obtained from the algorithm shown in Fig. 6.15, the algorithm is to identify lines which can participate in series compensation. Here $T_{cr6.4}$ is clearing time when machine 2 inertia is 6.4 with no compensation, $T_{cr5.2}$ is clearing time for inertia 5.2 with 80% compensation and X_{AB} is transmission line impedance is between bus A and B.

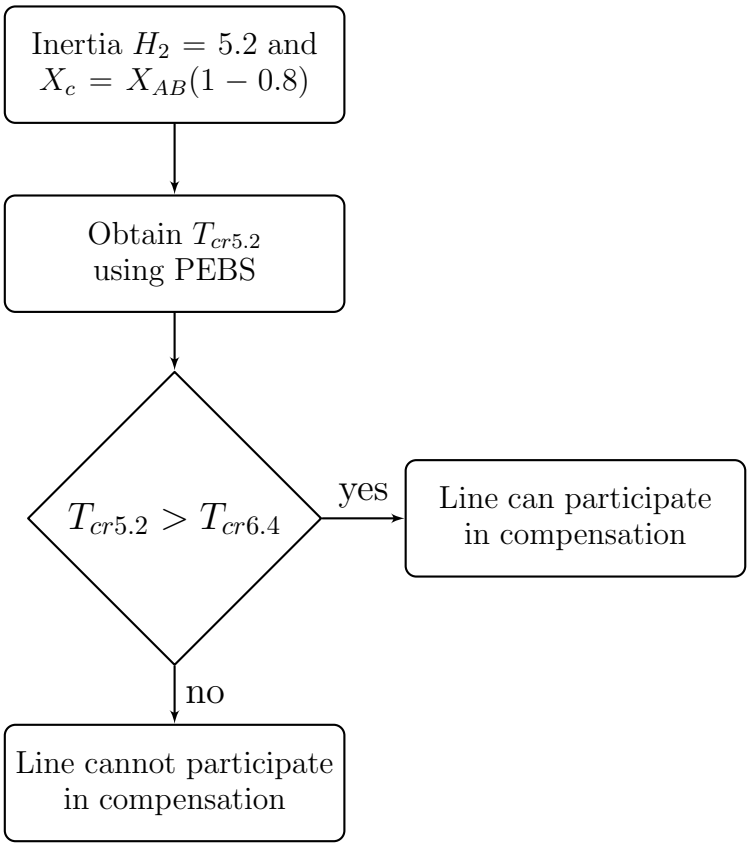

FIGURE 6.15: Algorithm to identify lines that participate in compensation

6.5 Summary

In this chapter we analyze how capacitive series compensation of transmission lines using bang-bang control strategy can achieve multi-swing transient stability if a machine inertia is reduced due to asynchronous generation. This was demonstrated on 3-machine 9-bus network, to find the value of series compensation that needed to be added in series of transmission lines when machine 2 inertia drops. PEBS techniques have been used to obtain clearing time. The estimated compensation value is sufficient to maintain CCT even with reduction in inertia of the machine. Algorithm was provided to obtain the lines which can participate in series compensation until 80% capacity. Equi-CCT contours are projected on compensation and inertia axis, which enables evaluating a quantifiable value of compensation required to be added in line series if a machine inertia is reduced. It clearly displays to help maintain desired transient stability margin, but only few specific lines seems to be able to participate in this compensation to improve stability.

In next and last chapter, a comprehensive conclusion, significance of contribution from this dissertation and direction for future work is provided.

Chapter 7

Conclusions and future works

This dissertation focuses on the transient stability assessment of power system networks with asynchronous generation like windfarms. Increasing amount of windfarms in existing power system network demands the need to understand existing transient stability methods.

Applying most traditional transient stability time-domain approach of observing rotor angle trajectory upon a fault, and see if the trajectory is bounded or diverging. This helps in arriving at a fault duration beyond which the trajectories diverge. This is a continuous trial and error method (performed offline using transient stability assessment tools) for large systems with detail models solved in time domain using high speed computational resources. An alternative approach for assessing transient stability is using the energy function method, which provides a faster solution and suitable for less detailed models but offers conservative results. Energy function method has been used in this thesis with an objective to understand the effect on existing transient stability margin i.e, without reducing inertia. This approach is being attempted for the very first time, for application to networks with asynchronous generation. The system used however are not large practical networks, but representative networks used in power system stability literature.

In chapter 2 energy function was derived and critical clearing time was obtained for SMIB system and three machine nine bus system. 39-bus 10-machine network was studied to identify coherent generator groups. By grouping generators this way, a network can be reduced to fewer buses. Chapter 3 provides thorough theoretical foundations for direct methods and algorithms which are thereafter illustrated by examples to obtain region of attraction for three machine systems. This provides a foundation for understating PEBS method used in obtaining transient critical energy and CCT for a contingency.

Chapter 4 provides results on effect of varying inertia of SMIB while obtaining CCT. It is observed that CCT decreases with reducing inertia, suggesting that lack of inertia quickly lets the system go into unstable region. PEBS method was used to obtain CCT and critical energy of three machine nine bus network. Although the method of obtaining CCT with PEBS is well established, utilising it to obtain CCT for wide range of reduced inertia of machines has never been explored before , which is thus a major contribution of this dissertation. Equi-CCT were plotted over inertia space to quantify the amount of inertia necessary from a machine, if inertia of other machine is reduced to maintain desired CCT. Anchoring of large inertia generator acts as a reference.

In chapter 5 coherent generator groups were identified when a windfarm displaces a synchronous generator in a 39-bus 10-machine system. It was found that generator groups remained same with relative deviations between machine angles and larger deviations to the machines close to windfarm bus. PEBS analysis done on a 3-machine 9-bus network, assuming windfarm as negative load offers a different initial solution and network, which makes it unsuitable for TSA with high wind energy penetration.

In chapter 6 dynamic series compensation of generators with reduced inertia to maintain desired first swing stability and application of bang-bang control to maintain multi-swing stability was demonstrated on SMIB and 3-machine 9-bus network. In three machine nine bus system, compensation quantity to be added in series to the machine is calculated. This quantity is sufficient to maintain critical clearing time even when there is reduction in inertia. PEBS method was employed to obtain critical energy and critical clearing time values.CCT contours are projected on compensation and inertia axis which provides quantifiable value of compensation required when machine inertia is reduced, still maintaining the desired transient stability margin. Optimal compensation values and lines are obtained, these lines can participate in compensation that can help to maintain transient stability limit during credible contingencies. It is found that only few lines can only participate with desired compensation amount upon reduction in inertia.

7.1 Significance of contributions

Study on SMIB and 3-machine 9-bus system to obtain CCT in event of decreasing inertia affirmatively demonstrates that transient stability margin reduces for all kind of contingencies. Simulation in MATLAB environment with machine modelled as constant voltage behind a transient reactance, being a standard practice for transient stability studies, is used in all our assessments.

The graphical representation (Fig .4.6) of CCT for several inertia combinations offers a quantifiable amount of inertia required in maintaining desired stability margin. This is unlike other researches done so far using proprietary software, where the effect of windfarm is assessed by observing rotor angles of neighbouring machines.

Equi-CCT contour representation also offers an index to proceed with a backward method of calculating inertia. From the CCT contour line plots, we can observe that it is a unique problem formulation. If for a multi-machine system, say 3 machines, exposed to contingency with similar pre-fault initial conditions inertia of any two machines and CCT are provided (which can be obtained from any energy function method or a time domain method) one can using the method described in this thesis estimate the inertia of third machine. This implies that one can estimate the pseudo inertia offered by aggregated asynchronous generator or from a generation bus. This backward method can be of special interest for windfarm integration and system planning group to incorporate the lack of inertial ability.

Equi-CCT contour representation in inertia space are like characteristic curves of system inertia for a contingency. It can be used as a reference guide for planning, operation/control of windfarms, especially to address the aspiration towards participating in ancillary services like providing inertial support. Even if necessary modification is required for existing protection setting, the new CCT obtained due to reduced inertia can help provide a roadmap for modifying existing protection setting. The bang-bang control ensures the system remain in region of attraction. The equi-CCT contour lines which are plotted along with capacitive compensation can be used as a characteristic curve for specific contingency which will help decide appropriate protection setting modifications.

7.2 Challenges

Simulation packages use different type of models and therefore it is challenging to compare results derived using different packages. This generates more confusions and uncertainties while dealing with simulation and validation of results. For this research, the author has primarily used MATLAB simulation environment for SMIB and 3-machine 9-bus system simulations, and DIgSILENT Powerfactory using library models for 39-bus 10-machine system RMS simulations. Powerfactory provides time domain results and does not have an energy function program. As proprietary software are complex and do not provide much flexibility that help to understand accurate parameters affecting the transient stability, the author sought to use MATLAB environment using PEBS method. In this study, the asynchronous generator of the windfarm is considered as a conventional synchronous generator with negligible inertia. Since the focus of the thesis

was to develop fundamental understanding of energy function application to transient stability, it can be considered acceptable.

The equi-CCT lines plotted in chapter 4 for varying inertia is only suitable for three machine system with one machine anchored. For machines more than three representing in inertia space and extracting information will be challenging. For larger machine assessment we can still obtain CCTs as usual multi-machine system. A large scale system can be reduced into an equivalent smaller machine network. Then an existing procedure to obtain CCT, involves grouping of generators and selective contingencies can be used.

7.3 Future work

7.3.1 Detail machine model analysis

- In this thesis much of investigation is done to obtain critical clearing time and energy in MATLAB environment, with simple machine and lossless network models that generally suffice for transient stability studies. Also with an assumption that windfarms are traditional synchronous machine with negligible or reduced inertia. This investigation can be redone and results can be verified to obtain accurate values using PSCAD software, with detailed machine and windfarm models.
- Similarly use of detail models in Powerfactory software in EMT mode and writing a script to compute energy function for multi-machine can be a possible direction.

7.3.2 Large network energy function analysis

- Direct methods have always suffered the inability to be applied on-line and for large networks. Direct method transient stability analysis on 39-bus 10-machine system can be pursued in future in MATLAB environment, and compared with rotor angles and speed deviation results from a network developed in PSCAD.
- Reducing a 39-bus 10-machine system, with and without windfarm developed in Powerfactory from chapter 3 and 5, into a smaller machine system can be possible future work direction. This task will help to verify generation aggregation and network reduction methods and identify the stability analysis fidelity of reducing a large network into a simple three machine network.
- In chapter 3, obtaining region of attraction for 3-machine 9-bus system and obtaining coherent generator groups has been clearly outlined. Using the coherent generator group information to reduce to three machine, smaller bus network and obtaining controllable unstable equilibrium points can be a taken up in future.

7.3.3 Control of FACT devices in large network

- In this thesis bang-bang control is proposed whereas in future this discrete control strategy or other novel strategies for transient stability enhancement can be verified with different FACT devices. Investigations can be done using Powerfactory, MATLAB or PSCAD packages on a multi-machine multi-bus network with simple or detailed models of synchronous generator and windfarms. Compensation can be verified from load bus locations and other non-generator locations.

Appendix A

IEEE 10 Generator 39 Bus System Data

A.1 Network single line diagram

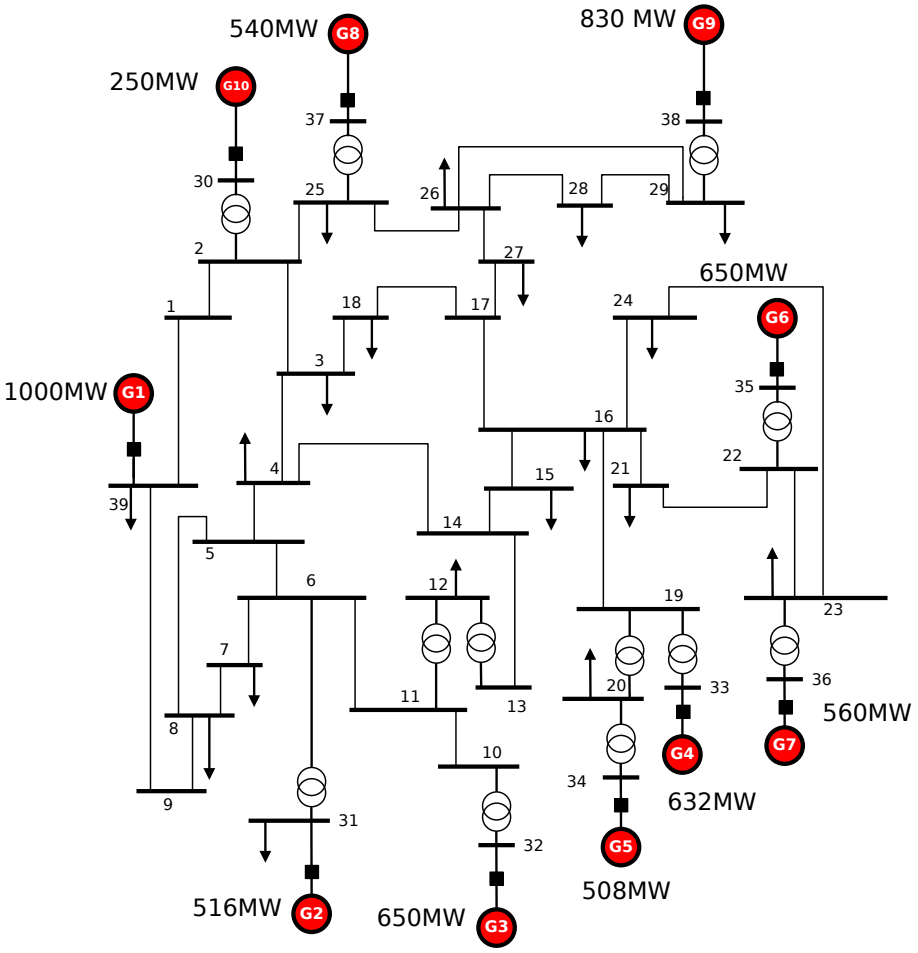

A.2 Basic data and characteristics

Parameters for the two-axis model of the synchronous machines are shown in tables as follows. All values are given on 100 MVA base [28, 97]

TABLE A.1: Generator data

bus	P_g	Q_g	Q_{max}	Q_{min}	V_g
30	250	161.762	161.762	140	1.0499
31	516	221.574	300	-100	0.982
32	650	206.965	300	150	0.9841
33	632	108.293	250	0	0.9972
34	508	166.688	167	0	1.0123
35	650	210.661	300	-100	1.0494
36	560	100.165	240	0	1.0636
37	540	-1.36945	250	0	1.0275
38	830	21.7327	300	-150	1.0265
39	1000	78.4674	300	-100	1.03

TABLE A.2: Detailed synchronous machines data

Gen.	H	r_a	x'_d	x'_q	x_d	x_q	T'_{do}	T'_{qo}	x_l
1	500.0	0	0.006	0.008	0.02	0.019	7.0	0.7	0.003
2	30.3	0	0.0697	0.170	0.295	0.282	6.56	1.5	0.035
3	35.8	0	0.0531	0.0876	0.2495	0.237	5.7	1.5	0.0304
4	28.6	0	0.0436	0.166	0.262	0.258	5.69	1.5	0.0295
5	26.0	0	0.132	0.166	0.67	0.62	5.4	0.44	0.054
6	34.8	0	0.05	0.0814	0.254	0.241	7.3	0.4	0.0224
7	26.4	0	0.049	0.186	0.295	0.292	5.66	1.5	0.0322
8	24.3	0	0.057	0.0911	0.290	0.280	6.7	0.41	0.028
9	34.5	0	0.057	0.0587	0.2106	0.205	4.79	1.96	0.0298
10	42.0	0	0.03 1	0.008	0.1	0.069	10.2	0.0	0.0125

A.2.1 network data, power and voltage set points

Table A.3: Network data

from bus	to bus	Resistance	Reactance	Suseptance	Tap ratio
1	2	0.0035	0.0411	0.6987	0
1	39	0.001	0.025	0.75	0
2	3	0.0013	0.0151	0.2572	0
2	25	0.007	0.0086	0.146	0
2	30	0	0.0181	0	1.025
3	4	0.0013	0.0213	0.2214	0
3	18	0.0011	0.0133	0.2138	0
4	5	0.0008	0.0128	0.1342	0
4	14	0.0008	0.0129	0.1382	0
5	6	0.0002	0.0026	0.0434	0
5	8	0.0008	0.0112	0.1476	0
6	7	0.0006	0.0092	0.113	0
6	11	0.0007	0.0082	0.1389	0
6	31	0	0.025	0	1.07
7	8	0.0004	0.0046	0.078	0
8	9	0.0023	0.0363	0.3804	0
9	39	0.001	0.025	1.2	0
10	11	0.0004	0.0043	0.0729	0
10	13	0.0004	0.0043	0.0729	0
10	32	0	0.02	0	1.07
12	11	0.0016	0.0435	0	1.006
12	13	0.0016	0.0435	0	1.006
13	14	0.0009	0.0101	0.1723	0
14	15	0.0018	0.0217	0.366	0
15	16	0.0009	0.0094	0.171	0
16	17	0.0007	0.0089	0.1342	0
16	19	0.0016	0.0195	0.304	0
16	21	0.0008	0.0135	0.2548	0
16	24	0.0003	0.0059	0.068	0
17	18	0.0007	0.0082	0.1319	0
17	27	0.0013	0.0173	0.3216	0
19	20	0.0007	0.0138	0	1.06
19	33	0.0007	0.0142	0	1.07
20	34	0.0009	0.018	0	1.009
21	22	0.0008	0.014	0.2565	0
22	23	0.0006	0.0096	0.1846	0
22	35	0	0.0143	0	1.025
23	24	0.0022	0.035	0.361	0
23	36	0.0005	0.0272	0	1
25	26	0.0032	0.0323	0.531	0
25	37	0.0006	0.0232	0	1.025
26	27	0.0014	0.0147	0.2396	0
26	28	0.0043	0.0474	0.7802	0
26	29	0.0057	0.0625	1.029	0
28	29	0.0014	0.0151	0.249	0
29	38	0.0008	0.0156	0	1.025

TABLE A.4: Bus data - power and voltage set points after load flow

Bus	P_i	Q_i	V_i	θ_i
1	97.6	44.2	1.0393836	-13.536602
2	0	0	1.0484941	-9.7852666
3	322	2.4	1.0307077	-12.276384
4	500	184	1.00446	-12.626734
5	0	0	1.0060063	-11.192339
6	0	0	1.0082256	-10.40833
7	233.8	84	0.99839728	-12.755626
8	522	176.6	0.99787232	-13.335844
9	6.5	-66.6	1.038332	-14.178442
10	0	0	1.0178431	-8.170875
11	0	0	1.0133858	-8.9369663
12	8.53	88	1.000815	-8.9988236
13	0	0	1.014923	-8.9299272
14	0	0	1.012319	-10.715295
15	320	153	1.0161854	-11.345399
16	329	32.3	1.0325203	-10.033348
17	0	0	1.0342365	-11.116436
18	158	30	1.0315726	-11.986168
19	0	0	1.0501068	-5.4100729
20	680	103	0.99101054	-6.8211783
21	274	115	1.0323192	-7.6287461
22	0	0	1.0501427	-3.1831199
23	247.5	84.6	1.0451451	-3.3812763
24	308.6	-92.2	1.038001	-9.9137585
25	224	47.2	1.0576827	-8.3692354
26	139	17	1.0525613	-9.4387696
27	281	75.5	1.0383449	-11.362152
28	206	27.6	1.0503737	-5.9283592
29	283.5	26.9	1.0501149	-3.1698741
30	0	0	1.0499	-7.3704746
31	9.2	4.6	0.982	0
32	0	0	0.9841	-0.1884374
33	0	0	0.9972	-0.19317445
34	0	0	1.0123	-1.631119
35	0	0	1.0494	1.7765069
36	0	0	1.0636	4.4684374
37	0	0	1.0275	-1.5828988
38	0	0	1.0265	3.8928177
39	1104	250	1.03	-14.535256

Bibliography

[1] J. Ekanayake, L. Holdsworth, and N. Jenkins, "Control of dfig wind turbines," *Power Engineer*, vol. 17, no. 1, pp. 28–32, Feb 2003.

[2] T. Ackermann, *Wind Power in Power Systems*. Wiley, 2005.

[3] B. Wu, Y. Lang, N. Zargari, and S. Kouro, *Power Conversion and Control of Wind Energy Systems*, ser. IEEE Press Series on Power Engineering. Wiley, 2011.

[4] H. Ahmadi and H. Ghasemi, "Maximum penetration level of wind generation considering power system security limits," *Generation, Transmission Distribution, IET*, vol. 6, no. 11, pp. 1164–1170, November 2012.

[5] K. H. LaCommare and J. H. Eto, "Understanding the cost of power interruptions to u.s. electricity consumers," p. 70, 09/2004 2004.

[6] D. Lineweber, S. McNulty, and E. P. R. Institute, *The Cost of Power Disturbances to Industrial & Digital Economy Companies*. EPRI, 2001.

[7] P. Kundur, J. Paserba, V. Ajjarapu, G. Andersson, A. Bose, C. Canizares, N. Hatziargyriou, D. Hill, A. Stankovic, C. Taylor, T. Van Cutsem, and V. Vittal, "Definition and classification of power system stability ieee/cigre joint task force on stability terms and definitions," *Power Systems, IEEE Transactions on*, vol. 19, no. 3, pp. 1387–1401, Aug 2004.

[8] P. Kundur, N. Balu, and M. Lauby, *Power system stability and control*, ser. EPRI power system engineering series. McGraw-Hill, 1994.

[9] P. Anderson and A. Fouad, *Power System Control and Stability*. The Iowa State University Press, 1977.

[10] O. Anaya-Lara, N. Jenkins, J. Ekanayake, P. Cartwright, and M. Hughes, *Wind Energy Generation: Modelling and Control*. Wiley, 2011.

[11] "Wind generation investigation project (wgip)-investigation 7 (stage 2): Effect of wind generation on transient stability," March 2008. [Online].

Available: http://www.ea.govt.nz/about-us/what-we-do/our-history/archive/dev-archive/work-programmes/power-systems-and-common-quality/wgip/

[12] D. Gautam, V. Vittal, and T. Harbour, "Impact of increased penetration of dfig-based wind turbine generators on transient and small signal stability of power systems," *Power Systems, IEEE Transactions on*, vol. 24, no. 3, pp. 1426–1434, Aug 2009.

[13] L. Mariotto, H. Pinheiro, G. Junior, and M. R. Muraro, "An analytical tool for computing transient stability margins of power systems with large amount of wind power," in *Clean Electrical Power, 2007. ICCEP '07. International Conference on*, May 2007, pp. 747–753.

[14] S. Dai, L. Shi, Y. Ni, L. Yao, and M. Bazargan, "Transient stability evaluations of power system with large dfig based wind farms," in *Power and Energy Engineering Conference (APPEEC), 2010 Asia-Pacific*, March 2010, pp. 1–4.

[15] J. Machowski, J. Bialek, and J. Bumby, *Power System Dynamics: Stability and Control*. Wiley, 2011.

[16] J. Rodriguez-Amenedo, S. Arnalte, and J. Burgos, "Automatic generation control of a wind farm with variable speed wind turbines," *Energy Conversion, IEEE Transactions on*, vol. 17, no. 2, pp. 279–284, Jun 2002.

[17] P. Naik, W. Qureshi, and N.-K. Nair, "Identification of coherent generator groups in power system networks with windfarms," in *Universities Power Engineering Conference (AUPEC), 2011 21st Australasian*, Sept 2011, pp. 1–5.

[18] E. Vittal, M. O'Malley, and A. Keane, "Rotor angle stability with high penetrations of wind generation," *Power Systems, IEEE Transactions on*, vol. 27, no. 1, pp. 353–362, Feb 2012.

[19] J. Slootweg and W. Kling, "Impacts of distributed generation on power system transient stability," in *Power Engineering Society Summer Meeting, 2002 IEEE*, vol. 2, July 2002, pp. 862–867 vol.2.

[20] D. Trudnowski, A. Gentile, J. Khan, and E. Petritz, "Fixed-speed wind-generator and wind-park modeling for transient stability studies," *Power Systems, IEEE Transactions on*, vol. 19, no. 4, pp. 1911–1917, Nov 2004.

[21] M. V. A. Nunes, J. Peas Lopes, H. Zurn, U. Bezerra, and R. Almeida, "Influence of the variable-speed wind generators in transient stability margin of the conventional generators integrated in electrical grids," *Energy Conversion, IEEE Transactions on*, vol. 19, no. 4, pp. 692–701, Dec 2004.

[22] E. Vittal, P. Cuffe, and A. Keane, "Transient stability impacts from distribution connected wind farms," in *Power and Energy Society General Meeting, 2012 IEEE*, July 2012, pp. 1–5.

[23] P. Anderson and A. Bose, "Stability simulation of wind turbine systems," *Power Apparatus and Systems, IEEE Transactions on*, vol. PAS-102, no. 12, pp. 3791–3795, Dec 1983.

[24] J. Zaborszky, G. Huang, B. Zheng, and T.-C. Leung, "On the phase portrait of a class of large nonlinear dynamic systems such as the power system," *Automatic Control, IEEE Transactions on*, vol. 33, no. 1, pp. 4–15, Jan 1988.

[25] G. E. Gless, "Direct method of liapunov applied to transient power system stability," *Power Apparatus and Systems, IEEE Transactions on*, vol. PAS-85, no. 2, pp. 159–168, Feb 1966.

[26] H.-D. Chiang, F. Wu, and P. Varaiya, "Foundations of direct methods for power system transient stability analysis," *Circuits and Systems, IEEE Transactions on*, vol. 34, no. 2, pp. 160–173, Feb 1987.

[27] A. Fouad and V. Vittal, *Power system transient stability analysis using the transient energy function method*. Prentice Hall, 1992.

[28] A. Pai, *Energy Function Analysis for Power System Stability*, ser. Kluwer international series in engineering and computer science. Springer, 1989.

[29] J. Grainger and W. Stevenson, *Power system analysis*, ser. McGraw-Hill series in electrical and computer engineering: Power and energy. McGraw-Hill, 1994.

[30] E. Kimbark, *Power System Stability*. John Wiley & Sons, 1950.

[31] S. Crary, *Power System Stability: Transient stability*, ser. General Electric series. John Wiley, 1947.

[32] A. Pai, *Power system stability: Analysis by the direct method of Lyapunov*, ser. Kluwer international series in engineering and computer science. North Holland Publishing Co. New York, 1981.

[33] A. H. El-Abiad and K. Nagappan, "Transient stability regions of multimachine power systems," *Power Apparatus and Systems, IEEE Transactions on*, vol. PAS-85, no. 2, pp. 169–179, Feb 1966.

[34] A. Michel, A. Fouad, and V. Vittal, "Power system transient stability using individual machine energy functions," *Circuits and Systems, IEEE Transactions on*, vol. 30, no. 5, pp. 266–276, May 1983.

[35] B. N. Nityanandan, "Decomposition and aggregation of multimachine power systems for transient stability, ph.d. thesis."

[36] A. Rahimi and G. Schaffer, "Power system transient stability indexes for on-line analysis of "worst-case" dynamic contingencies," *Power Systems, IEEE Transactions on*, vol. 2, no. 3, pp. 660–666, Aug 1987.

[37] R. Podmore, "Identification of coherent generators for dynamic equivalents," *Power Apparatus and Systems, IEEE Transactions on*, vol. PAS-97, no. 4, pp. 1344 –1354, july 1978.

[38] J. Giri, "Coherency reduction in the epri stability program," *Power Apparatus and Systems, IEEE Transactions on*, vol. PAS-102, no. 5, pp. 1285 –1293, 1983.

[39] R. Schlueter and P. Rusche, "Dynamic equivalents in rapid analysis of transient stability methods," in *Proceedings of IEEE PES winter meeting*, New Orleans, USA, 1987, pp. 30–36.

[40] A. Germond and R. Podmore, "Dynamic aggregation of generating unit models," *Power Apparatus and Systems, IEEE Transactions on*, vol. PAS-97, no. 4, pp. 1060–1069, July 1978.

[41] P. W. Sauer and M. Pai, *Power system dynamics and stability*, ser. Kluwer international series in engineering and computer science. Prentice Hall Upper Saddle River, NJ, 1998.

[42] A. Miah, "Simple dynamic equivalent for fast online transient stability assessment," *Generation, Transmission and Distribution, IEE Proceedings-*, vol. 145, no. 1, pp. 49–55, Jan 1998.

[43] J. LaSalle and S. Lefschetz, *Stability by Liapunov's direct method: with applications*, ser. Mathematics in science and engineering. Academic Press, New York, 1961.

[44] A. Michel, N. Sarabudla, and R. Miller, "Stability analysis of complex dynamical systems," *Circuits, Systems and Signal Processing*, vol. 1, no. 2, pp. 171–202, 1982.

[45] W. Hahn and A. Baartz, *Stability of motion*, ser. Grundlehren der mathematischen Wissenschaften. Springer, 1967.

[46] S. Sastry, *Nonlinear Systems: Analysis, Stability and Control*, ser. Interdisciplinary applied mathematics: Systems and control. Springer, 1999.

[47] H.-D. Chiang, F. Wu, and P. Varaiya, "Foundations of the potential energy boundary surface method for power system transient stability analysis," *Circuits and Systems, IEEE Transactions on*, vol. 35, no. 6, pp. 712–728, Jun 1988.

[48] J. Guckenheimer and P. Holmes, *Nonlinear Oscillations, Dynamical Systems, and Bifurcations of Vector Fields*, ser. Applied Mathematical Sciences. Springer, 1983, no. v. 42.

[49] M. Hirsch, R. Devaney, and S. Smale, *Differential Equations, Dynamical Systems, and Linear Algebra*, ser. Pure and Applied Mathematics. Elsevier Science, 1974.

[50] M. Hirsch, S. Smale, and R. Devaney, *Differential Equations, Dynamical Systems, and an Introduction to Chaos*, ser. Differential equations, dynamical systems, and an introduction to chaos. Academic Press, 2004, no. v. 60.

[51] H. Khalil, *Nonlinear Systems*. Prentice Hall PTR, 2002.

[52] A. Michel, B. Nam, and V. Vittal, "Computer generated lyapunov functions for interconnected systems: Improved results with applications to power systems," *Circuits and Systems, IEEE Transactions on*, vol. 31, no. 2, pp. 189–198, Feb 1984.

[53] W. Price, K. Wirgau, A. Murdoch, J. V. Mitsche, E. Vaahedi, and M. El-Kady, "Load modeling for power flow and transient stability computer studies," *Power Systems, IEEE Transactions on*, vol. 3, no. 1, pp. 180–187, Feb 1988.

[54] M. Vidyasagar, *Nonlinear Systems Analysis*, ser. Classics in Applied Mathematics. Society for Industrial and Applied Mathematics, 2002.

[55] H. Chiang, *Direct Methods for Stability Analysis of Electric Power Systems: Theoretical Foundation, BCU Methodologies, and Applications*. Wiley, 2011.

[56] P. Varaiya, F. Wu, and R.-L. Chen, "Direct methods for transient stability analysis of power systems: Recent results," *Proceedings of the IEEE*, vol. 73, no. 12, pp. 1703–1715, Dec 1985.

[57] H.-D. Chiang, F. Wu, and P. Varaiya, "A bcu method for direct analysis of power system transient stability," *Power Systems, IEEE Transactions on*, vol. 9, no. 3, pp. 1194–1208, Aug 1994.

[58] N. Kakimoto, Y. Ohnogi, H. Matsuda, and H. Shibuya, "Transient stability analysis of large-scale power system by lyapunov's direct method," *Power Apparatus and Systems, IEEE Transactions on*, vol. PAS-103, no. 1, pp. 160–167, Jan 1984.

[59] T. Athay, R. Podmore, and S. Virmani, "A practical method for the direct analysis of transient stability," *Power Apparatus and Systems, IEEE Transactions on*, vol. PAS-98, no. 2, pp. 573–584, March 1979.

[60] K. Padiyar and K. Ghosh, "Direct stability evaluation of power systems with detailed generator models using structure-preserving energy functions," *International Journal of Electrical Power & Energy Systems*, vol. 11, no. 1, pp. 47 – 56, 1989.

[61] P. Sauer, A. Behera, M. A. Pai, J. Winkelman, and J. Chow, "Trajectory approximations for direct energy methods that use sustained faults with detailed power system models," *Power Systems, IEEE Transactions on*, vol. 4, no. 2, pp. 499–506, May 1989.

[62] A. A. Fouad, V. Vittal, S. Rajagopal, V. F. Carvalho, M. A. El-Kady, C. K. Tang, J. V. Mitsche, and M. Pereira, "Direct transient stability analysis using energy functions application to large power networks," *Power Systems, IEEE Transactions on*, vol. 2, no. 1, pp. 37–43, Feb 1987.

[63] G. Simões and F. Farret, *Renewable Energy Systems: Design and Analysis with Induction Generators*, ser. Power Electronics and Applications Series. Taylor & Francis, 2004.

[64] S. Muller, M. Deicke, and R. De Doncker, "Doubly fed induction generator systems for wind turbines," *Industry Applications Magazine, IEEE*, vol. 8, no. 3, pp. 26–33, May 2002.

[65] L. Holdsworth, X. Wu, J. Ekanayake, and N. Jenkins, "Comparison of fixed speed and doubly-fed induction wind turbines during power system disturbances," *Generation, Transmission and Distribution, IEE Proceedings-*, vol. 150, no. 3, pp. 343–352, May 2003.

[66] L. Wang, M. Klein, S. Yirga, and P. Kundur, "Dynamic reduction of large power systems for stability studies," *Power Systems, IEEE Transactions on*, vol. 12, no. 2, pp. 889–895, May 1997.

[67] E. Pires de Souza and A. Leite da Silva, "An efficient methodology for coherency-based dynamic equivalents [power system analysis]," *Generation, Transmission and Distribution, IEE Proceedings C*, vol. 139, no. 5, pp. 371–382, Sep 1992.

[68] A. Germond and R. Podmore, "Dynamic aggregation of generating unit models," *Power Apparatus and Systems, IEEE Transactions on*, vol. PAS-97, no. 4, pp. 1060–1069, July 1978.

[69] S. E. De Oliveira and J. F. De Queiroz, "Modal dynamic equivalent for electric power systems. i. theory," *Power Systems, IEEE Transactions on*, vol. 3, no. 4, pp. 1723–1730, Nov 1988.

[70] X. Lei, D. Povh, and O. Ruhle, "Industrial approaches for dynamic equivalents of large power systems," in *Power Engineering Society Winter Meeting, 2002. IEEE*, vol. 2, 2002, pp. 1036–1042 vol.2.

[71] R. J. Newell, M. D. Risan, L. Allen, I. Rao, and D. Stuehm, "Utility experience with coherency-based dynamic equivalents of very large systems," *Power Apparatus and Systems, IEEE Transactions on*, vol. PAS-104, no. 11, pp. 3056–3063, Nov 1985.

[72] M. Pavella, D. Ernst, and D. Ruiz-Vega, *Transient Stability of Power Systems: A Unified Approach to Assessment and Control*, ser. Kluwer International Series in Engineering & Computer Science. Springer London, Limited, 2000.

[73] M. El-Kady, C. K. Tang, V. F. Carvalho, A. Fouad, and V. Vittal, "Dynamic security assessment utilizing the transient energy function method," *Power Systems, IEEE Transactions on*, vol. 1, no. 3, pp. 284–291, Aug 1986.

[74] S. Nishida, "On-line identification of potential energy at the unstable equilibrium point and its application to adaptive emergency control of power system," *Electrical Engineering in Japan*, vol. 104, no. 4, pp. 113–123, 1984.

[75] F. Rahimi, M. Lauby, J. Wrubel, and K. Lee, "Evaluation of the transient energy function method for on-line dynamic security analysis," *Power Systems, IEEE Transactions on*, vol. 8, no. 2, pp. 497–507, May 1993.

[76] S. Horowitz and A. Phadke, *Power system relaying*, ser. Electronic & electrical engineering research studies: Lines and cables for power transmission series. Research Studies Press, 1995.

[77] C. Liu and J. Thorp, "Application of synchronised phasor measurements to real-time transient stability prediction," *Generation, Transmission and Distribution, IEE Proceedings-*, vol. 142, no. 4, pp. 355–360, Jul 1995.

[78] M. Adamiak, A. Apostolov, M. Begovic, C. Henville, K. Martin, G. Michel, A. Phadke, and J. Thorp, "Wide area protection technology and infrastructures," *Power Delivery, IEEE Transactions on*, vol. 21, no. 2, pp. 601–609, April 2006.

[79] M. Donnelly, J. Smith, R. Johnson, J. Hauer, R. W. Brush, and R. Adapa, "Control of a dynamic brake to reduce turbine-generator shaft transient torques," *Power Systems, IEEE Transactions on*, vol. 8, no. 1, pp. 67–73, Feb 1993.

[80] S. Krishna and K. Padiyar, "Discrete control of unified power flow controller for stability improvement," *Electric Power Systems Research*, vol. 75, no. 2–3, pp. 178 – 189, 2005.

[81] K. Padiyar and K. U. Rao, "Discrete control of series compensation for stability improvement in power systems," *International Journal of Electrical Power and Energy Systems*, vol. 19, no. 5, pp. 311 – 319, 1997.

[82] K. Padiyar, *Structure Preserving Energy Functions in Power Systems: Theory and Applications*. Taylor & Francis, 2013.

[83] J. Gronquist, W. Sethares, F. Alvarado, and R. Lasseter, "Power oscillation damping control strategies for facts devices using locally measurable quantities," *Power Systems, IEEE Transactions on*, vol. 10, no. 3, pp. 1598–1605, Aug 1995.

[84] S. Rahimzadeh, M. Tavakoli Bina, and A. Viki, "Simultaneous application of multi-type facts devices to the restructured environment: achieving both optimal number and location," *Generation, Transmission Distribution, IET*, vol. 4, no. 3, pp. 349–362, March 2010.

[85] D. Chatterjee and A. Ghosh, "Transient stability assessment of power systems containing series and shunt compensators," *Power Systems, IEEE Transactions on*, vol. 22, no. 3, pp. 1210–1220, Aug 2007.

[86] I. P. S. Engineering, "A description of discrete supplementary controls for stability," *Power Apparatus and Systems, IEEE Transactions on*, vol. PAS-97, no. 1, pp. 149–165, Jan 1978.

[87] J. Chang and J. Chow, "Time-optimal control of power systems requiring multiple switchings of series capacitors," *Power Systems, IEEE Transactions on*, vol. 13, no. 2, pp. 367–373, May 1998.

[88] N. Rama Rao and D. Reitan, "Improvement of power system transient stability using optimal control: Bang-bang control of reactance," *Power Apparatus and Systems, IEEE Transactions on*, vol. PAS-89, no. 5, pp. 975–984, May 1970.

[89] O. J. M. Smith, "Power system transient control by capacitor switching," *Power Apparatus and Systems, IEEE Transactions on*, vol. PAS-88, no. 1, pp. 28–35, Jan 1969.

[90] "Improvement of system stability by switched series capacitors," *Power Apparatus and Systems, IEEE Transactions on*, vol. PAS-85, no. 2, pp. 180–188, Feb 1966.

[91] N. Hingorani and L. Gyugyi, *Understanding FACTS: Concepts and Technology of Flexible AC Transmission Systems*. Wiley, 2000.

[92] K. Padiyar, *Facts Controllers In Power Transmission And Distribution*. New Age International (P) Limited, 2007.

[93] M. Athans and P. Falb, *Optimal control: an introduction to the theory and its applications*, ser. Lincoln Laboratory publications. McGraw-Hill, 1966.

[94] D. Reitan and N. RamaRao, "A method of improving transient stability by bang-bang control of tie-line reactance," *Power Apparatus and Systems, IEEE Transactions on*, vol. PAS-93, no. 1, pp. 303–311, Jan 1974.

[95] R. Mathur and R. Varma, *Thyristor-Based FACTS Controllers for Electrical Transmission Systems*, ser. IEEE Press series on microelectronic systems. Wiley, 2002.

[96] A. Chakrabarti and S. Halder, *Power System Analysis: Operation And Control*. Prentice-Hall Of India Pvt. Limited, 2006.

[97] R. D. Zimmerman, C. E. Murillo-Sánchez, and D. Gan, "A matlab power system simulation package," 1997.